

BLEJSKE DELAVNICE IZ FIZIKE

BLED WORKSHOPS IN PHYSICS

LETNIK 13, ŠT. 1

VOL. 13, NO. 1

ISSN 1580-4992

Proceedings of the Mini-Workshop
Hadronic Resonances

Bled, Slovenia, July 1 – 8, 2012

Edited by

Bojan Golli

Mitja Rosina

Simon Širca

University of Ljubljana and Jožef Stefan Institute

DMFA – ZALOŽNIŠTVO
LJUBLJANA, NOVEMBER 2012

The Mini-Workshop *Hadronic Resonances*

was organized by

*Jožef Stefan Institute, Ljubljana
Department of Physics, Faculty of Mathematics and Physics, University of Ljubljana*

and sponsored by

*Slovenian Research Agency
Department of Physics, Faculty of Mathematics and Physics, University of Ljubljana
Society of Mathematicians, Physicists and Astronomers of Slovenia*

Organizing Committee

Mitja Rosina, Bojan Golli, Simon Širca

List of participants

*Marko Bračko, Ljubljana, marko.bracko@ijs.si
Saša Ceci, Zagreb, sasa.ceci@gmail.com
Joseph Day, Graz, jday21@gmail.com
Veljko Dmitrašinović, Belgrade, dmitrasin@yahoo.com
Bojan Golli, Ljubljana, bojan.golli@ijs.si
Atsushi Hosaka, Osaka, hosaka@rcnp.osaka-u.ac.jp
Regina Kleinhappel, Graz, regina.kleinhappel@gmx.at
Daniel Kupelwieser, Graz, daniel.kupelwieser@uni-graz.at
Michael Ostrick, Mainz, ostrick@kph.uni-mainz.de
Willi Plessas, Graz, willibald.plessas@uni-graz.at
Deborah Roenchen, Bonn, roenchen@hiskp.uni-bonn.de
Saša Prelovšek, Ljubljana, Sasa.Prelovsek@ijs.si
Mitja Rosina, Ljubljana, mitja.rosina@ijs.si
Wolfgang Schweiger, Graz, wolfgang.schweiger@uni-graz.at
Vikram Soni, New Delhi, v.soni@airtelmail.in
Ica Stancu, Liege, fstancu@ulg.ac.be
Simon Širca, Ljubljana, simon.sirca@fmf.uni-lj.si
Alfred Švarc, Zagreb, svarc@irb.hr
Lothar Tiator, Mainz, tiator@kph.uni-mainz.de*

Electronic edition

<http://www-fl.ijs.si/BledPub/>

Contents

Preface	V
Predgovor	VII
The Road to Extraction of S-Matrix Poles from Experimental Data <i>Saša Ceci, Milorad Korolija, and Branimir Zauner</i>	1
Unified Model for Light- and Heavy-Flavor Baryon Resonances <i>J. P. Day, W. Plessas, Ki-Seok Choi</i>	5
A chiral theory of scalar heavy-light (D, D_s) and (B, B_s) mesons <i>V. Dmitrašinović</i>	12
Low-lying states of the Y-string in two dimensions <i>V. Dmitrašinović, I. Salom</i>	13
Exotic molecules of heavy quark hadrons <i>Atsushi Hosaka</i>	17
Spin-Flavor Formalism for the Relativistic Coupled-Channels Quark Model <i>Regina Kleinhappel, Willibald Plessas, Wolfgang Schweiger</i>	20
Resonances in photo-induced reactions <i>M. Ostrick</i>	23
Electroweak Form Factors of Baryon Ground States and Resonances <i>Ki-Seok Choi, W. Plessas, M. Rohrmoser</i>	32
Pion- and photon-induced hadronic reactions in a combined coupled-channel analysis <i>Deborah Rönchen</i>	36
The implications of the two solar mass neutron star for the strong interactions <i>Vikram Soni, Pawel Haensel and Mitja Rosina</i>	42

Highly excited states of baryons in large N_c QCD	
<i>N. Matagne, Fl. Stancu</i>	47
Poles as a link between QCD and scattering theory (old and contemporary knowledge)	
<i>A. Švarc</i>	54
Complete Experiments for Pion Photoproduction	
<i>L. Tiator</i>	55
News from Belle: Recent Spectroscopy Results	
<i>M. Bračko</i>	62
Meson electro-production in the region of the Delta(1700) D33 resonance	
<i>B. Golli</i>	66
Scattering phase shifts and resonances from lattice QCD	
<i>S. Prelovšek</i>	74
Scattering of nucleon on a superheavy neutron	
<i>Norma Mankoč Borštnik and Mitja Rosina</i>	78
Approaching the spin structure of ^3He by polarization observables	
<i>S. Širca</i>	84

Preface

The activities and achievements of our encounter at Bled 2012 can be easily summarized. We were caught in a resonance! However, there was also no shortage of interesting “background”.

We learned many things about the development of analytical methods for the search of resonances and for implementing the influence of nearby thresholds and interferences in the determination of resonance parameters. In many cases, the interplay between quark and mesonic degrees of freedom is particularly significant, for example in the $\Delta(1700)$ resonance. Resonance parameters, especially poles in the complex energy plane, can sometimes be better determined from the calculation of the time delay instead of the shape of the resonance curve. It was a great encouragement that nowadays Lattice QCD can be used as well to calculate phase shifts for the pion-meson scattering, even in the resonance region.

New mesonic resonances deserved particular attention. One of our experimental colleagues from Belle reported the results on the hypothetical excited states of charmonium, dimesons and tetraquarks. We heard also the prediction that some highly excited states of D and B mesons might be tetraquarks, as well as proposals for its experimental verification. There is also some interesting progress in speculations about “hadronic molecules” DN and BN.

New double polarizaton measurements in Jefferson Lab have clarified several features of the spin structure of ^3He and of resonance parameters in electroproduction of pions on nucleons.

The description of baryon spectra, their electroweak structure and decay widths has been successfully extended to hyperons and charmed baryons. There has been noticeable progress in the classification of high-lying baryonic multiplets ($N = 3$) using the expansion in $1/N_c$ and the $O(3) \times SU(4)$ symmetry; in the description of pionic and photonic reactions by using coupled channels; in the scattering of a superheavy hadron which might be a candidate for dark matter.

As a surprise came the recently discovered magnetar which is too heavy to be supported by quark gas or plasma in its core. This suggests that the three-quark cluster should be stable also at five times the nuclear density, extending the nuclear equation of state into this region.

As you can see, there is no shortage of problems and surprises, but also the strategy of a sequence of small steps can be fruitful! Therefore we hope that our traditional “Bled Workshops” will be continued.

Ljubljana, November 2012

*M. Rosina
B. Golli
S. Širca*

Predgovor

Aktivnosti in dosežke našega letošnjega blejskega druženja zlahka povzamemo. Ujeli smo se v resonanco! Pa tudi zanimivega "ozadja" ni manjkalo.

Seznanili smo se z razvojem analitskih metod za iskanje resonanc in študijem vpliva bližnjih pragov in interferenc na določitev resonančnih parametrov. Ponekod je izrazito pomembna povezava med kvarkovskimi in mezonskimi prostostnimi stopnjami, na primer pri resonanci $\Delta(1700)$. Resonančne parametre, zlasti pole v kompleksni energijski ravnini, včasih boljše določimo z izračunom časovnega zamika kot z obliko resonančne krivulje. Prijetno nas je vzpodbudilo, da lahko dandanes s kromodinamiko na mreži že računamo fazne premike za sipanje piona na mezonih, celo v območju resonanc.

Posebno pozornost smo namenili novim mezonskim resonancam. Naš eksperimentalni sodelavec v laboratoriju Belle je poročal o rezultatih, ki zadevajo domnevna vzbujena stanja čarmonija, dimezonov in tetrakvarkov. Slišali pa smo tudi napoved, da so nekatera visoka stanja mezonov D in B tetrakvarki ter predloge za eksperimente, s katerimi bi lahko te trditve preverili. Zanimiv je tudi napredek pri spekulacijah o "hadronskih molekulah" DN in BN.

Nove meritve z dvojno polarizacijo v laboratoriju Jefferson Lab so razjasnile nekatere značilnosti spinske strukture jeder ${}^3\text{He}$ ter resonančnih parametrov pri elektroprodukciji pionov na nukleonih.

Opis spektrov barionov, njihove elektro-šibke strukture in razpadnih širin se je uspešno razširil na hiperone in čarobne barione. Napredek je opazen tudi pri razvrščanju visokih barionskih multipletov ($N = 3$) z razvojem po recipročnem številu barv in s simetrijo $O(3) \times SU(4)$; pri obravnavanju pionskih in fotonskih reakcij s sklopljenimi kanali; pri sipanju supertežkega hadrona, ki je morda tudi kandidat za temno snov.

Presenečenje predstavlja nedavno odkriti magnetar, ki je pretežak, da bi njegovo jedro pojasnili s kvarkovskim plinom oziroma plazmo. Zdi se, da so trikvarkovske gručice obstojne tudi pri petkratni jedrski gostoti in tudi velja kar jedrska enačba stanja.

Problemov in presenečenj torej ne zmanjka, in tudi zaporedje majhnih korakov očitno tvori plodno pot! Upamo torej, da se bodo naše tradicionalne "Blejske delavnice" še nadaljevale.

Ljubljana, novembra 2012

*M. Rosina
B. Golli
S. Širca*

Workshops organized at Bled

- ▷ *What Comes beyond the Standard Model* (June 29–July 9, 1998), Vol. 0 (1999) No. 1
- ▷ *Hadrons as Solitons* (July 6–17, 1999)
- ▷ *What Comes beyond the Standard Model* (July 22–31, 1999)
- ▷ *Few-Quark Problems* (July 8–15, 2000), Vol. 1 (2000) No. 1
- ▷ *What Comes beyond the Standard Model* (July 17–31, 2000)
- ▷ *Statistical Mechanics of Complex Systems* (August 27–September 2, 2000)
- ▷ *Selected Few-Body Problems in Hadronic and Atomic Physics* (July 7–14, 2001), Vol. 2 (2001) No. 1
- ▷ *What Comes beyond the Standard Model* (July 17–27, 2001), Vol. 2 (2001) No. 2
- ▷ *Studies of Elementary Steps of Radical Reactions in Atmospheric Chemistry*
- ▷ *Quarks and Hadrons* (July 6–13, 2002), Vol. 3 (2002) No. 3
- ▷ *What Comes beyond the Standard Model* (July 15–25, 2002), Vol. 3 (2002) No. 4
- ▷ *Effective Quark-Quark Interaction* (July 7–14, 2003), Vol. 4 (2003) No. 1
- ▷ *What Comes beyond the Standard Model* (July 17–27, 2003), Vol. 4 (2003) Nos. 2-3
- ▷ *Quark Dynamics* (July 12–19, 2004), Vol. 5 (2004) No. 1
- ▷ *What Comes beyond the Standard Model* (July 19–29, 2004), Vol. 5 (2004) No. 2
- ▷ *Exciting Hadrons* (July 11–18, 2005), Vol. 6 (2005) No. 1
- ▷ *What Comes beyond the Standard Model* (July 18–28, 2005), Vol. 6 (2005) No. 2
- ▷ *Progress in Quark Models* (July 10–17, 2006), Vol. 7 (2006) No. 1
- ▷ *What Comes beyond the Standard Model* (September 16–29, 2006), Vol. 7 (2006) No. 2
- ▷ *Hadron Structure and Lattice QCD* (July 9–16, 2007), Vol. 8 (2007) No. 1
- ▷ *What Comes beyond the Standard Model* (July 18–28, 2007), Vol. 8 (2007) No. 2
- ▷ *Few-Quark States and the Continuum* (September 15–22, 2008), Vol. 9 (2008) No. 1
- ▷ *What Comes beyond the Standard Model* (July 15–25, 2008), Vol. 9 (2008) No. 2
- ▷ *Problems in Multi-Quark States* (June 29–July 6, 2009), Vol. 10 (2009) No. 1
- ▷ *What Comes beyond the Standard Model* (July 14–24, 2009), Vol. 10 (2009) No. 2
- ▷ *Dressing Hadrons* (July 4–11, 2010), Vol. 11 (2010) No. 1
- ▷ *What Comes beyond the Standard Model* (July 12–22, 2010), Vol. 11 (2010) No. 2
- ▷ *Understanding hadronic spectra* (July 3–10, 2011), Vol. 12 (2011) No. 1
- ▷ *What Comes beyond the Standard Model* (July 11–21, 2011), Vol. 12 (2011) No. 2
- ▷ *Understanding hadronic spectra* (July 1–8, 2012), Vol. 13 (2012) No. 1
- ▷ *What Comes beyond the Standard Model* (July 9–19, 2012), Vol. 13 (2012) No. 2

Also published in this series

- ▷ *Book of Abstracts, XVIII European Conference on Few-Body Problems in Physics*, Bled, Slovenia, September 8–14, 2002, Edited by Rajmund Krivec, Bojan Golli, Mitja Rosina, and Simon Širca, Vol. 3 (2002) No. 1–2





The Road to Extraction of S-Matrix Poles from Experimental Data ^{*}

Saša Ceci, Milorad Korolija, and Branimir Zauner

Rudjer Bosković Institute, Bijenička 54, HR-10000 Zagreb, Croatia

Abstract. By separating data points close to a resonance into intervals, and fitting all possible intervals to a simple pole with constant coherently added background, we obtained a substantial number of convergent fits. After a chosen set of statistical constraints was imposed, we calculated the average of a resonance pole position from the statistically acceptable results. We used this method to find pole positions of Z boson.

Breit-Wigner (BW) parameters are often used for the description of unstable particles (see *e.g.*, *Review of Particle Physics* [1]), although shortcomings of such choice have been pointed out on numerous occasions. For example, Sirlin showed that the BW parameters of the Z boson were gauge dependent [2]. To resolve this issue he redefined BW parameters, but also suggested usage of the S-matrix poles as an alternative, since poles are fundamental properties of the S-matrix and therefore gauge independent by definition. In a somewhat different study, Höhler advocated using S-matrix poles for characterization of nucleon resonances [3] in order to reduce confusion that arises when different definitions of BW parameters are used [4]. However, loosely defined [5] BW parameters of mesons and baryons are still being extracted from experimental analyses, compared among themselves [1], and used as input to QCD-inspired quark models [6] and as experiment-to-theory matching points for lattice QCD [7].

Our group has been very interested in reducing human and model dependence from resonance parameters' extraction procedures (from scattering matrices). We developed the regularization method for pole extraction from S-matrix elements [8]. Its main disadvantage is that it needs very dense data, one that is attainable only after an energy dependent partial-wave analysis. The other method was the K-matrix pole extraction method [9] which needed the whole unitary S-matrix to begin with, making it impossible to use on any single reaction. Both of those methods were purely mathematical, and the only assumption were that there is a pole in the complex energy plane of an S-matrix. We had no physical input into our procedures. Therefore, we proclaimed these procedures model-independent. The only thing missing, was a method which could be applied directly to the experimental data, *e.g.*, total cross sections.

In this proceeding, we illustrate a method for model-independent extraction of S-matrix pole positions directly from the data.

^{*} Talk delivered by S. Ceci

The first step in devising a method for extraction of the pole parameters from the experimental data is to set up an appropriate parameterization. The parameterization presented here is based on the assumption that close to a resonance, the T matrix will be well described with a simple pole and a constant background. The similar assumption was used in Höhler's speed plot technique [3]. The speed plot is a method used for the pole parameter extraction from the known scattering amplitudes. It is based on calculating the first order energy derivative of the scattering amplitude, with the key assumption that the first derivative of the background is negligible.

The T matrix with a single pole and constant background term is given by

$$T(W) = r_p \frac{\Gamma_p/2}{M_p - W - i\Gamma_p/2} + b_p, \quad (1)$$

where W is center-of-mass energy, r_b and b_b are complex, while M_p and Γ_p are real numbers. Total cross section is then proportional to $|T|^2/q^2$, where q is the initial center-of-mass momentum. Equation (1), as well as other similar forms (see e.g. [1]), are standardly called Breit-Wigner parameterizations, which can be somewhat misleading since M_p and Γ_p are generally not Breit-Wigner, but pole parameters (hence the index p). The square of the T matrix defined in Eq. (1) is given by

$$|T(W)|^2 = T_\infty^2 \frac{(W - M_z)^2 + \Gamma_z^2/4}{(W - M_p)^2 + \Gamma_p^2/4}, \quad (2)$$

where, for convenience, we simplified the numerator by combining the old parameters into three new real-valued ones: T_∞ , M_z , and Γ_z . Pole parameters M_p and Γ_p are retained in the denominator.

With such a simple parameterization, it is crucial to use only data points close to the resonance peak. To avoid picking and choosing the appropriate data points by ourselves, we analyzed the data from a wider range around the resonance peak, and fitted locally the parameterization (2) to each set of seven successive data points (seven data points is minimum for our five-parameter fit). Then we increased the number of data points in the sets to eight and fitted again. We continued increasing the number of data points in sets until we fitted the whole chosen range. Such procedure allowed different background term for each fit, which is much closer to reality than assuming a single constant background term for the whole chosen data set (see e.g. discussion on the problems with speed plot in Ref. [8]). In the end, we imposed a series of statistical constraints to all fits to distinguish the good ones. The whole analysis was done in Wolfram Mathematica 8 using NonlinearModelFit routine [11].

Having defined the fitting strategy, we tested the method by applying it to the case of the Z boson. The data set we used is from the PDG compilation [1], and shown in Fig. 1. Extracted pole masses are shown in the same figure: filled histogram bins show pole masses from the good fits, while the empty histogram bins are stacked to the solid ones to show masses obtained in the discarded fits. Height of the pole-mass histogram in Fig. 1 is scaled for convenience.

Extracted S-matrix pole mass and width of Z boson are given in Table 1. The pole masses are in excellent agreement, while the pole widths are reasonably close.

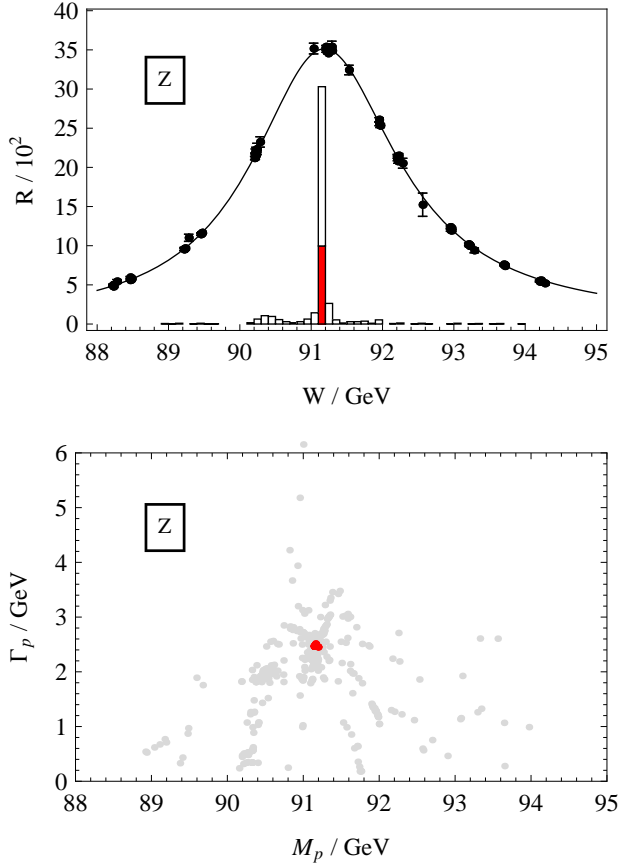


Fig. 1. [Upper figure] PDG compilation of Z data [1] and histogram of obtained pole masses. Line is the fit result with the lowest reduced χ^2 (just for illustration). Dark (red online) colored histogram bins are filled with statistically preferred results. [Lower figure] Pole masses vs. pole widths. Dark (red online) circles show statistically preferred results we use for averages.

It is important to stress that the difference between the pole and BW mass of the Z boson is fundamental and statistically significant. Distribution of discarded and good results is shown in the lower part of Fig. 1.

Table 1. Pole parameters of Z obtained in this work. PDG values of pole and BW parameters are given for comparison.

	Pole	Pole PDG [1]	BW PDG [1]
M/MeV	91159 ± 8	91162 ± 2	91188 ± 2
Γ/MeV	2484 ± 10	2494 ± 2	2495 ± 2

In conclusion, we have illustrated here a model-independent method for extraction of resonance pole parameters from total cross sections and partial waves. Very good estimates for Z boson pole position were obtained.

We are today witnessing the dawn of ab-initio calculations in low-energy QCD. In order to compare theoretical predictions with experimentally determined resonance states, we need first to establish proper point of comparison. We hope that our method, once it becomes fully operational, will help connecting experiment and theory.

References

1. J. Beringer *et al.*, (Particle Data Group), Phys. Rev. D**86**, 010001 (2012)
2. A. Sirlin, Phys. Rev. Lett. **67**, 2127 (1991).
3. G. Höhler, π N Newsletter **9**, 1 (1993).
4. R. E. Cutkosky *et al.*, Phys. Rev. D**20**, 2839 (1979); D. M. Manley and E. M. Saleski, Phys. Rev. D**45**, 4002 (1992).
5. G. Höhler, "A pole-emic" in *Review of particle properties*, D. E. Groom *et al.* Eur. Phys. J. C**15**, 1 (2000).
6. S. Capstick and W. Roberts Prog. Part. Nucl. Phys. **45**, S241-S331 (2000); T. Melde, W. Plessas, and B. Sengl, Phys. Rev. D**77**, 114002 (2008).
7. S. Dürr, *et al.*, Science **322**, 1224 (2008).
8. S. Ceci *et al.*, J. Stahov, A. Švarc, S. Watson, and B. Zauner, Phys. Rev. D**77**, 116007 (2008).
9. S. Ceci, A. Švarc, B. Zauner, D. M. Manley, and S. Capstick, Phys. Lett. **B659**, 228 (2008).
10. http://gwuac.phys.gwu.edu/analysis/pin_analysis.html Current PWA solution (June, 2010).
11. <http://reference.wolfram.com/mathematica/ref/NonlinearModelFit.html>



Unified Model for Light- and Heavy-Flavor Baryon Resonances *

Joseph P. Day^a, W. Plessas^a, and Ki-Seok Choi^b

^a Theoretical Physics, Institute of Physics, University of Graz, Universitätsplatz 5, A-8010 Graz, Austria

^b Department of Physics, Soongsil University, Seoul 156-743, Republic of Korea

Abstract. We report on the construction of a relativistic constituent-quark model capable of describing the spectroscopy of baryons with all flavors u , d , s , c , and b . Some selective spectra are presented, where comparisons to experimental data are yet possible.

1 Introduction

Over the decades the constituent-quark model (CQM) has ripened into a stage where its formulation and solution are well based on a relativistic (i.e. Poincaré-invariant) quantum theory (for a thorough review of relativistic Hamiltonian dynamics see ref. [1]). In such an approach one relies on an invariant mass operator \hat{M} , where the interactions are introduced according the so-called Bakamjian-Thomas construction [2]. If the conditions of the Poincaré algebra are fulfilled by \hat{M} , this leads to relativistically invariant mass spectra.

Relativistic constituent-quark models (RCQM) have been developed by several groups, however, with limited domains of validity. Of course, it is desirable to have a framework as universal as possible for the description of all kinds of hadron processes in the low- and intermediate-energy regions. This is especially true in view of the advent of ever more data on heavy-baryon spectroscopy from present and future experimental facilities.

We have developed a RCQM that comprises all known baryons with flavors u , d , s , c , and b within a single framework [3]. There have been only a few efforts so far to extend a CQM from light- to heavy-flavor baryons. We may mention, for example, the approach by the Bonn group who have developed a RCQM, based on the 't Hooft instanton interaction, along a microscopic theory solving the Salpeter equation [4] and extended their model to charmed baryons [5], still not yet covering bottom baryons. A further quark-model attempt has been undertaken by the Mons-Liège group relying on the large- N_c expansion [6,7], partially extended to heavy-flavor baryons [8]. Similarly, efforts are invested to expand other approaches to heavy baryons, such as the employment of Dyson-Schwinger equations together with either quark-diquark or three-quark calculations [9,10].

* Talk delivered by J. P. Day

Also an increased amount of more refined lattice-QCD results has by now become available on heavy-baryon spectra (see, e.g., the recent work by Liu et al. [11] and references cited therein).

2 The Model

Our RCQM is based on the invariant mass operator

$$\hat{M} = \hat{M}_{\text{free}} + \hat{M}_{\text{int}}, \quad (1)$$

where the free part corresponds to the total kinetic energy of the three-quark system and the interaction part contains the dynamics of the constituent quarks Q . In the rest frame of the baryon, where its three-momentum $\mathbf{P} = \sum_i^3 \mathbf{k}_i^2 = 0$, we may express the terms as

$$\hat{M}_{\text{free}} = \sum_{i=1}^3 \sqrt{\hat{m}_i^2 + \hat{\mathbf{k}}_i^2}, \quad (2)$$

$$\hat{M}_{\text{int}} = \sum_{i<j}^3 \hat{V}_{ij} = \sum_{i<j}^3 (\hat{V}_{ij}^{\text{conf}} + \hat{V}_{ij}^{\text{hf}}). \quad (3)$$

Here, the $\hat{\mathbf{k}}_i$ correspond to the three-momentum operators of the individual quarks with rest masses m_i and the Q-Q potentials \hat{V}_{ij} are composed of confinement and hyperfine interactions. By employing such a mass operator $\hat{M}^2 = \hat{\mathbf{P}}^\mu \hat{\mathbf{P}}_\mu$, with baryon four-momentum $\hat{\mathbf{P}}_\mu = (\hat{H}, \hat{\mathbf{P}}_1, \hat{\mathbf{P}}_2, \hat{\mathbf{P}}_3)$, the Poincaré algebra involving all ten generators $\{\hat{H}, \hat{\mathbf{P}}_i, \hat{\mathbf{J}}_i, \hat{\mathbf{K}}_i\}$, ($i = 1, 2, 3$), or equivalently $\{\hat{\mathbf{P}}_\mu, \hat{\mathbf{J}}_{\mu\nu}\}$, ($\mu, \nu = 0, 1, 2, 3$), of time and space translations, spatial rotations as well as Lorentz boosts, can be guaranteed. The solution of the eigenvalue problem of the mass operator \hat{M} yields the relativistically invariant mass spectra as well as the baryon eigenstates (the latter, of course, initially in the standard rest frame).

We adopt the confinement depending linearly on the Q-Q distance r_{ij}

$$V_{ij}^{\text{conf}}(\mathbf{r}_{ij}) = V_0 + Cr_{ij} \quad (4)$$

with the strength $C = 2.33 \text{ fm}^{-2}$, corresponding to the string tension of QCD. The parameter $V_0 = -402 \text{ MeV}$ is only necessary to set the ground state of the whole baryon spectrum, i.e., the proton mass; it is irrelevant for level spacings.

The hyperfine interaction is most essential to describe all of the baryon excitation spectra. In a unified model the hyperfine potential must be explicitly flavor-dependent. Otherwise, e.g., the N and Λ spectra with their distinct level orderings could not be reproduced simultaneously. Therefore we have advocated for the hyperfine interaction of our universal RCQM the $SU(5)_F$ GBE potential

$$V_{\text{hf}}(\mathbf{r}_{ij}) = \left[V_{24}(\mathbf{r}_{ij}) \sum_{\alpha=1}^{24} \lambda_i^\alpha \lambda_j^\alpha + V_0(\mathbf{r}_{ij}) \lambda_i^0 \lambda_j^0 \right] \boldsymbol{\sigma}_i \cdot \boldsymbol{\sigma}_j. \quad (5)$$

Here, we take into account only its spin-spin component, which produces the most important hyperfine forces for the baryon spectra; the other possible force components together play only a minor role for the excitation energies [16]. While σ_i represent the Pauli spin matrices of $SU(2)_S$, the λ_i^α are the generalized Gell-Mann flavor matrices of $SU(5)_F$ for quark i . In addition to the exchange of the pseudoscalar 24-plet also the flavor-singlet is included because of the $U(1)$ anomaly. The radial form of the GBE potential resembles the one of the pseudoscalar meson exchange

$$V_\beta(\mathbf{r}_{ij}) = \frac{g_\beta^2}{4\pi} \frac{1}{12m_i m_j} \left[\mu_\beta^2 \frac{e^{-\mu_\beta r_{ij}}}{r_{ij}} - 4\pi\delta(\mathbf{r}_{ij}) \right] \quad (6)$$

for $\beta = 24$ and $\beta = 0$. Herein the δ -function must be smeared out leading to [13, 14]

$$V_\beta(\mathbf{r}_{ij}) = \frac{g_\beta^2}{4\pi} \frac{1}{12m_i m_j} \left[\mu_\beta^2 \frac{e^{-\mu_\beta r_{ij}}}{r_{ij}} - \Lambda_\beta^2 \frac{e^{-\Lambda_\beta r_{ij}}}{r_{ij}} \right]. \quad (7)$$

Contrary to the earlier GBE RCQM [13], which uses several different exchange masses μ_γ and different cut-offs Λ_γ , corresponding to $\gamma = \pi, K$, and $\eta=\eta_8$ mesons, we here managed to get along with a universal GBE mass μ_{24} and a single cut-off Λ_{24} for the 24-plet of $SU(5)_F$. Only the singlet exchange comes with another mass μ_0 and another cut-off Λ_0 with a separate coupling constant g_0 . Consequently the number of open parameters in the hyperfine interaction could be kept as low as only three (see Tab. 1).

Table 1. Free parameters of the present GBE RCQM determined by a best fit to the baryon spectra.

Free Parameters		
$(g_0/g_{24})^2$	$\Lambda_{24} [\text{fm}^{-1}]$	$\Lambda_0 [\text{fm}^{-1}]$
1.5	3.55	7.52

Table 2. Fixed parameters of the present GBE RCQM predetermined from phenomenology and not varied in the fitting procedure.

Fixed Parameters						
Quark masses [MeV]				Exchange masses [MeV]		Coupling
$m_u = m_d$	m_s	m_c	m_b	μ_{24}	μ_0	$g_{24}^2/4\pi$
340	480	1675	5055	139	958	0.7

All other parameters entering the model have judiciously been predetermined by existing phenomenological insights. In this way the constituent quark

masses have been set to the values as given in Tab. 2. The 24-plet Goldstone-boson (GB) mass has been assumed as the value of the π mass and similarly the singlet mass as the one of the η' . The universal coupling constant of the 24-plet has been chosen according to the value derived from the π -N coupling constant via the Goldberger-Treiman relation.

3 Results for Baryon Spectra

We have calculated the baryon spectra of the relativistically invariant mass operator \hat{M} to a high accuracy both by the stochastic variational method [17] as well as the modified Faddeev integral equations [18, 19]. The present universal GBE RCQM produces the spectra in the light and strange sectors with similar or even better quality than the previous GBE RCQM [13]. In Figs. 1 and 2 we show the ground states and the first two excitations of $SU(3)_F$ singlet, octet, and decuplet baryons up to $J = \frac{7}{2}$, for which experimental data of at least three stars are quoted by the PDG [15] and J^P is known. Evidently a good overall description is achieved. Most importantly, the right level orderings specifically in the N, Δ , and Λ spectra as well as all other $SU(3)_F$ ground and excited states are reproduced in accordance with phenomenology. The reasons are exactly the same as for the previous GBE RCQM, what has already been extensively discussed in the literature [12–14]. Unfortunately, the case of the $\Lambda(1405)$ excitation could still not be resolved. It remains as an intriguing problem that can possibly not be solved by RCQMs relying on $\{QQQ\}$ configurations only; an explicit coupling to the K-N decay channel whose threshold lies nearby might be needed.

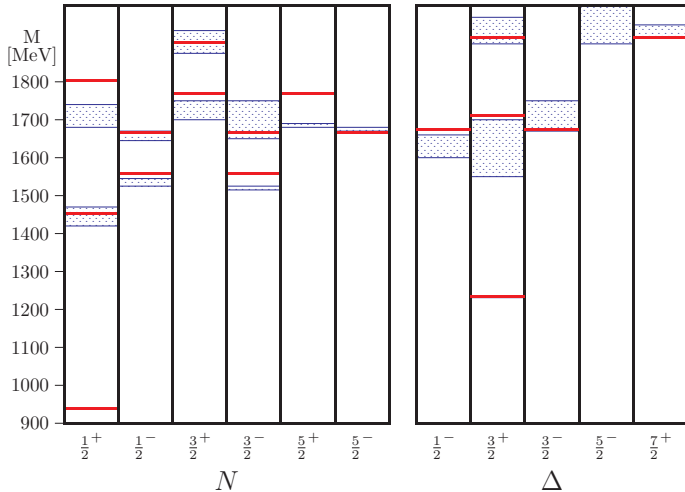


Fig. 1. Nucleon and Δ excitation spectra (solid/red levels) as produced by the universal GBE RCQM in comparison to phenomenological data [15] (the gray/blue lines and shaded/blue boxes show the masses and their uncertainties).

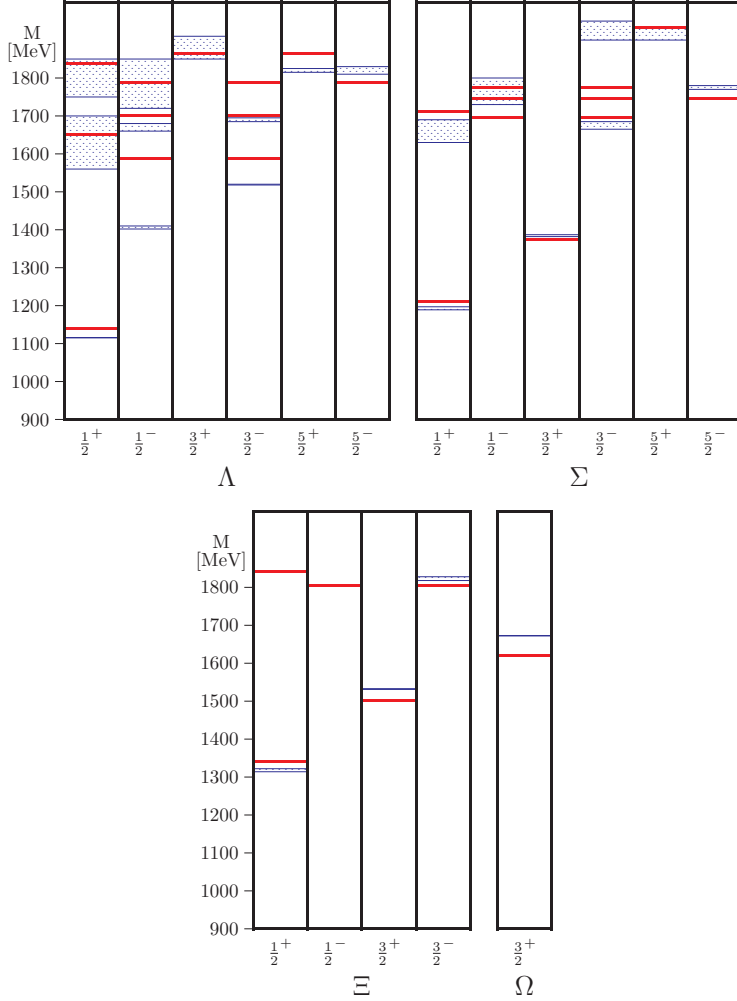


Fig. 2. Same as Fig. 1 but for the strange baryons.

What is most interesting in the context of the present work are the very properties of the light-heavy and heavy-heavy Q-Q hyperfine interactions. Can the GBE dynamics reasonably account for them? In Figs. 3 and 4 we show the spectra of all charm and bottom baryons that experimental data with at least three- or four-star status by the PDG exist for [15]. As is clearly seen, our universal GBE RCQM can reproduce all levels with respectable accuracy. In the Λ_c and Σ_c spectra some experimental levels are not known with regard to their spin and parity J^P . They are shown in the right-most columns of Fig. 3. Obviously they could easily be accommodated in accordance with the theoretical spectra, once their J^P 's are determined. Furthermore the model predicts some additional excited states for charm and bottom baryons that are presently missing in the phenomenological data base.

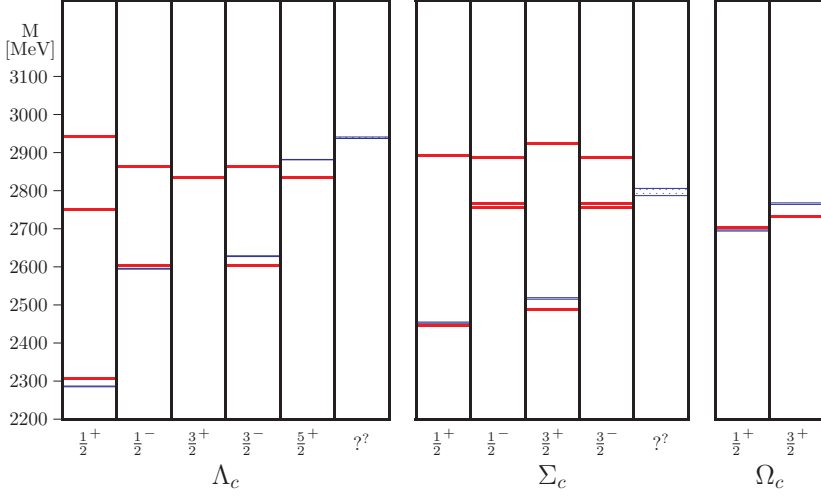


Fig. 3. Same as Fig. 1 but for charm baryons.

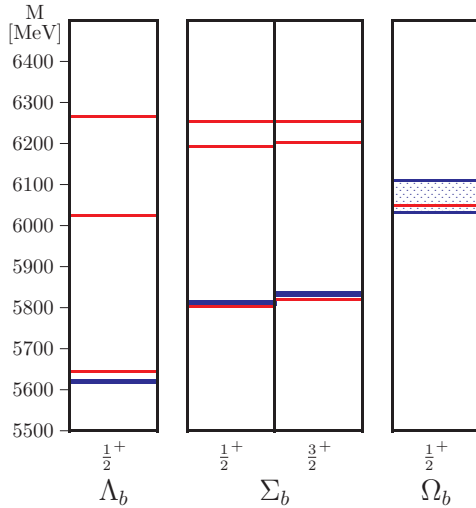


Fig. 4. Same as Fig. 1 but for bottom baryons.

Of course, the presently available data base on charm and bottom baryon states is not yet very rich and thus not particularly selective for tests of effective Q-Q hyperfine forces. The situation will certainly improve with the advent of further data from ongoing and planned experiments. Beyond the comparison to experimental data, we note that the theoretical spectra produced by our present GBE RCQM are also in good agreement with existing lattice-QCD results for heavy-flavor baryons. This is especially true for the charm baryons vis-à-vis the recent work by Liu et al. [11].

4 Discussion and Conclusion

We emphasize that the most important ingredients into the present RCQM are relativity, specifically Poincaré invariance, and a hyperfine interaction that is derived from an interaction Lagrangian built from effective fermion (constituent quark) and boson (Goldstone boson) fields connected by a pseudoscalar coupling [12]. It appears that such kind of dynamics is quite appropriate for constituent quarks of any flavor.

As a result we have demonstrated by the proposed GBE RCQM that a universal description of all known baryons is possible in a single model. Here, we have considered only the baryon masses (eigenvalues of the invariant mass operator \hat{M}). Beyond spectroscopy the present model will be subject to further tests with regard to the baryon eigenstates, which are simultaneously obtained from the solution of the eigenvalue problem of \hat{M} . They must prove reasonable in order to make the model a useful tool for the treatment of all kinds of baryons reactions within a universal framework.

5 Acknowledgement

This work was supported by the Austrian Science Fund, FWF, through the Doctoral Program on *Hadrons in Vacuum, Nuclei, and Stars* (FWF DK W1203-N16).

References

1. B. D. Keister and W. N. Polyzou, *Adv. Nucl. Phys.* **20**, 225 (1991)
2. B. Bakamjian and L. H. Thomas, *Phys. Rev.* **92**, 1300 (1953)
3. J. P. Day, W. Plessas, and K. -S. Choi, arXiv:1205.6918 [hep-ph].
4. U. Löring, B.C. Metsch, and H.-R. Petry, *Eur. Phys. J. A* **10**, 395 (2001); *ibid.* 447 (2001)
5. S. Migura, D. Merten, B. Metsch, and H.-R. Petry, *Eur. Phys. J. A* **28**, 41 (2006)
6. C. Semay, F. Buisseret, N. Matagne, and F. Stancu, *Phys. Rev. D* **75**, 096001 (2007)
7. C. Semay, F. Buisseret, and F. Stancu, *Phys. Rev. D* **76**, 116005 (2007)
8. C. Semay, F. Buisseret, and F. Stancu, *Phys. Rev. D* **78**, 076003 (2008)
9. H. Sanchis-Alepuz, R. Alkofer, G. Eichmann, and R. Williams, *PoS QCD-TNT-II*, 041 (2011) [arXiv:1112.3214]
10. H. Sanchis-Alepuz, PhD Thesis, University of Graz (2012)
11. L. Liu, H.-W. Lin, K. Orginos, and A. Walker-Loud, *Phys. Rev. D* **81**, 094505 (2010)
12. L.Ya. Glozman and D.O. Riska, *Phys. Rept.* **268**, 263 (1996)
13. L.Ya. Glozman, W. Plessas, K. Varga, and R.F. Wagenbrunn, *Phys. Rev. D* **58**, 094030 (1998)
14. L.Ya. Glozman, Z. Papp, W. Plessas, K. Varga, and R.F. Wagenbrunn, *Phys. Rev. C* **57**, 3406 (1998)
15. J. Beringer *et al.* [Particle Data Group Collaboration], *Phys. Rev. D* **86**, 010001 (2012)
16. K. Glantschnig, R. Kainhofer, W. Plessas, B. Sengl and R. F. Wagenbrunn, *Eur. Phys. J. A* **23**, 507 (2005)
17. Y. Suzuki and K. Varga, *Stochastic Variational Approach to Quantum-Mechanical Few-Body Problems*, Lecture Notes in Physics **54**, 1 (1998)
18. Z. Papp, A. Krassnigg, and W. Plessas, *Phys. Rev. C* **62**, 044004 (2000)
19. J. McEwen, J. Day, A. Gonzalez, Z. Papp, and W. Plessas, *Few-Body Syst.* **47**, 225 (2010)
20. R. M. Woloshyn, *Phys. Lett. B* **476**, 309 (2000)



A chiral theory of scalar heavy-light (D, D_s) and (B, B_s) mesons

V. Dmitrašinović

Institute of Physics, Belgrade University, Pregrevica 118, Zemun, P.O.Box 57, 11080
Beograd, Serbia

Abstract. The talk with the above title delivered at the Bled 2012 workshop was based on the paper “Chiral symmetry of heavy-light scalar mesons with $U_A(1)$ symmetry breaking” that has been published in the meantime as *Phys. Rev. D* **86**, 016006 (2012). For all details we refer the interested reader to that publication.



Low-lying states of the Y-string in two dimensions ^{*}

V. Dmitrašinović, I. Salom

Institute of Physics, Belgrade University, P.O.Box 57, Pregrevica 118, 11080 Zemun, Serbia

Abstract. We use $SU(2) \times SU(2)$ algebraic methods to calculate the energy-splitting pattern of the $K=2,3$ excited states of the Y-string in two dimensions. To this purpose we use the dynamical $O(2)$ symmetry of the Y-string in the shape space of triangles and compare our results with known results in three dimensions and find qualitative agreement.

1 Introduction

The three-quark confinement problem has been attacked in many ways: 1) by way of the harmonic oscillator models with some non-harmonic two-body potential components [1–3]; 2) by way of Y-string three-body potentials, Refs. [4–15]; 3) by way of the hyperspherical formalism applied to two-quark potentials, Refs. [16, 17] and 4) by way of dynamical symmetry Lie-algebraic methods, Refs. [18–23], with some success for the low-lying bands of states (up to $K \leq 3$). The higher-lying bands ($K \leq 4$) have generally not been studied systematically (to our knowledge), only individual states with highest values of the orbital angular momentum, for purposes of Regge analyses, with one significant exception ($K = 4$), the Ref. [11].

QCD seems to demand a genuine three-body confining potential: the so-called Y-junction string three-quark potential, defined by

$$V_Y = \sigma \min_{\mathbf{x}_0} \sum_{i=1}^3 |\mathbf{x}_i - \mathbf{x}_0|, \quad (1)$$

or, explicitly

$$V_{\text{string}} = V_Y = \sigma \sqrt{\frac{3}{2}(\rho^2 + \lambda^2 + 2|\boldsymbol{\rho} \times \boldsymbol{\lambda}|)}. \quad (2)$$

The $|\boldsymbol{\rho} \times \boldsymbol{\lambda}|$ term is proportional to the area of the triangle subtended by the three quarks. The Y-string potential was proposed as early as 1975, see Refs. [4, 5] and the first schematic calculation (using perturbation theory) of the baryon spectrum up to $K \leq 2$ followed soon thereafter, Ref. [6]. Refs. [7–9], elaborated on this. The first non-perturbative calculations (variational approximation) of the $K=3$ band with the Y-string potential were published in the early 1990's, Ref. [10] and extended to the $K=4$ band later in that decade, Ref. [11]. Yet, some of the most basic

^{*} Talk delivered by V. Dmitrašinović

properties of this potential, such as the ordering of the low-lying states in the spectrum, without the “QCD hyperfine interaction” and/or relativistic kinematics remain unknown.

The first systematic attempt to solve the Y-string spectrum, albeit only up to the $K=2$ band, can be found in Ref. [12]. That paper used the hyperspherical harmonics formalism, which led to the discovery of a new dynamical $O(2)$ symmetry in the Y-string potential, with the permutation group $S_3 \subset O(2)$ as the subgroup of the dynamical $O(2)$ symmetry, see Ref. [13]. That symmetry was further elaborated in Ref. [15]. The present work is a continuation of that line, which has also been represented in this series of workshops [14]. The three-body sum of two-body potentials has only the permutation group S_3 as its symmetry.

2 $O(4)$ algebraic method

The existence of an additional dynamical symmetry strongly suggests an algebraic approach, such as those used in Refs. [18–23]. A careful perusal of Ref. [18,19] shows, however, that an $O(2)$ group had been used as an enveloping structure for the (discrete) permutation group $S_3 \subset O(2)$, but was not interpreted as a (possible) dynamical symmetry. Refs. [20–23] did not use this symmetry, however. We start an algebraic study of Y-string-like potentials with this in mind. For the sake of technical simplicity we confine ourselves to the two-dimensional case here. We say here “Y-string-like potentials”, rather than the Y-string potential, because the complete Y-string potential contains “additional” two-body terms that are valid only in certain parts of the tree-particle configuration space (a.k.a. triangle “shape space”) and that do not have the $O(2)$ dynamical symmetry. This wider class of three-body potentials has the same dynamical $O(2)$ symmetry in shape space as the Y-string potential, thus making them equivalent in the algebraic sense. We must therefore first establish the basic properties of the dynamical symmetry of the Y-string potential.

In two dimensions (2D) the non-relativistic three-body kinetic energy is a quadratic form of the two Jacobi two-vector velocities, $\dot{\mathbf{p}}, \dot{\boldsymbol{\lambda}}$, so its “hyper-spherical symmetry” is $O(4)$, and the residual dynamical symmetry of the Y-string potential is $O(2) \otimes O_L(2) \subset O(4)$, where $O_L(2)$ is the (orbital) angular momentum. As the $O(4)$ Lie group can be “factored” in two mutually commuting $O(3)$ Lie groups: $O(4) \simeq O(3) \otimes O(3)$, one may use for our purposes many of the $O(3)$ group results, such as the Clebsch-Gordan coefficients. The 3D case is substantially more complicated than the 2D one: the three-body “hyper-spherical symmetry” is $O(6)$, and the residual dynamical symmetry of the Y-string potential is $O(2) \otimes O_L(3) \subset O(6)$. The $O(6)$ Lie group cannot be “factored” in two mutually commuting $O(3)$ Lie groups and one cannot simply reduce this problem to one in the $O(3)$ group. For these reasons we limit ourselves to the two-dimensional case in this paper.

Thus we are looking for the “chain” of symmetries $O(2) \otimes O_L(2) \subset O(3) \otimes O_L(2) \subset O(4)$. Rather than parametrize the energy E as a function of corresponding Casimir operators, and thus calculate the spectrum, as was done in Refs. [20–23], we reformulate the problem in terms of $O(4)$ variables and then

bring the potential into a form that can be (exactly) solved, i.e. we expand it in $O(4)$ hyperspherical harmonics. As the potential must be spherically symmetrical, this imposes an additional constraint on the allowed hyperspherical harmonics and one ends up with only a few (leading) terms: 1) the area-term containing the $O(4)$ hyperspherical harmonic \mathcal{Y}_{00}^{22} , which, in turn is related to the $O(3)$ spherical harmonic $Y_{20}(\alpha, \phi)$ of the shape space (hyper)spherical angles (α, ϕ) , i.e., the V_4 term in the notation of Richard and Taxil [16]), that is present in both the two-body and the Y-string potentials; and 2) the $O(2)$ symmetry-breaking term containing $\mathcal{Y}_{0\pm 3}^{33} \simeq Y_{3\pm 3}(\alpha, \phi)$, i.e., the V_6 term in the notation of Richard and Taxil [16], that is important in the two-body potential, and less so in the “complete” Y-string potential and not at all in Eq. (2). The energy spectrum is a function of the $O(4)$ hyperspherical expansion coefficients for the potential, and of the $O(4)$ Clebsch-Gordan coefficients, that are products of the ordinary $O(3)$ Clebsch-Gordan coefficients.

3 Results

Next we proceed to evaluate the $K=2,3$ bands’ splittings and compare them with the 3D case:

1) At the $K=2$ level, there are four $SU(6)$ multiplets (other than the hyper-radial excitation $[56, 0^+]'$ of the $K=0$ state): $[70, 0^+]$, $[56, 2^+]$, $[70, 2^+]$, $[20, 1^+]$ in 3D. The main difference between the 2D and 3D is that the $[20, 0^+]$ state has vanishing orbital angular momentum in 2D, rather than unity, as in the 3D state $[20, 1^+]$.

The only difference between the 2D and 3D $K=2$ states’ splittings is that the $[70, 0^+]$ and $[56, 2^+]$ states are degenerate in 2D, whereas in 3D they are split by one half of the energy difference between $[70, 2^+]$ and $[70, 0^+]$. This shows that the 2D case does relate fairly closely to the 3D one.

2) The energy splittings in the $K=3$ band, for the Y-string potential in 3D has not been worked out analytically, as yet, to our knowledge. Therefore, we compare our 2D Y-string potential $K=3$ results with the 3D $K=3$ two-body potential results of Ref. [16] and find certain similarities, and a few distinctions. There are six $SU(6)$ multiplets in the $K=3$ sector (other than the hyper-radial excitation $[70, 1^-]''$ of the $K=1$ state): $[20, 1^-]$, $[56, 1^-]$, $[70, 3^-]$, $[56, 3^-]$, $[70, 2^-]$, $[20, 3^-]$ in 3D. The main difference between the 2D and 3D is that the $[70, 2^-]$ state disappears in 2D.

In 3D two-body potential the energy splittings have been divided in two parts in Ref. [16]: a) those due to the V_4 perturbation; and b) due to the V_6 perturbation. This corresponds to our Y_{20} and $Y_{3\pm 3}$ terms, respectively.

a) In the $V_4 \neq 0, V_6 \rightarrow 0$ limit, the states are roughly divided in two groups: the $[20, 1^-]$, $[56, 1^-]$, $[70, 3^-]$ which are pushed down, and the $[56, 3^-]$, $[70, 2^-]$, $[20, 3^-]$ which are pushed up by the V_4 perturbation. Two pairs of states are left degenerate: ($[20, 1^-]$, $[56, 1^-]$) in the lower set and ($[56, 3^-]$, $[20, 3^-]$) in the upper set. In this limit in 2D we find complete degeneracy of all three members of the lower- ($[20, 1^-]$, $[56, 1^-]$, $[70, 3^-]$) and upper levels ($[56, 3^-]$, $[70, 2^-]$, $[20, 3^-]$).

b) In the $V_4 \neq 0, V_6 \neq 0$ case, the remaining degeneracy of states is removed in 3D: the $[20, 1^-]$ and the $[56, 1^-]$ are split in the “lower set” and the $[56, 3^-]$ and

the $[20, 3^-]$ in the “upper set”. In 2D we find the same sort of splitting, and in almost the same ratio of strengths.

So, in the $K=2,3$ bands, one sees similarities of dynamical symmetry-breaking patterns in 2D and 3D. This lends credence to the belief that this similarity may persist at higher values of K , where there are no known 3D results, at present.

Acknowledgments

This work was supported by the Serbian Ministry of Science and Technological Development under grants number OI 171037 and III 41011.

References

1. D. Faiman and A. W. Hendry, *Phys. Rev.* **173**, 1720 (1968).
2. D. Gromes and I. O. Stamatescu, *Nucl. Phys. B* **112**, 213 (1976); *Z. Phys. C* **3**, 43 (1979).
3. N. Isgur and G. Karl, *Phys. Rev. D* **19**, 2653 (1979) [Erratum-ibid. *D* **23**, 817 (1981)].
4. X. Artru, *Nucl. Phys. B* **85**, 442 (1975).
5. H. G. Dosch and V. F. Muller, *Nucl. Phys. B* **116**, 470 (1976).
6. R. E. Cutkosky and R. E. Hendrick, *Phys. Rev. D* **16**, 786 (1977).
7. J. Carlson, J. B. Kogut and V. R. Pandharipande, *Phys. Rev. D* **27**, 233 (1983).
8. J. Carlson, J. B. Kogut and V. R. Pandharipande, *Phys. Rev. D* **28**, 2807 (1983).
9. S. Capstick and N. Isgur, *Phys. Rev. D* **34**, 2809 (1986).
10. F. Stancu and P. Stassart, *Phys. Lett. B* **269**, 243 (1991).
11. P. Stassart and F. Stancu, *Z. Phys. A* **359**, 321 (1997).
12. V. Dmitrašinović, T. Sato and M. Šuvakov, *Eur. Phys. J. C* **62**, 383 (2009) [arXiv:0906.2327 [hep-ph]].
13. V. Dmitrašinović, T. Sato and M. Šuvakov, *Phys. Rev. D* **80**, 054501 (2009) [arXiv:0908.2687 [hep-ph]].
14. V. Dmitrašinović and M. Šuvakov, p.27-28 (Bled Workshops in Physics. Vol. 11 No. 1)
15. Milovan Šuvakov and V. Dmitrašinović *Phys. Rev. E* **83**.056603, (2011)
16. J. -M. Richard and P. Taxil, *Nucl. Phys. B* **329**, 310 (1990).
17. J. -M. Richard, *Phys. Rep.* **212**, 1-76, (1992).
18. K. C. Bowler, P. J. Corvi, A. J. G. Hey, P. D. Jarvis and R. C. King, *Phys. Rev. D* **24**, 197 (1981).
19. K. C. Bowler and B. F. Tynemouth, *Phys. Rev. D* **27**, 662 (1983).
20. R. Bijker, F. Iachello and A. Leviatan, *Annals Phys.* **236**, 69 (1994) [nucl-th/9402012].
21. R. Bijker, F. Iachello and E. Santopinto, *J. Phys. A* **31**, 9041 (1998) [nucl-th/9801051].
22. R. Bijker, F. Iachello and A. Leviatan, *Phys. Rev. C* **54**, 1935 (1996) [nucl-th/9510001].
23. R. Bijker, F. Iachello and A. Leviatan, *Annals Phys.* **284**, 89 (2000) [nucl-th/0004034].



Exotic molecules of heavy quark hadrons

Atsushi Hosaka

Research Center for Nuclear Physics (RCNP)
Osaka University, Ibaraki, 567-0047, Japan

Abstract. We discuss hadronic molecules containing both heavy and light quarks. The interactions are provided by meson exchanges between light quarks in the constituent hadrons. The tensor force in the one-pion exchange potential mixes states of different spins and angular momenta. This provides attraction and generates rich structure in exotic channels in the heavy quark sectors. The method has been applied to exotic baryons with a \bar{c} or \bar{b} quark, and exotic mesons containing $b\bar{b}$ including the recently found Z'_b 's.

Recent interest in hadron physics has been largely motivated by the observations of candidates for exotic multi-quark states which are not (easily) explained by the conventional quark model [1–4]. Many of them appear near the threshold region of their possible decay channels. The finding of the twin Z'_b 's is perhaps the most striking in that they appear very close to the BB^* and B^*B^* thresholds [4–6].

Strictly, multi-quarks does not make much sense for light flavors especially for u and d quarks when the quark number is not a conserved quantity. In fact, they interact strongly at the energy scale of Λ_{QCD} , creating $q\bar{q}$ pairs and generating massive constituent quarks. It is known that it is a consequence of spontaneous breaking of chiral symmetry. In the low energy region we expect that such constituent quarks become active degrees of freedom as almost on-shell particles, forming exotic multi-quark states. Contrary to the light flavor sector heavy quarks such as c and b with mass $M \gg \Lambda_{\text{QCD}}$ conserve their quark number. Thus we can treat them as almost on shell particles with non-relativistic kinematics at low energies of typical hadron resonances.

Starting from the conventional quark model picture for orbitally excited states, multi-quark configurations can mix with them because the typical excitation energy of about 0.5-1 GeV is sufficient to create a (constituent) $q\bar{q}$ pair. A color singlet multi-quark system of more than the minimal number ($\bar{q}q$ or qqq) may form color singlet sub-systems (clusters) of hadrons. Clustering phenomena of multiparticle systems have been extensively studied in nuclear physics for many years [7]. Alpha particles saturate the dominant component of spin and isospin dependent nuclear force. The spin-isospin neutral alpha particles interact rather weakly and can form loosely bound states near the threshold regions of alpha decay.

In QCD, the state corresponding to alpha particle is a hadron which saturates the strong color dependent force. If these hadrons have sufficient amount of attraction (but weak as compared to the color force), they may form a bound or

resonant state, which is the hadronic molecule. it must be a rather loosely bound state having an extending spatial structure to retain the identity of hadronic constituents. We expect that the relevant energy scale of binding and resonant states should be sufficiently small as compared to Λ_{QCD} of some hundreds MeV.

To establish exotic states is interesting not only for its own sake, but also because it is expected to reveal important aspects of non-perturbative dynamics of QCD. In this respect, as experimental observations imply, hadrons of light and heavy quarks are interesting, where more candidates of exotic states are observed. There, heavy quark symmetry and chiral symmetry play simultaneously. The former suppresses the spin dependent interactions, leading to degeneracy of different spin states. On the other hand, the latter is responsible for the pion coupling to the light quarks, which provides the source of the strong one pion exchange potential between heavy flavor hadrons. When these two conditions are satisfied, we expect the formation of exotic hadronic molecules. The spin and isospin dependent nature of the pion exchange potential as well as its orientation dependence of the tensor structure are the cause of the rich structure of hadron spectrum.

Based on these ideas, we have studied hadronic molecular states for exotic heavy baryons in Refs. [8–10], and for exotic heavy mesons in Ref. [11–13]. They are exotic not only due to hadronic molecular structure but also due to their exotic quantum numbers which are not accessible by the minimal number of quarks. In forming the hadronic molecular state, the following three points are important; (1) heavy mass which suppresses kinetic energy of constituent hadrons, (2) one pion exchange force of tensor nature which mixes the 0^- and 1^- states (DD^* and BB^*), and (3) degeneracy of 0^- and 1^- states which makes the wider space of coupled channels more effective to gain more attraction.

Hadronic molecules have been also studied for DN systems of ordinary quantum numbers [14,15]. These channels allow even more attraction leading to deeply bound states of a binding energy of order a few hundred MeV with much spatially compact configuration. Here $q\bar{q}$ annihilation is also possible, the treatment of which is more difficult than in the case of exotic channel without $q\bar{q}$ annihilation.

Turning to the exotic channels, employing an interactions between heavy flavor hadrons in a boson exchange model including one pion exchange potential, we find several bound and resonant states near the threshold regions. Many of them with small binding energy of order ten MeV or less have a rather extended size compatible to hadronic molecules. For baryons, we have found bound states of $J^P = 1/2^-$ states of exotic quark content $\bar{c}q\text{-}qqq$ and $\bar{b}q\text{-}qqq$ just below the threshold of $\bar{D}N$ and BN , respectively. Other resonant states are also found for $J^P = 3/2^-, 1/2^+, 3/2^+, 5/2^+$ with similar structure of mass spectrum for c and b quark sectors [9,10].

For mesons, in the hidden bottom sector, we have found ten $B\bar{B}$, $B\bar{B}^*$, $B^*\bar{B}^*$ molecules for low lying spin $J \leq 2$. In particular, the hidden bottom exotic mesons Z_b 's are well predicted [11]. Further exotic states of double heavy flavor (charm and bottom) mesons are also found [12]. In Ref. [13], we have estimated the decay and production rates of various states in the limit of heavy quarks which are

characteristic to the hadronic molecular structure. These theoretical predictions for rich structure of hadronic molecules can be studied in the facilities such as Belle, JPARC and LHC.

Acknowledgements:

The author thanks, S. Yasui, S. Ohkoda, Y. Yamaguchi, K. Sudoh for discussions. This work is partly supported by the Grant-in-Aid for Scientific Research on Priority Areas titled "Elucidation of New Hadrons with a Variety of Flavors" (E01: 21105006).

References

1. T. Nakano *et al.* [LEPS Collaboration], Phys. Rev. Lett. **91**, 012002 (2003) [arXiv:hep-ex/0301020].
2. B. Aubert *et al.* [BABAR Collaboration], Phys. Rev. Lett. **90**, 242001 (2003) [arXiv:hep-ex/0304021].
3. S.K. Choi *et al.* (Belle Collaboration), Phys. Rev. Lett. **91**, 262001 (2003).
4. I. Adachi [Belle Collaboration], arXiv:1105.4583 [hep-ex].
5. A. Bondar *et al.* [Belle Collaboration], Phys. Rev. Lett. **108**, 122001 (2012) [arXiv:1110.2251 [hep-ex]].
6. J. Beringer *et al.* (Particle Data Group), Phys. Rev. D **86**, 010001 (2012).
7. K. Ikeda, H. Horiuchi and S. Saito, Prog. Theor. Phys. Suppl. **68**, 1 (1980).
8. S. Yasui and K. Sudoh, Phys. Rev. D **80**, 034008 (2009) [arXiv:0906.1452 [hep-ph]].
9. Y. Yamaguchi, S. Ohkoda, S. Yasui and A. Hosaka, Phys. Rev. D **84**, 014032 (2011) [arXiv:1105.0734 [hep-ph]].
10. Y. Yamaguchi, S. Ohkoda, S. Yasui and A. Hosaka, Phys. Rev. D **85**, 054003 (2012) [arXiv:1111.2691 [hep-ph]].
11. S. Ohkoda, Y. Yamaguchi, S. Yasui, K. Sudoh and A. Hosaka, Phys. Rev. D **86**, 014004 (2012) [arXiv:1111.2921 [hep-ph]].
12. S. Ohkoda, Y. Yamaguchi, S. Yasui, K. Sudoh and A. Hosaka, Phys. Rev. D **86**, 034019 (2012) [arXiv:1202.0760 [hep-ph]].
13. S. Ohkoda, Y. Yamaguchi, S. Yasui and A. Hosaka, arXiv:1210.3170 [hep-ph].
14. J. Hofmann and M. F. M. Lutz, Nucl. Phys. A **763**, 90 (2005) [hep-ph/0507071].
15. T. Mizutani and A. Ramos, Phys. Rev. C **74**, 065201 (2006) [hep-ph/0607257].



Spin-Flavor Formalism for the Relativistic Coupled-Channels Quark Model^{*}

Regina Kleinhappel, Willibald Plessas, Wolfgang Schweiger

Theoretical Physics, Institute of Physics, University of Graz,
Universitätsplatz 5, A-8010 Graz, Austria

Abstract. The ongoing progress in our group of treating hadron resonances within a relativistic coupled-channels quark model is shortly discussed. Following earlier calculations along a simplified toy model for mesons, now all spin and flavor degrees of freedom are being included. Furthermore the approach is now extended also to baryons considered as genuine three-quark states.

Covariant calculations of properties of hadron resonances, such as hadronic decay widths, with relativistic constituent quark models (RCQM) have so far been limited to treating the resonant states as excited bound states rather than true resonances with finite widths. Corresponding predictions in general have been found to underestimate existing experimental data for hadronic decay widths [1–5]. The shortcomings are probably due to the usage of inadequate wave functions for the hadron resonances within single-channel models, such as the Goldstone-boson-exchange (GBE) RCQM [6,7]. Explicit couplings to mesonic channels might be needed.

We have started a project towards setting up a coupled-channels (CC) RCQM. A corresponding toy model applied to meson-like systems of scalar particles has already produced promising results, hinting to a broadening of the decay widths, when the coupling to the decay channels is included [8,9]. We are now aiming at more realistic calculations both for meson and baryon resonances including all spin and flavor degrees of freedom. The corresponding formalism has been worked out and the implementation into the computer programs is under way.

For a CC RCQM we start out from an invariant mass operator in matrix form that includes beyond the channel of i particles in addition a channel $i+1$ with a further degree of freedom, say, the meson produced in a decay process. By eliminating the decay channel according to the Feshbach method one arrives at a complex mass operator, whose eigenvalue equation reads

$$\left[M_i + K (m - M_{i+1} + i0)^{-1} K^\dagger \right] |\psi_i \rangle = m |\psi_i \rangle . \quad (1)$$

Here, M_i and M_{i+1} are the invariant mass operators of the i -particle and $(i+1)$ -particle systems and K^\dagger describes the transition dynamics (emission of the decay product). It should be noted that the mass eigenvalue m appears both in the

^{*} Talk delivered by R. Kleinhappel

optical-potential term and also on the right-hand side of the eigenvalue equation. It assumes real values for bound states and complex values above the resonance thresholds. In the latter case its imaginary part is the half-width of the decaying resonance.

We exemplify the introduction of spin and flavor degrees of freedom in a CC RCQM along the ω -meson decaying into a ρ and a π . Here, the ω - and ρ -mesons are assumed to be built up by a constituent quark and a constituent antiquark, while the π is considered as a fundamental particle (namely, a Goldstone boson, much in analogy to the RCQM proposed in Refs. [6,7]). The dynamics is thus mediated by GBE according to the interaction Lagrangian density in $SU(3)_F$

$$\mathcal{L}_I = ig_{PS}\bar{\psi}\gamma^5\lambda^F\psi\Phi, \quad (2)$$

where $\bar{\psi}$ and ψ represent the (anti)quark fields and Φ the boson (pseudoscalar meson) fields; λ^F are the Gell-Mann flavor matrices.

In the construction of the optical potential in Eq.(1), the first channel thus consists of confined quark-antiquark bound states, whereas the second channel adds the π . The spin and flavor degrees of freedom of the process in question are introduced as follows.

Spin states:

$$\rho, \omega: \begin{cases} |1, 1\rangle = |\uparrow\uparrow\rangle \\ |1, 0\rangle = \frac{1}{\sqrt{2}}(|\uparrow\downarrow\rangle + |\downarrow\uparrow\rangle) \\ |1, -1\rangle = |\downarrow\downarrow\rangle \end{cases}$$

Flavor states:

$$\chi = \begin{pmatrix} u \\ d \end{pmatrix}, \quad \bar{\chi} = \begin{pmatrix} \bar{d} \\ -\bar{u} \end{pmatrix}$$

$$\omega = -\frac{1}{\sqrt{2}}(u\bar{u} + d\bar{d}), \quad \begin{aligned} \rho^+ &= u\bar{d} \\ \rho^0 &= \frac{1}{\sqrt{2}}(d\bar{d} - u\bar{u}) \\ \rho^- &= -d\bar{u} \end{aligned}$$

In the optical potential, the spin degrees of freedom undergo Wigner rotations according to Lorentz boosts, and the flavor degrees of freedom specify the various possible decay modes.

The same process can also be treated at a hadronic level. The decay dynamics is then described by the coupling of the fundamental meson fields ρ^β , π , and ω^γ following the Lagrangian density [10]

$$\mathcal{L}_{\omega\rho\pi} = \frac{g_{\omega\rho\pi}}{\sqrt{m_\rho m_\omega}} \epsilon_{\alpha\beta\mu\nu} (\partial^\alpha \rho^\beta) \cdot (\partial^\mu \pi) \omega^\nu. \quad (3)$$

Here, the vector notation in the ρ and π cases is related to the isospin degrees of freedom, and $\epsilon_{\alpha\beta\mu\nu}$ denotes the Levi-Civita antisymmetric tensor. The macroscopic approach at the hadronic level relies on the assumption of vertex form

factors. By comparing with the calculation at the quark level, a microscopic explanation of these form factors can be obtained.

The same approach can also be applied to baryons as three-quark systems. Here we will first consider the couplings of the N and the Δ to the π . Again the GBE dynamics is furnished by the Lagrangian in Eq. (2).

At the hadronic level the following Lagrangian densities are suggested [11]

$$\mathcal{L}_{NN\pi} = -\frac{f_{NN\pi}}{m_\pi} \bar{\Psi} \gamma_5 \gamma^\mu \Psi \partial_\mu \phi, \quad (4)$$

$$\mathcal{L}_{\Delta N\pi} = -\frac{f_{\Delta N\pi}}{m_\pi} \bar{\Psi} \Psi^\mu \partial_\mu \phi + \text{h.c.}, \quad (5)$$

where the Ψ and Ψ^μ now represent N and Δ fields, respectively. The phenomenological vertex form factors needed here, can again be deduced with the help of the microscopic calculation along the CC RCQM, just by comparing the two approaches.

Acknowledgment

This work was supported by the Austrian Science Fund, FWF, through the Doctoral Program on *Hadrons in Vacuum, Nuclei, and Stars* (FWF DK W1203-N16).

References

1. T. Melde, W. Plessas, and R.F. Wagenbrunn, Phys. Rev. C 72, 015207 (2005);
Erratum: Phys. Rev. C 74, 069901 (2006)
2. T. Melde, W. Plessas and B. Sengl, Phys. Rev. C 76, 025204 (2007)
3. B. Sengl, T. Melde, and W. Plessas, Phys. Rev. D 76, 054008 (2007)
4. T. Melde, W. Plessas, and B. Sengl, Phys. Rev. D 77, 114002 (2008)
5. B. Metsch, U. Löring, D. Merten, and H. Petry, Eur. Phys. J. A 18, 189 (2003)
6. L.Y. Glozman, W. Plessas, K. Varga, and R.F. Wagenbrunn, Phys. Rev. D 58, 094030 (1998)
7. L.Y. Glozman, Z. Papp, W. Plessas, K. Varga, and R.F. Wagenbrunn, Phys. Rev. C 57, 3406 (1998)
8. R. Kleinhappel, Diploma Thesis, University of Graz, 2010
9. R. Kleinhappel and W. Schweiger, in *Dressing Hadrons* (Proceedings of the Mini-Workshop, Bled, Slovenia, 2010), ed. by B. Golli, M. Rosina, and S. Sirca, DMFA, Ljubljana (2010), p. 33; arXiv:1010.3919
10. K. Nakayama, Y. Oh, J. Haidenbauer and T.-S.H. Lee, Phys. Lett. B 648, 351 (2007)
11. T. Melde, L. Canton and W. Plessas, Phys. Rev. Lett. 102, 132002 (2009)



Resonances in photo-induced reactions

M. Ostrick

Institut für Kernphysik, Johannes-Gutenberg-Universität Mainz, J.-J.-Becher-Weg 45,
55128 Mainz, Germany

Abstract. The extraction of baryon resonance parameters from experimental data and their interpretation within QCD are central issues in hadron physics. To achieve these goals it is an essential prerequisite to have a sufficient amount of precision data which allows an unambiguous reconstruction of partial wave amplitudes for different reactions. Over the last years an intense effort has started to study photon-induced meson production. Many single and double spin-observables have been measured for the first time. This experimental progress will be illustrated by means of single and double π^0 photo-production. The focus will be on the impact of the new data for the unambiguous reconstruction of partial wave amplitudes.

1 Introduction

Meson scattering and meson production reactions below 3 GeV distinctively exhibit resonances, clearly organized in terms of flavor content, spin and parity, sitting on top of a non resonant "background. In lack of stringent predictions from strong QCD these resonances are usually interpreted in constituent quark models as excitations of massive quasi-particles bound by a confining potential. However, also the strong meson-baryon and meson-meson interaction could give rise to dynamically generated resonances. Chiral unitary methods and coupled channel calculations provide a theoretical framework to study the importance of resonances without including them explicitly in a model. Furthermore, lattice QCD simulations started to become predictive for dynamical quantities like strong decay widths of resonances and scattering phase shifts [1]. In the past, only calculations of approximate mass spectra in the heavy pion limit, where excited baryons are stable particles, were possible.

Empirically, N^* and Δ^* baryon resonance parameters like mass, width or pole position have been extracted for many years by partial-wave analyses of elastic and charge-exchange pion-nucleon scattering experiments. The most recent analysis of existing πN data has been performed by the George Washington Group [2]. Today there is no running experiment dedicated to study πN scattering anymore. However, options for a new generation of experiments with pion beams at Hades/GSI [3], ITEP [4] and J-PARC [5] are presently under discussion.

Instead of πN scattering, an immense effort started during the last decade to study baryon resonances with electromagnetic probes at various laboratories,

mainly ELSA, Graal, JLAB, LEPS, LNS and MAMI. The motivation for this ongoing effort is 2-fold. The initial idea was to substantiate or to disprove the existence of questionable resonances or even to discover new states that couple only weakly to πN . Especially, above 2 GeV an abundance of states is predicted by quark models which are not identified in πN partial wave analyses. This fact is often called the “missing resonance” problem. As historically all information about resonances came from pionic reaction, the hope was to discover new states in e.g. $K\Lambda$, $K\Sigma$, ηN or ωN final states. The PDG lists in their latest edition a couple of new states which have been seen in some analyses of recent data [6]. However, there are still many ambiguities and the discussion is ongoing.

The second objective are high precision measurements of the excitation of established resonances with real and virtual photons in order to relax the model constraints in the analyses and understand the influence of background on the extraction and interpretation of resonance properties. Single and double spin observables turned out to be an indispensable prerequisite to address both issues. Such measurements with sufficient acceptance and statistics became technically feasibly only recently. A brief overview of the facilities is given in section 2.

A completely different approaches to baryon spectroscopy are presently being developed at the BES-III e^+e^- collider, where decays like $J/\psi \rightarrow \bar{N}N^* \rightarrow \bar{N}N\pi$ have been observed, or at the COMPASS experiment at CERN, where diffractive processes like $pp \rightarrow pp\pi\pi$ clearly show resonant structures. One important milestone in future experimental baryon spectroscopy will be the combination of all empirical information from very different experiments in order to identify universal, i.e. process independent, properties of genuine nucleon excitations and to quantify the impact of coupled channel dynamics.

2 Photon beam facilities

During the last ten years we noticed an enormous increase in high precision measurements of many single and double spin observables in photo-induced meson production. The experiments are still ongoing and many results are still preliminary. The reason for this unprecedented development was the combination of high-intensity polarized beams, polarized targets and hermetic detector systems which was technically realized at the CLAS spectrometer in Hall B at Jefferson Lab [7], the Crystal-Barrel experiment at the ELSA stretcher ring [8] and the Crystal Ball experiment at the Mainz Microtron MAMI [9]. CLAS is a large acceptance spectrometer based on a toroidal magnetic field configuration. Tracking chambers and time-of-flight detectors provide charge particle identification and momentum resolution. At CLAS, energy tagged, polarized photon beams with up to 6 GeV can be used. The Crystal Barrel calorimeter consisting of 1230 CsI(Tl) crystals is the core of the experimental setup at ELSA and provides excellent acceptance and resolution for multi-photon final states. The Crystal Ball at MAMI (see Fig. 2) consists of 672 NaI(Tl) crystals covering 93% of the full solid angle with an energy resolution of 1.7% for electromagnetic showers at 1 GeV. For charged particle tracking and identification two layers of coaxial multi-wire proportional

chambers and a barrel of 24 scintillation counters surrounding the target are installed. The forward angular range is covered by the TAPS calorimeter consisting of BaF2 detectors and a Cerenkov detector.

The polarized target technique at all labs is based on Dynamic Nucleon Polarization (DNP) of solid-state target materials such as butanol, deuterated butanol, NH_3 or ${}^6\text{LiD}$. The material is spin polarized by microwave pumping in an external magnetic field of 2.5T at temperatures of about 100mK. During the measurements, the spin orientation is frozen at temperatures of down to 20mK by a moderate longitudinal or transverse magnetic holding field of about 0.5T. The main technical challenge was the construction of a horizontal cryostat that fits into the detector geometry and keeps a temperature of about 20mK without adding too much material that would limit the particle detection. The underlying concept of the targets presently used at ELSA, JLAB and MAMI was developed in Bonn [10] and was successfully used for the first time in 1998 for measurements of the GDH sum rule in Mainz [11].



Fig. 1. Crystal-Ball detector at MAMI and the horizontal cryostat of the frozen spin target, which keeps temperatures of about 20mK.

3 $\gamma\text{N} \rightarrow \pi\text{N}$

The photo-production of pseudoscalar mesons has four spin degrees of freedom which define four complex scattering amplitudes for each isospin. These amplitudes manifest themselves in 16 different single and double spin observables, including experiments with polarized target, beam and nucleon recoil polarimetry. It is well known for a long time that the full knowledge of 8 selected observables at each energy and scattering angle completely determines all amplitudes in a mathematical sense. Such a procedure is called a "Complete Experiment" [12]. It would then allow us to predict all remaining observables. However, in a real situation with statistical and systematic uncertainties this procedure is much more difficult. Furthermore, the goal is not a "Complete Experiment" and the reconstruction of the 4 helicity amplitudes but an understanding of the underlying dynamics. For this, the knowledge of all relevant partial wave or multipole amplitudes is much more important.

Up to a certain maximum orbital angular momentum l_{max} , all $4l_{\text{max}}$ complex multipole amplitudes have to be determined from experiment (see Table 1). It can be shown that even a "Complete Experiment" is only of limited value to reach this goal because of the freedom to choose an angular and energy dependent overall phase [13]. Therefore, one has to determine the relevant multipoles directly from experimental data. Each observable, $O_i(W, \theta)$, can be expanded in term on Legendre polynomials:

$$O_i(W, \theta) = \sin^{\alpha_i} \theta \sum_{k=0}^{k_{\text{max}}} a_{ik}(W) P_k(\cos(\theta)), \quad \alpha_i = \{0, 1, 2\}. \quad (1)$$

Here k_{max} is given by the truncation to a certain maximum angular momentum. The coefficients $a_{ik}(W)$ are bilinear combinations of the $4l_{\text{max}}$ complex multipole amplitudes which can be reconstructed from the coefficients. For a detailed discussion of the concepts of a "Complete Experiment" and such a truncated partial wave analysis see [13].

Table 1. Multipole decomposition of the pion photo-production amplitude for $l_\pi \leq l_{\text{max}} = 2$. For each isospin, $4l_{\text{max}}$ complex multipoles have to be determined from experiment.

l_π	0		1		2	
J^P	$\frac{1}{2}^-$	$\frac{1}{2}^+$	$\frac{3}{2}^+$		$\frac{3}{2}^-$	$\frac{5}{2}^-$
multipole	E_{0+}	M_{1-}	M_{1+}	E_{1+}	M_{2-}	E_{2+}

A direct reconstruction of the relevant partial wave amplitudes was achieved for the first time in the energy region of the $\Delta(1232)$ resonance using a truncation to s- and p-waves ($l_{\text{max}} < 2$) and additional theoretical constraints [14].

At higher energies this procedure requires precision measurements of several spin observables with a sufficiently fine energy binning, e.g. 10 MeV, and a full angular coverage. Below $E_{\text{CM}} \sim 2$ GeV, where a truncation to F- or G-wave ($l_{\text{max}} < 3$ or 4) is possible, already the measurement of 4-6 spin and double-spin observables could provide sufficient constraints for such a direct reconstruction. This has been shown in [15] using generated pseudo-data with realistic uncertainties that will be achieved with the Crystal-Ball experiment at MAMI within the next years. Preliminary results for many new target and beam-target asymmetries from ELSA, JLAB and MAMI have been presented e.g. at the last NSTAR conference [16]. However, the direct reconstruction of multipoles has not yet been achieved above the $\Delta(1232)$ resonance region and one has to rely on fits using models for the energy-dependent amplitudes. Figure 3 summarizes the current status of such model dependent analyses in the case of the important lowest order multipole amplitudes, $J^P = 1/2^+(M_{1-})$ and $J^P = 1/2^-(E_{0+})$. Even at relatively low energies in the second resonance region there are significant deviations between different models. A summary of our current knowledge of multipole amplitudes for different flavor states can be found in [21].

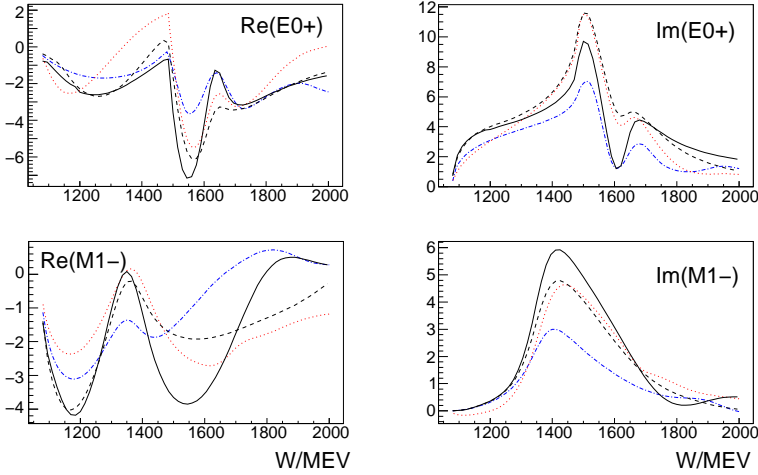


Fig. 2. Lowest order multipole amplitudes of the $\gamma\pi^0 p$ reaction in units of $10^{-3}/M_\pi$. The curves are derived from fits of different models to existing data. The black solid and dashed lines represent the SAID 2011 and the SAID Chew-Mandelstam fits [17, 18], the MAID analysis gives the red dotted line [19]. Finally, the blue dashed-dotted curve is derived from the Bonn-Gatchina analysis [20].

In the case of the $\gamma\pi^0 p$ reaction close to threshold a direct reconstruction of the amplitudes is more simple as the dynamics is dominated only by one s-wave, E_{0+} and 3 p-waves, M_{1-} , M_{1+} and E_{1+} . Furthermore, these multipoles are real between the $\pi^0 p$ and $\pi^+ n$ production thresholds. Above the $\pi^+ n$ threshold the E_{0+} amplitude becomes complex and shows a strong energy dependence due to the unitary cusp [22]. The imaginary parts of the p-waves remain negligible below ~ 180 MeV. With this truncation, the real parts of the multipoles can be reconstructed from measurements of two observables only, namely the differential cross section and the photon beam asymmetry

$$\Sigma = \frac{\sigma_\perp - \sigma_\parallel}{\sigma_\perp + \sigma_\parallel}. \quad (2)$$

Here σ_\perp and σ_\parallel denote the differential cross sections with the photon polarization vector perpendicular and parallel to the $p\pi^0$ reaction plane. Both observables have recently been measured from threshold up to the Δ resonance region with unprecedented accuracy at the Crystal-Ball experiment at MAMI [23]. Fig. 3 show as an example the results of these measurements at the CM angle of 90° as function of the incoming photon energy. The new data are compared to existing data and ChPT calculations with updated low-energy parameters [25] as well as the 2001 version of the DMT dynamical model [26]. The reconstruction of the multipoles is almost final and will be published soon [24].

With all relevant multipoles fixed by experiment the additional measurement of target (T) and beam-target (F) spin asymmetries will provide sensitivity to the charge exchange $\pi^+ n \rightarrow \pi^0 p$ scattering length from the unitary cusp which enters directly in the imaginary part of the E_{0+} amplitude. Therefore, threshold

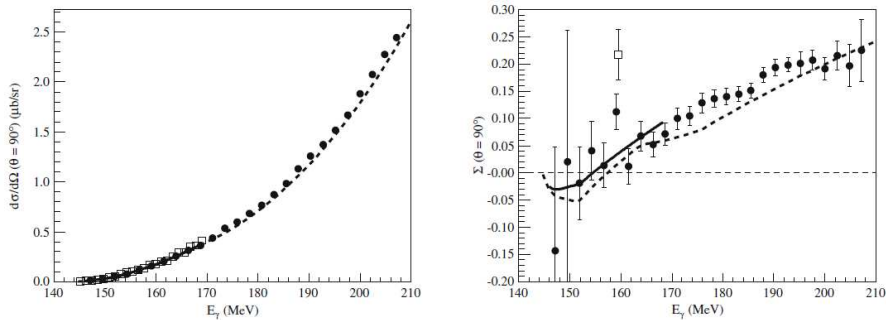


Fig. 3. Preliminary results from Crystal Ball at MAMI (solid circles) of the differential cross section and photon asymmetry for the $\gamma p \rightarrow \pi^0 p$ reaction at pion CM angle of 90° compared to the older data from MAMI ([22], open squares) as well as some theory calculations. The solid lines are preliminary ChPT fits to the new data [25] and the dashed lines are a dynamical model [26].

π^0 photo-production will enable us to study strong and electromagnetic isospin breaking in πN scattering by comparing the charge exchange scattering lengths for $\pi^+ n \rightarrow \pi^0 p$ and $\pi^- p \rightarrow \pi^0 n$ [23]. The latter has recently been measured in pionic hydrogen [27].

4 $\gamma N \rightarrow \pi\pi N$

When looking at the production of meson pairs like $\pi\pi$ or $\pi\eta$ it is obvious that the dynamics can be much more complex and an analysis will be even more model dependent than in the case of single meson photo-production. Nevertheless, $\pi\pi N$ and $\pi\eta N$ final states have attracted a lot of interest during the last years. These processes allow us to study resonances which have no significant branching ratio for a direct decay into the nucleon ground state. This is possible via sequential decays which involve intermediate excited states like $R \rightarrow R'\pi \rightarrow N\pi\pi$. Here R and R' denote nucleon resonances. Such decay chains are a phenomenon that can be observed in other quantum systems like atoms or nuclei as well. The theoretical interpretation is usually based on isobar models or effective field theories [28–32]. Typically, the reaction amplitude is constructed as a sum of background and resonance contributions. The background part contains nucleon Born terms as well as meson exchange in the t channel. The resonance part is a coherent sum of s -channel resonances decaying into $\pi\pi N$ via intermediate formation of meson-nucleon and meson-meson states (“isobars”). Despite significant differences between the models, all of them provide an acceptable description of the existing data. This observation clearly demonstrates, that further experimental and theory studies are necessary.

With the Crystal-Ball at MAMI we have recently studied the $\gamma N \rightarrow \pi^0\pi^0 N$ reactions by measurements of cross sections [33] and beam helicity asymmetries [34, 35].

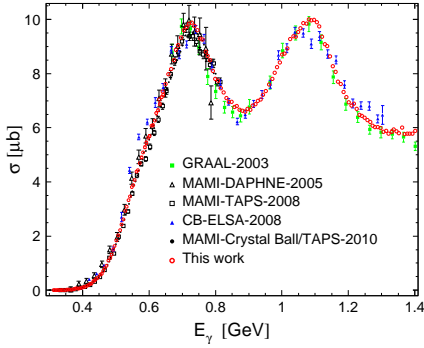


Fig. 4. Total cross section for the $\gamma p \rightarrow \pi^0 \pi^0 p$ reaction as function of the incoming photon energy. The open circles show the precision that has been obtained at MAMI. Further information and references can be found in [33].

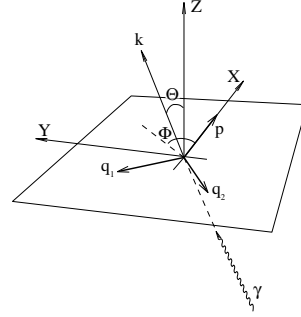


Fig. 5. The coordinate system is fixed by the momenta of the incident-photon, \mathbf{k} , out-going proton, \mathbf{p} and the two pions, \mathbf{q}_1 , and \mathbf{q}_2 , in the center of mass system.

Fig. 4 shows the existing data for the total cross section. It is widely accepted that the $D_{13}(1520)$ resonance decaying to $\pi\Delta$ channel is responsible for the first peak at $E_\gamma \approx 730$ MeV. However, the underlying dynamics down to threshold as well as the behavior at higher energies have not been well understood so far. E.g., the minimum at $W = 1.6$ GeV and the second maximum at $W = 1.7$ GeV are described in Ref. [32] by the destructive interference between D_{13} and D_{33} partial wave amplitudes. In other models this behavior is explained by different resonance contributions, e.g. in the F_{15} partial wave. The high accuracy of the MAMI new data allowed us to make first steps towards a model independent partial wave analysis for the first time. In case of meson pair production the helicity amplitudes depend on the incoming photon energy, E_γ , the meson energies, ω_1 and ω_2 (Dalitz-Plot) and two angles, Θ and Φ , which are explained in Fig. 5. The angular distributions normalized to the total cross section, $W(E_\gamma, \omega_1, \omega_2, \Theta, \Phi) = \frac{1}{\sigma} \cdot \frac{d\sigma}{d\Omega}$ can now be expanded in terms of spherical harmonics $Y_{LM}(\Theta, \Phi)$. In a first step, we average the distributions over the meson energies, ω_1, ω_2 :

$$W(E_\gamma, \Theta, \Phi) \equiv \frac{1}{\sigma} \int d\omega_1 d\omega_2 \frac{d\sigma}{d\Omega} = \sum_{L \geq 0} \sum_{M=-L}^L \sqrt{\frac{2J+1}{4\pi}} W_{LM}(E_\gamma) \cdot Y_{LM}(\Theta, \Phi) \quad (3)$$

This expansion determines the general structure of an angular distribution analogous to the expansion of the cross section for single-meson photo-production in terms of the Legendre polynomials (see Eq. 1). The moments $W_{LM}(E_\gamma)$ are bilinear combinations of the partial wave amplitudes. The exact relations have been worked out explicitly by Fix and Arenhoevel in ref. [36]. With the high precision data from MAMI it was possible to determine the moments $W_{LM}(E_\gamma)$ for the first time. The results are shown in Fig. 6. In case of the production of two

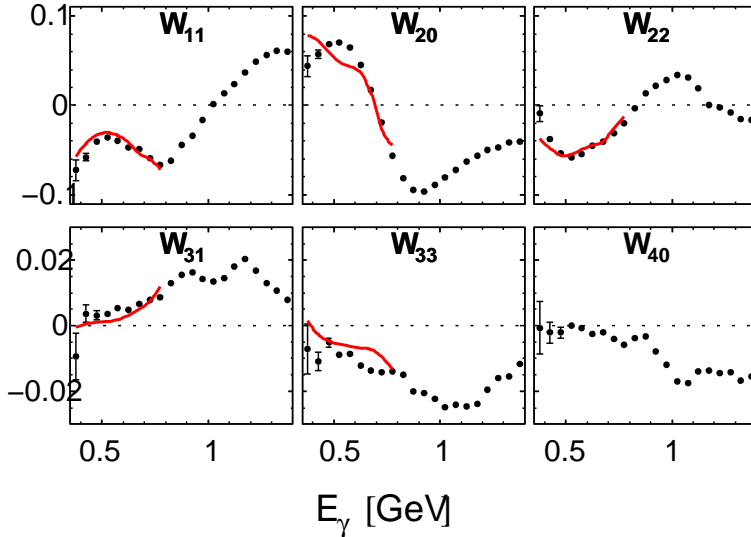


Fig. 6. First moments W_{LM} (normalized such that $W_{00} = 1$) as a function of the incident-photon energy. Our experimental results are shown by filled circles. The solid lines show the results of an isobar model fit [37].

identical particles, e.g. $\gamma p \rightarrow \pi^0 \pi^0 p$, it can be shown, that the imaginary parts vanish exactly ($\text{Im}(W_{LM}) = 0$). Already at low energies, the quantities W_{20} and W_{22} , which are given by an incoherent sum $J^P = 3/2^-$ and $3/2^+$ partial wave amplitudes, achieve relatively large values. This observation indicates an additional strong $3/2^-$ contribution, interfering with the $D_{13}(1520)$ resonance. This could support the dynamics found in Ref. [32] where a strong contribution from the $D_{33}(1700)$ resonance was found. Of course, the analysis of the moments $W_{LM}(E_\gamma)$ is only a very first step towards a full partial wave analysis of meson pair production processes. Nevertheless, it shows that data with very high precision, which will be available also for other observables in the future, will allow us to reduce the model dependence in the analysis procedures even for more complex final states significantly.

5 Conclusion

During the last decade an immense effort started to study baryon resonances in photo-induced meson production at various laboratories, mainly ELSA, Graal, JLAB, LEPS, LNS and MAMI. New high precision data for many spin observables are expected in the near future. A prerequisite for an unambiguous, model-independent extraction of resonance parameters is the reconstruction of partial wave or multipole amplitudes from experimental data. Resonances as well as effects from coupled channel dynamics manifest themselves in the analytic properties of these amplitudes. The upcoming data will allow us to minimize the model dependence in the determination of partial wave amplitudes in a systematic way.

This goal has already been achieved in π^0 photo-production close to threshold. The methods will be extended to higher photon energies and other final states (ηN , $K\Lambda$, $\pi\pi N$, etc.).

References

1. S. Prelovsek, C. B. Lang, and D. Mohler, Bled Workshops in Physics **12**, 73 (2011).
2. R. Arndt et al., Physical Review C **74**, 045205 (2006).
3. Symposium on baryon resonance production and electromagnetic decays, www.hades2012.pl
4. I. I. Alekseev, arXiv:1204.6433v1 (2012).
5. H. Fujioka, Hadron and Nuclear Physics **9**, 150 (2010).
6. J. Beringer et al. (Particle Data Group), Phys. Rev. D **86**, 010001 (2012)
7. B. Mecking et al., Nucl. Instr. and Meth. A **503**, 513 (2003).
8. D. Elsner, Int. J. of Mod. Phys. E **19**, 869 (2010).
9. A. Thomas, Eur. Phys. J. Special Topics **198**, 171 (2011).
10. C. Bradtke et al., Nucl. Instr. and Meth. A **436**, 430 (1999).
11. J. Ahrens et al., Phys. Rev. Lett. **97**, 1 (2006).
12. I. Barker, A. Donnachie, and J. Storrow, Nucl. Phys. B **95**, 347 (1975).
13. L. Tiator, AIP Conf. Proc. **162**, 162 (2012) and contribution to this workshop.
14. R. Beck et al., Phys. Rev. C **61**, 1 (2000).
15. R. L. Workman et al., Eur. Phys. J. A **47**, 143 (2011).
16. V. Burkert, M. Jones, M. Pennington, D. Richards (ed.) AIP Conf. Proc. **1432**, 1 (2012).
17. R. L. Workman, W. J. Briscoe, M. W. Paris, and I. I. Strakovsky, Phys. Rev. C **85**, 025201 (2012).
18. R. Workman et al., Phys. Rev. C **86**, 1 (2012).
19. D. Drechsel, S. S. Kamalov, and L. Tiator, Eur. Phys. J. A **34**, 69 (2007).
20. A. V. Anisovich et al., Eur. Phys. J. A **48**, 15 (2012).
21. A. V. Anisovich et al., Eur. Phys. J. A **48**, 88 (2012).
22. A. Schmidt et al., Phys. Rev. Lett. **87**, 1 (2001).
23. D. Hornidge and a. M. Bernstein, Eur. Phys. J. Special Topics **198**, 133 (2011).
24. D. Hornidge et al., submitted to Phys. Rev. Lett. (2012).
25. C. Fernández-Ramírez et al., Phys. Lett. B **679**, 41 (2009).
26. S. Kamalov et al., Phys. Rev. C **64**, 1 (2001).
27. D. Gotta et al., AIP Conference Proceedings **1037**, 162 (2008).
28. J. Gómez Tejedor and E. Oset, Nucl. Phys. A **600**, 413 (1996).
29. M. Ripani et al., Nucl. Phys. A **672**, 220 (2000).
30. A. Fix and H. Arenhövel, Eur. Phys. J. A **135**, 115 (2005).
31. H. Kamano, B. Juliá-Díaz, T. S. H. Lee, a. Matsuyama, and T. Sato, Phys. Rev. C **80** (2009).
32. U. Thoma et al., Phys. Lett. B **659**, 87 (2008).
33. V. Kashevarov et al., Phys. Rev. C **85**, 1 (2012).
34. F. Zehr et al., Eur. Phys. J. A **48**, 1 (2012).
35. M. Oberle et al., submitted to Eur. Phys. J. A (2012).
36. A. Fix and H. Arenhövel, Phys. Rev. C **85**, 035502 (2012)
37. V. L. Kashevarov et al., Phys. Rev. C **85**, 1 (2012).



Electroweak Form Factors of Baryon Ground States and Resonances*

Ki-Seok Choi^a, W. Plessas^b, M. Rohrmoser^b

^a Department of Physics, Soongsil University, Seoul 156-743, Republic of Korea

^b Theoretical Physics, Institute of Physics, University of Graz, A-8010 Graz, Austria

Abstract. We report of our ongoing studies of the electroweak structures of baryon ground and resonant states with flavors u , d , and s . Particular emphasis is laid on the comparison of the theoretical predictions of our relativistic constituent-quark model with recent experimental data for individual flavor contributions to the nucleon electromagnetic form factors.

The original results of covariant predictions by the Goldstone-boson-exchange relativistic constituent-quark model (GBE RCQM) [1,2] for the elastic electromagnetic and axial form factors of the nucleons were published in [3–5]. They were followed by detailed studies of the electric radii as well as magnetic moments of all light and strange baryons [6]. Comparisons to corresponding predictions by other RCQM, such as the relativized one-gluon-exchange (OGE) RCQM of Bhaduri, Cohler, and Nogami, as parameterized in ref. [7], were given in [8]. In the latter paper also comparative studies of point-form and instant-form calculations of the nucleon electromagnetic form factors were made, in order to find out the essential differences between the spectator-model constructions in either the instant and point forms of Poincaré-invariant quantum mechanics [9]. More recently we have performed detailed investigations of the axial charges of the nucleon and N^* resonances [10]; this kind of studies have then also been extended to the axial charges of the whole octet and decuplet of light and strange baryons [11]. The axial charges are connected with the πNN coupling constant via the Goldberger-Treiman relation. Therefore it has been very interesting to study also the πNN as well as $\pi N\Delta$ interaction vertices [12]. With these investigations we have reached a microscopic description of the Q^2 dependences of the πNN and $\pi N\Delta$ form factors together with predictions for the corresponding coupling constants $f_{\pi NN}$ and $f_{\pi N\Delta}$, which were found in agreement with phenomenology.

Especially the point form results obtained from the GBE RCQM have been found to be everywhere in quite good an agreement with existing experimental data. Further fine-tuning of the description is probably only needed for such sensitive observables like the N electric radii, some baryon magnetic moments, and the N axial charge [5,6,10,11]. The studies have recently been extended to the Δ

* Talk delivered by W. Plessas

and the lowest hyperon states [13], for which, of course, no experimental data exist. In some instances, however, comparisons to data from lattice QCD have been possible, showing again a reasonable agreement in most cases.

With regard to the N elastic electromagnetic form factors an interesting issue has come about by the recent publication of phenomenological data for the flavor contributions to these form factors [14]. We were immediately interested in the performance of the GBE RCQM with regard to the u- and d-flavor contributions to the proton and neutron electromagnetic form factors as well as the electric radii and magnetic moments. First results were already reported at the Bled Workshop in 2011 (see [15]) and subsequently published in [16]. For the flavor contributions to the Sachs electric and magnetic form factors of both the proton and the neutron surprisingly good agreement with experimental data published in [14] is achieved. Slight deviations occur close to zero momentum transfer, since the electric radii and magnetic moments are not perfectly reproduced by the GBE RCQM [6].

Driven by these successes we have extended the flavor analyses to all the other octet and decuplet baryons [17]. Again, no experimental data exist. However, in some cases we can compare to calculations of flavor components to electromagnetic baryon form factors from lattice QCD [18]. This applies specifically to Σ^- , Σ^0 , Σ^+ , Ξ^- , and Ξ^0 baryons. In all cases a remarkably good agreement is found. In Figs. 1 and 2 we show as typical examples the electric and magnetic form factors of Σ^+ , for which also other lattice-QCD data exist.

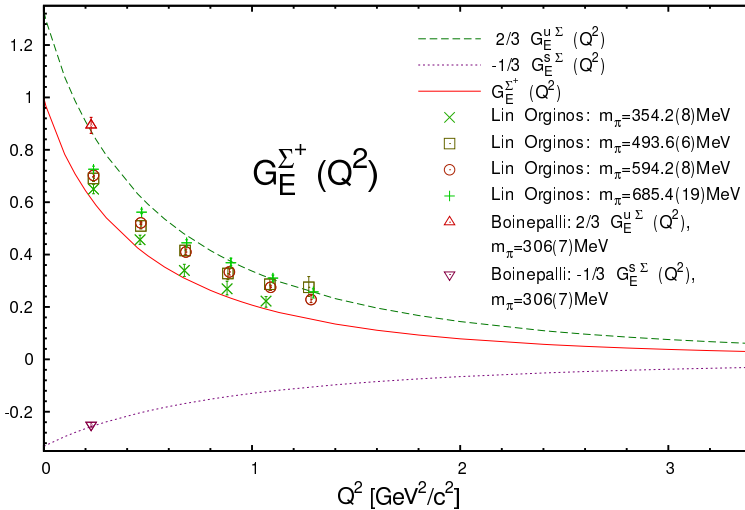


Fig. 1. Predictions of the GBE RCQM for the elastic electric form factor of Σ^+ (total: solid line, u-component: dashed line, s-component: dotted line) in comparison to data from lattice QCD for the total form factor [19] and for the u and s flavor contributions [18].

It should be emphasized that the covariant predictions of the GBE RCQM are parameter-free. No further parametrizations, such as meson-dressing effects

nor constituent quark anomalous magnetic moments etc., have been included for the calculation of the electromagnetic current matrix elements. Still, a remarkably good agreement with the whole existing experimental data base and also with lattice-QCD data is generally achieved. It means that the RCQM is a reliable tool to treat at least the lowest-lying baryon states on reasonable grounds. Of course, refined wave functions such as the ones produced by the GBE RCQM must be employed and the framework must be fully relativistic.

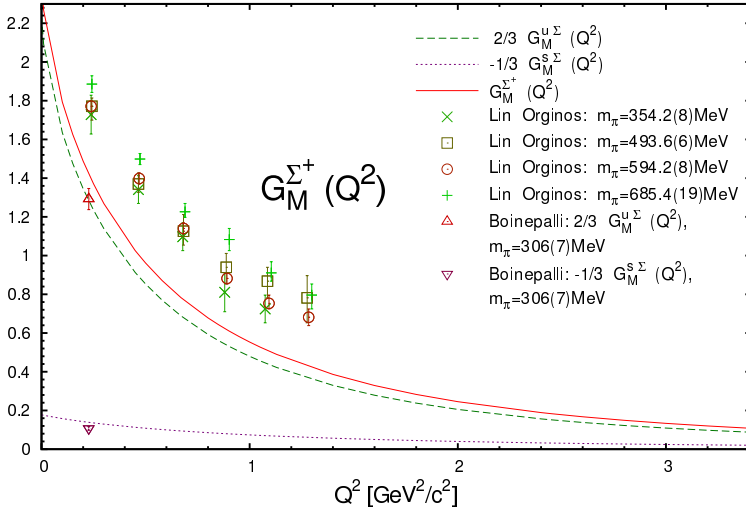


Fig. 2. Same as in Fig. 1 but for the elastic magnetic form factor of Σ^+ .

Acknowledgment

This work was supported by the Austrian Science Fund, FWF, through the Doctoral Program on *Hadrons in Vacuum, Nuclei, and Stars* (FWF DK W1203-N16).

References

1. L. Y. Glozman, W. Plessas, K. Varga, and R. F. Wagenbrunn, Phys. Rev. D **58**, 094030 (1998).
2. L. Y. Glozman, Z. Papp, W. Plessas, K. Varga, and R. F. Wagenbrunn, Phys. Rev. C **57**, 3406 (1998).
3. R. F. Wagenbrunn, S. Boffi, W. Klink, W. Plessas, and M. Radici, Phys. Lett. B **511**, 33 (2001)
4. S. Boffi, L. Y. Glozman, W. Klink, W. Plessas, M. Radici, and R. F. Wagenbrunn, Eur. Phys. J. A **14**, 17 (2002)
5. L. Y. Glozman, M. Radici, R. F. Wagenbrunn, S. Boffi, W. Klink, and W. Plessas, Phys. Lett. B **516**, 183 (2001)
6. K. Berger, R. F. Wagenbrunn and W. Plessas, Phys. Rev. D **70**, 094027 (2004)

7. L. Theussl, R. F. Wagenbrunn, B. Desplanques, and W. Plessas, *Eur. Phys. J. A* **12**, 91 (2001)
8. T. Melde, K. Berger, L. Canton, W. Plessas, and R. F. Wagenbrunn, *Phys. Rev. D* **76**, 074020 (2007)
9. T. Melde, L. Canton, W. Plessas, and R. F. Wagenbrunn, *Eur. Phys. J. A* **25**, 97 (2005).
10. K. S. Choi, W. Plessas, and R. F. Wagenbrunn, *Phys. Rev. C* **81**, 028201 (2010)
11. K. S. Choi, W. Plessas, and R. F. Wagenbrunn, *Phys. Rev. D* **82**, 014007 (2010)
12. T. Melde, L. Canton, and W. Plessas, *Phys. Rev. Lett.* **102**, 132002 (2009)
13. K.-S. Choi, PhD Thesis, Univ. of Graz (2011)
14. G. D. Cates, C. W. de Jager, S. Riordan, and B. Wojtsekhowski, *Phys. Rev. Lett.* **106**, 252003 (2011)
15. M. Rohrmoser, K.-S. Choi, and W. Plessas, in: *Proceedings of the Workshop "Understanding Hadronic Spectra"*, Bled, 2011, ed. by B. Golli, M. Rosina, and S. Sirca (DMFA-Zaloznistvo, Ljubljana, 2011), p. 47
16. M. Rohrmoser, K.-S. Choi, and W. Plessas, arXiv:1110.3665 [hep-ph]
17. M. Rohrmoser, Diploma Thesis, Univ. of Graz, 2012
18. S. Boinepalli, D. B. Leinweber, A. G. Williams, J. M. Zanotti, and J. B. Zhang, *Phys. Rev. D* **74** (2006) 093005
19. H.-W. Lin and K. Orginos, *Phys. Rev. D* **79** (2009) 074507



Pion- and photon-induced hadronic reactions in a combined coupled-channel analysis

Deborah Rönchen

Institut für Kernphysik and Jülich Center for Hadron Physics, Forschungszentrum Jülich, D-52425 Jülich, Germany

1 Introduction and Formalism

To gain insight into the non-perturbative sector of Quantum Chromodynamics the knowledge of the excited hadron spectrum is essential, providing the connection between experiment and QCD. Most resonances have been identified through elastic πN scattering in the past to present day. On the other hand, combining different reactions for resonance extraction allows to determine those states which couple only weakly to πN . The simultaneous analysis of different final states of pion- and photon-induced reactions is especially interesting regarding the new experimental window that has opened through the recent high-precision photon beam facilities, e.g., at ELSA, JLab and MAMI. Among other approaches, dynamical coupled-channel (DCC) models provide a sophisticated tool to analyze those data on excited baryons as they obey a maximum of theoretical requirements of the S -matrix such as analyticity to allow for a reliable extraction of resonances.

The DCC model developed and employed in this study (*Jülich model*) is based on an approach pursued over the years [1–9]. The scattering amplitude is obtained as the solution of a Lippmann-Schwinger equation (Eq. (1)) which guarantees two-body unitarity and approximates three-body unitarity,

$$\begin{aligned} \langle L'S'k' | T_{\mu\nu}^{IJ} | LSk \rangle &= \langle L'S'k' | V_{\mu\nu}^{IJ} | LSk \rangle \\ &+ \sum_{\gamma L''S''} \int_0^{\infty} k''^2 dk'' \langle L'S'k' | V_{\mu\gamma}^{IJ} | L''S''k'' \rangle \frac{1}{z - E_{\gamma}(k'') + i\epsilon} \langle L''S''k'' | T_{\gamma\nu}^{IJ} | LSk \rangle \end{aligned} \quad (1)$$

In Eq. 1 z is the scattering energy, $J(L)$ is the total angular (orbital angular) momentum, $S(I)$ is the total spin (isospin), $k(k', k'')$ are the incoming (outgoing, intermediate) momenta, and μ, ν, γ are channel indices. E_{γ} is the on-mass shell energy in channel γ [4]. The pseudo-potential V iterated in Eq. (1) is constructed from an effective interaction based on the Lagrangians of Wess and Zumino, supplemented by additional terms [2, 3] for including the Δ isobar, the ω, η, α_0 meson, and the σ . The channel space is given by $N\pi, N\eta, N\sigma, \Delta\pi, N\rho, \Lambda K$ and ΣK . The non-resonant interactions are constructed of t - and u -channel exchanges

of known mesons and baryons, while bare resonances can be considered as s -channel processes. The explicit treatment of the background in terms of t - and u -channel diagrams introduces strong correlations between the different partial waves and generates a non-trivial energy and angular dependence of the observables. Analyticity is respected in the sense that dispersive, real parts of intermediate states are included, as well as the correct structure of branch points, some of them being in the complex plane, and the correct off-shell behavior as dictated by the interaction Lagrangians. Thus, a reliable determination of resonance properties given in terms of pole positions and residues is possible. In the *Jülich model* SU(3) flavor symmetry is exploited to link the different reaction channels, while it is broken e.g. by physical masses and different cut-offs in the form factors of the vertices.

The extension of the model to photoproduction within a fully gauge-invariant approach has been accomplished recently [9].

In the following, the results of a simultaneous analysis of elastic π N-scattering and pion-induced K and η production within the framework of the *Jülich model* will be presented. In the present study, we perform a resonance analysis of the isospin $I = 1/2$ and $I = 3/2$ sector, considering the world data on the set of reactions $\pi^- p \rightarrow \eta n$, $K^0 \Lambda$, $K^0 \Sigma^0$, $K^+ \Sigma^-$, and $\pi^+ p \rightarrow K^+ \Sigma^+$, together with π N $\rightarrow \pi$ N scattering. Within the framework of DCC approaches, this is the first analysis of this type realized. The approach also includes the three effective $\pi\pi$ N channels $\pi\Delta$, σ N and ρ N. The considered energy range has been extended beyond 2 GeV and resonances up to $J = 9/2$ are included in this study.

The present study is the first step towards a global analysis of pion- and photon-induced production of π N, η N, K Λ and K Σ .

2 Results

While for the reaction π N $\rightarrow \pi$ N the partial waves from the GWU/SAID analysis [10] are used, for the inelastic channels, π N $\rightarrow \eta$ N and π N \rightarrow KY, we fit directly to total and differential cross sections as well as to polarization observables. The bulk of the existing data for the inelastic channels was obtained in the 1960's and 70's. Though many experiments have been carried out at different facilities, unfortunately, there are still energy ranges where the data situation is not ideal. All in all we include about 6000 data points in our analysis. The present solution was obtained in a fit procedure using MINUIT on the JUROPA supercomputer at the *Forschungszentrum Jülich*.

In the previous analysis [5], the reaction $\pi^+ p \rightarrow K^+ \Sigma^+$ and π N scattering were considered and only resonance parameters, i.e. bare masses and couplings of the resonances to the different channels, were fitted. In this study, in addition the important T^{NP} parameters are varied. Those are the cut-offs of the form factors in t - and u -channel exchange diagrams.

Resonances with a total spin up to $J = 9/2$ are included, with the corresponding new parameters. One bare s -channel state is included in each of the $I = 1/2$ partial waves D13, D15, F15, P13, F17, H19 and G19, while we have two in S11

and P11. In the $I = 3/2$ sector, one bare s -channel state is included in the S31, D33, F35, P31, D35, F37, G37 and G39 partial waves and two are included in P33. These states couple to all channels πN , ρN , ηN , $\pi\Delta$, $K\Lambda$ and $K\Sigma$ if allowed by isospin. In total, we have 196 free parameters, of which 128 are resonance parameters and 68 belong to the T^{NP} part (t - and u -channel exchanges). The values of the parameters will be quoted elsewhere.

In Figs. 1, 2 and 3 we show a selection of our present results at typical energies.

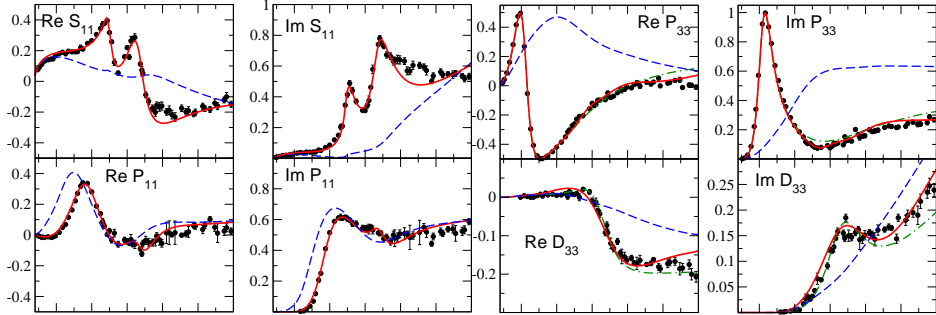


Fig. 1. Reaction $\pi N \rightarrow \pi N$, real and imaginary part of the S11, P11, P33 and D33 partial waves. (Red) solid lines: present solution. (Blue) dashed lines: only T^{NP} . (Green) dash-dotted lines: Jülich model, solution 2011 from Ref. [5]. Data points: GWU/SAID partial wave analysis (single energy solution) from Ref. [10]. (Preliminary)

In summary, a first combined analysis of the reactions $\pi N \rightarrow \pi N$, ηN , $K\Lambda$, and the three measured $K\Sigma$ final states $K^+\Sigma^+$, $K^0\Sigma^0$, and $K^+\Sigma^-$ within a dynamical coupled-channel framework has been performed. In the Lagrangian-based calculation, the full off-shell solution of the Lippman-Schwinger equation provides the correct analytic structure allowing for a reliable extrapolation into the complex plane to extract resonance pole positions and residues up to $J^P = 9/2^\pm$. The amplitude features also effective $\pi\pi N$ channels with branch points in the complex plane and a dispersive treatment of σ and ρ t -channel exchanges.

A publication of the full results together with a resonance analysis in terms of poles and residues is in progress.

The present results, in combination with the recent extension to pion photoproduction [9], will be used as input into a global study of pion- and photon-induced production of πN , ηN , $K\Lambda$ and $K\Sigma$. This means a major step towards the analysis of high-precision photoproduction data of ηN , $K\Lambda$, and $K\Sigma$ data produced, e.g., at ELSA, JLab, and MAMI.

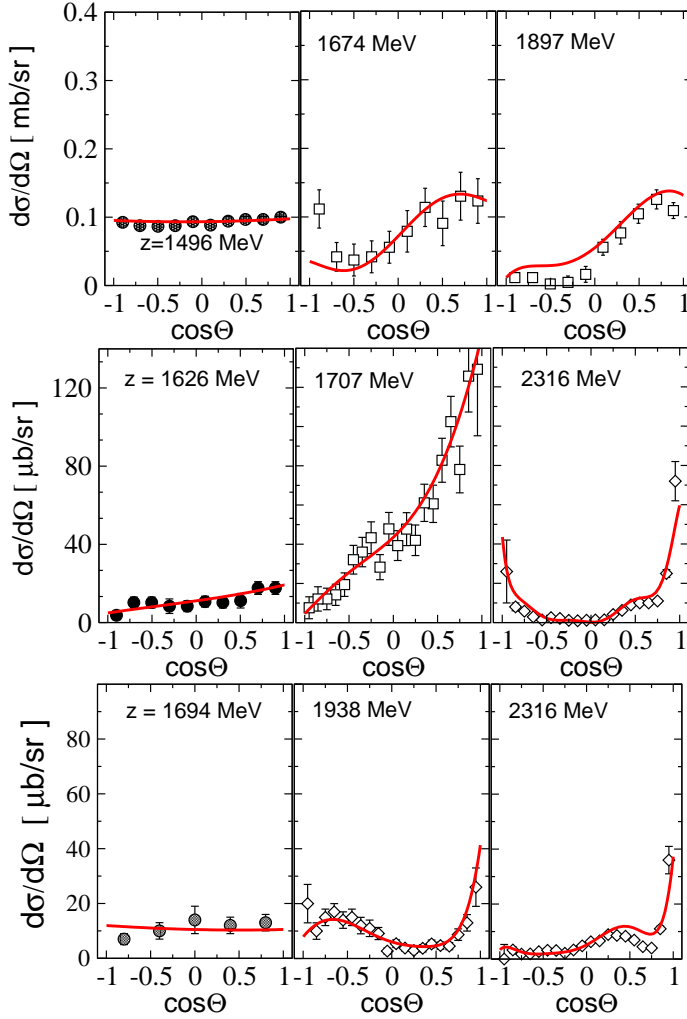


Fig. 2. Differential cross section for the reactions $\pi^-p \rightarrow \eta n$ (upper row), $\pi^-p \rightarrow K^0\Lambda$ (middle) and $\pi^-p \rightarrow K^0\Sigma^0$ (lower). (Red) solid lines: present solution. Selected results (Preliminary).

Acknowledgment

This work has been carried out in collaboration with M. Döring, F. Huang, H. Haberzettl, J. Haidenbauer, C. Hanhart, S. Krewald, U.-G. Meißner and K. Nakayama. I am also grateful to the German Academic Exchange Service (DAAD) for financial support within a “DAAD-Doktorandenstipendium”.

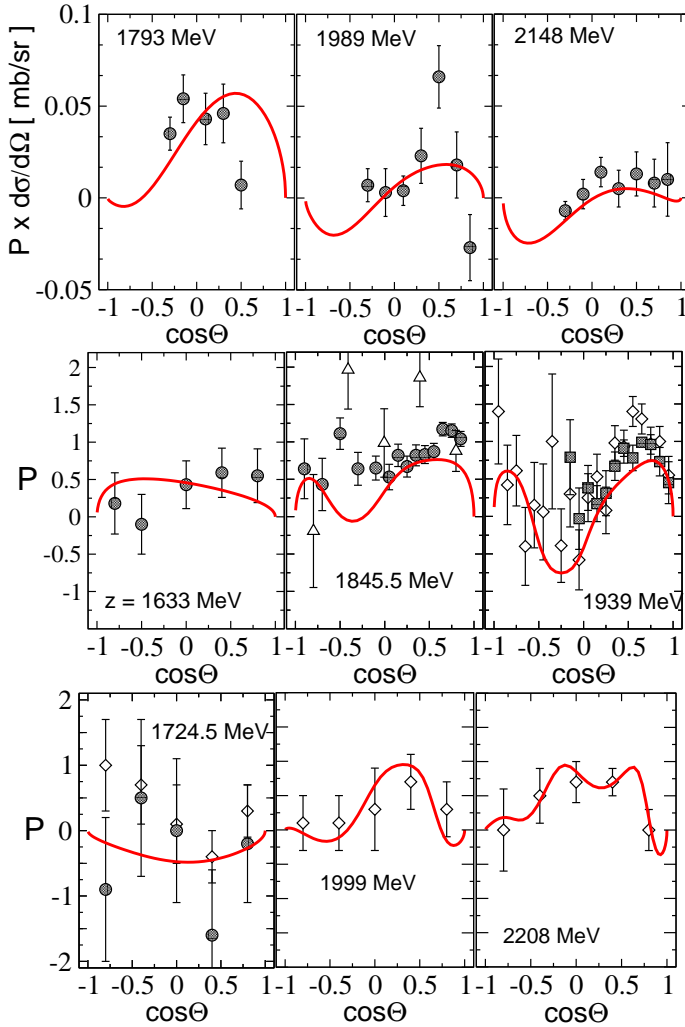


Fig. 3. Polarization for the reactions $\pi^- p \rightarrow \eta n$ (upper row), $\pi^- p \rightarrow K^0 \Lambda$ (middle) and $\pi^- p \rightarrow K^0 \Sigma^0$ (lower). (Red) solid lines: present solution. Selected results (Preliminary).

References

1. Schütz C, Haidenbauer J, Speth J and Durso J W 1998, Phys. Rev. C **57** 1464 (1998).
2. O. Krehl, C. Hanhart, S. Krewald and J. Speth, Phys. Rev. C **62**, 025207 (2000).
3. A. M. Gasparyan, J. Haidenbauer, C. Hanhart and J. Speth, Phys. Rev. C **68**, 045207 (2003).
4. M. Döring, C. Hanhart, F. Huang, S. Krewald and U.-G. Meißner, Nucl. Phys. A **829**, 170 (2009).
5. M. Döring, C. Hanhart, F. Huang, S. Krewald, U.-G. Meißner and D. Rönchen, Nucl. Phys. A **851**, 58 (2011).
6. H. Haberzettl, Phys. Rev. C **56** (1997) 2041.
7. H. Haberzettl, K. Nakayama, S. Krewald, Phys. Rev. C **74** (2006) 045202.

8. H. Haberzettl, F. Huang and K. Nakayama, *Phys. Rev. C* **83** (2011) 065502.
9. F. Huang, M. Döring, H. Haberzettl, J. Haidenbauer, C. Hanhart, S. Krewald, U.-G. Meißner and K. Nakayama, *Phys. Rev. C* **85**, 054003 (2012).
10. R. A. Arndt, W. J. Briscoe, I. I. Strakovsky and R. L. Workman, *Phys. Rev. C* **74**, 045205 (2006).



The implications of the two solar mass neutron star for the strong interactions ^{*}

Vikram Soni^a, Pawel Haensel^b and Mitja Rosina^{c,d}

^aNational Physical Laboratory, K.S. Krishnan Marg, New Delhi 110012, India

^bNicolaus Copernicus Astronomical Center, Polish Academy of Sciences, Bartycka 18, PL-00-716 Warszawa, Poland

^cFaculty of Mathematics and Physics, University of Ljubljana, Jadranska 19, P.O. Box 2964, 1001 Ljubljana, Slovenia

^dJ. Stefan Institute, 1000 Ljubljana, Slovenia

Abstract. The existence of a star with such a large mass means that the equation of state is stiff enough to provide a high enough pressure up to a fairly large density, about four times the nuclear density.

1 Introduction

Equations of state (EOS) that involve nonrelativistic constituents counteract gravitational infall of matter through a fermi pressure that is proportional to the density to the $(5/3)$ power, unlike fermi pressures of relativistic constituents that go as density to the $(4/3)$ power. Clearly the nonrelativistic nucleons are favoured over quarks for stiffer EOS's that can lead to larger mass for the stars.

However, a pure nonrelativistic fermi gas of neutrons is not sufficient to give large masses for neutron stars. Such a non interacting gas can give stars of maximum mass 0.7 solar mass - this a general relativistic effect coming from the Oppenheimer - Volkoff equation where the pressure needs to be proportional to density to a power greater than $(5/3)$. On the other hand, for white dwarfs fermi pressure of a nonrelativistic electron gas is all that is needed to counteract gravity and have stable stars. This enhanced pressure is provided by nuclear interactions like the hard core.

It is known that stars with soft, relativistic quark matter cores surrounded by a nonrelativistic $n+p+e$ plasma in beta equilibrium can give maximum mass for neutron stars ~ 1.6 solar mass [1, 2].

It is also known that there are many nucleon based neutron stars models that have neutron stars with maximum mass above 2 solar masses, eg. the APR 98 EOS of Akmal, Pandharipande and Ravenhall [3].

If we can show that matter in neutron stars is entirely composed of nucleon degrees of freedom then we can have a simple resolution of this problem. *Can we?*

^{*} Talk delivered by V. Soni

2 The Maxwell construction between nuclear matter and quark matter

A simple way to look at whether nucleons can dissolve into quark matter is to plot E_B , the energy per baryon in the ground state of both phases versus $1/n_B$, where n_B is the baryon density. The slope of the common tangent between the two phases then gives the pressure and the intercept the common baryon chemical potential. For the quark matter equation of state see Fig.1.

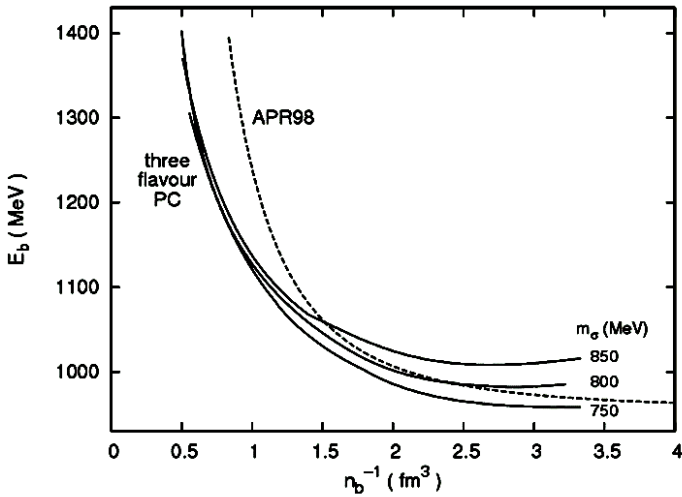


Fig. 1. The Maxwell construction: Energy per baryon plotted against the reciprocal of the baryon number density for APR98 equation of state (dashed line) and the 3-flavour pion-condensed phase (PC) for three different values of m_σ (solid lines). A common tangent between the PC phase and the APR98 phase in this diagram gives the phase transition between them. The slope of a tangent gives the negative of the pressure at that point, and its intercept gives the chemical potential. As this figure indicates, the transition pressure moves up with increasing m_σ , and at m_σ below ~ 750 MeV a common tangent between these two phases cannot be obtained. (From Fig. 2 of Soni and Bhattacharya [2] or Fig. 3 of the preprint [4])

This is based on an effective chiral symmetric theory that is QCD coupled to a chiral sigma model. The theory thus preserves the symmetries of QCD. In this effective theory chiral symmetry is spontaneously broken and the degrees of freedom are constituent quarks which couple to colour singlet, sigma and pion fields as well as gluons. The nucleon in such a theory is a colour singlet quark soliton with three valence quark bound states [5]. The quark meson couplings are set by matching mass of the nucleon to its experimental value and the meson self coupling which sets the tree level sigma particle mass is set from pi-pi scattering to be of order 800 MeV. Such an effective theory has a range of validity up to

centre of mass energies (or quark chemical potentials) of ~ 800 MeV. For details we refer the reader to ref. [2].

This is the simplest effective chiral symmetric theory for the strong interactions at intermediate scale and we use this consistently to describe, both, the composite nucleon of quark boundstates and quark matter. We expect it to be valid till the intermediate scales quoted above. Of course inclusion of the higher mesonic degrees of freedom like the rho and A1 would make for a more complete description. We work at the mean field level the gluon interactions are subsumed in the colour singlet sigma and pion fields they generate. We could further add perturbative gluon mediated corrections but they do not make an appreciable difference.

As can be seen from Fig.1, it is the tree level value of the sigma mass that determines the intersection of the two phases; the higher the mass the higher the density at which the transition to quark matter will take place. In [2] it was found that above, $m_\sigma \sim 850$ MeV, stars with quark matter cores become unstable as their mass goes up beyond the allowed maximum mass. So, if we want purely nuclear stars we should, in this model, work at, $m_\sigma \geq 850$ MeV [2].

From Fig. 1, for the tree level value of the sigma mass ~ 850 MeV, the common tangent in the two phases starts at $1/n_B \sim 1.75 \text{ fm}^3$ ($n_B \sim 0,57/\text{fm}^3$) in the nuclear phase of APR [A18 + dv +UIX] and ends up at $1/n_B \sim 1.25 \text{ fm}^3$ ($n_B \sim 0.8/\text{fm}^3$) in the quark matter phase.

At the above densities between the two phases there is a mixed phase at the pressure given by the slope of the common tangent and the at a baryon chemical potential given by the intercept of the common tangent on the vertical axis. If we are to stay in the nuclear phase the best way is to look at the central density of the nuclear (APR) stars and if it so happens that they are at lower density than that at which the above phase transition begins the we can safely say that the star remains in the nuclear phase.

Going Back to the APR phase in in fig 11 of APR [3] we find that for the APR [A18 + dv +UIX] the central density of a star of 1.8 solar mass is $n_B \sim 0.62 /\text{fm}^3$, very close to the initial density at which the phase transition begins.

The reason we are taking a static star mass of 1.8 solar mass from APR [3] is that for PSR-1614, the star is rotating fast at a period of 3 millisecc and we expect a $\sim 15\%$ diminution of the central density from the rotation [6]. Equivalently, since the above paper reports results for static stars, the central density of a fast rotating 1.97 solar mass star \sim the central density of a static 1.8 solar mass star.

Now we have found that in above scenario the central density is of the same order as the density at which the above phase transition begins in the nuclear phase. Ideally we would like the central density to be a little less than the initial density at which the above phase transition begins in the nuclear phase.

3 Beyond the Maxwell tangent construction for the phase transition

How do we change the crossover and Maxwell tangent construction for the phase transition? There are 2 ways of moving the crossover between the 2 phases and

also the initial density at which the above phase transition begins in the nuclear phase to higher density.

(i) By increasing the tree level mass of the sigma we can move the quark matter curve up (Fig. 1), thus moving the initial density at which the above phase transition begins in the nuclear phase to higher density. However we have to be careful. There is not much freedom here, as this is what also determines the $\pi - \pi$ scattering.

(ii) By softening the nuclear EOS at high density, e.g. by including hyperons or pi condensates. But this will increase the central density of the star and also reduce its maximum mass.

Of these the option (i) is a safer option as it does not disturb the central density or maximum mass of the nuclear star. However, the Maxwell construction is not the final word on the phase transition. The exact nature of the transition is not just given by the energy /baryon in the quark matter phase (which depends mainly on m_σ) but will depend on the quark binding inside the nucleon (which depends mainly o the quark meson coupling) and the nucleon nucleon repulsion as we squeeze them. This is not captured by the Maxwell construction.

The nucleon binding in this model is very high (Fig. 2) [5]

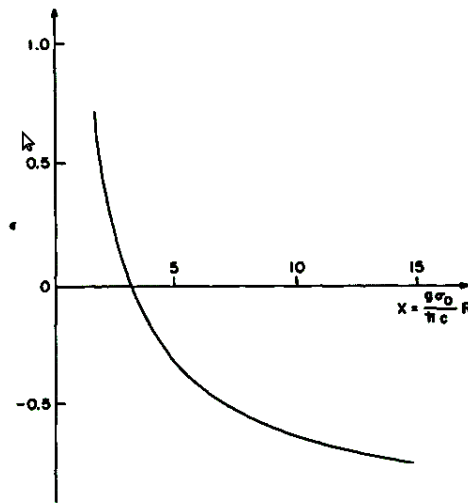


Fig.2. Dependence of the quark energy on the soliton size X in the quark soliton model (From Fig. 2 of Kahana, Ripka and Soni [5])

The quark eigenfunctions are smaller than the radius of the nucleon; they spread over about 0.5 fermi. This yields a quark wave function size of ~1 fermi or kinetic energy of about 200 MeV. The unbound mass of the quark is given by $gf_\pi \sim 500$ MeV and effectively they must contribute 313 MeV to the mass of the nucleon , giving the quark binding energy of ~ 400 MeV.

We can see that the quarks will become unbound (go to the continuum) when the energy eigenvalue is larger than the unbound mass of the quark which

is given by $m_{\text{free}} = gf_{\pi} \sim 500$ MeV. This happens when in the dimensionless units used in Fig. 2 $\epsilon \geq 1$ at $X = 3.12/1.94 = 1.6$. This translates into $R = (1.6/2.5) \text{ fm}^{-1} \sim 0.6 \text{ fm}^{-1}$. This is the effective radius of the squeezed nucleon at which the bound state quarks are liberated to the continuum. By inverting the volume occupied by the nucleon and assuming hexagonal close packing, this translates to nucleon density of $1/(6R^3) \sim 0.77 \text{ fm}^{-3}$.

Thus the quark bound states in nucleon persist until a much higher density $\sim 0.8/\text{fm}^3$. In other words, nucleons can survive well above the density at which the Maxwell phase transition begins and appreciably above the central density of the APR 2-solar-mass star.

Another feature is the the nucleon nucleon potential. It has been found for skyrmions and such quark-quark solitons with skyrmion configurations that there is a strong N-N repulsion that forces the lowest baryon number $N_B = 2$ configuration to become toroidal [7]. This is an indication that nucleon nucleon potential becomes strongly repulsive.

It thus follows that the phase transition from nuclear to quark matter will encounter a potential barrier before the quarks can go free. This effect cannot be seen by the coarse Maxwell construction which does not track their transition. This will modify the simple minded Maxwell construction which assumes only the energy and pressure that exist independently in the 2 phases. Here is where the internal structure of the nucleon will delay the transition.

All in all this produces a very plausible scenario of how the ~ 2 solar mass star can be achieved in a purely nuclear phase.

4 Consequences and discussion

A simple consequence of this unexpected scenario at high density is that the the phase diagram of QCD which plots temperature versus baryon chemical potential, the quark matter transition for finite density (in the range above) will be lifted up along the temperature axis.

References

1. J. M. Lattimer and M. Prakash, *Astrophysical J.* **550** (2001) 426;
2. V. Soni and D. Bhattacharya, *Phys. Lett. B* **643** (2006) 158.
3. A. Akmal, V. R. Pandharipande and D. G. Ravenhall, *Phys. Rev. C* **58** (1998) 1804.
4. V. Soni and D. Bhattacharya, arXiv. Hep-ph/0504041 v2.
5. S. Kahana, G. Ripka and V. Soni, *Nuclear Physics A* **415** (1984) 351.
6. Haensel et al., *New Astronomy Reviews* **51** (2008) 785; arXiv:0805.1820; arXiv:1109.1179 v2.
7. M. S. Sriram et al., *Phys. Lett. B* **342** (1995) 201.



Highly excited states of baryons in large N_c QCD*

N. Matagne^a, Fl. Stancu^b

^a Service de Physique Nucléaire et Subnucléaire, University of Mons, Place du Parc, B-7000 Mons, Belgium

^b Institute of Physics, B5, University of Liège, Sart Tilman, B-4000 Liège 1, Belgium

Abstract. The masses of highly excited negative parity baryons belonging to the $N = 3$ band are calculated in the $1/N_c$ expansion method of QCD. We use a procedure which allows to write the mass formula by using a small number of linearly independent operators. The numerical fit of the dynamical coefficients in the mass formula show that the pure spin and pure flavor terms are dominant in the expansion, like for the $N = 1$ band. We present the trend of some important dynamical coefficients as a function of the band number N or alternatively of the excitation energy.

1 The status of the $1/N_c$ expansion method

The large N_c QCD, or alternatively the $1/N_c$ expansion method, proposed by 't Hooft [1] in 1974 and implemented by Witten in 1979 [2] became a valuable tool to study baryon properties in terms of the parameter $1/N_c$ where N_c is the number of colors. According to Witten's intuitive picture, a baryon containing N_c quarks is seen as a bound state in an average self-consistent potential of a Hartree type and the corrections to the Hartree approximation are of order $1/N_c$. These corrections capture the key phenomenological features of the baryon structure.

Ten years after 't Hooft's work, Gervais and Sakita [3] and independently Dashen and Manohar in 1993 [4] derived a set of consistency conditions for the pion-baryon coupling constants which imply that the large N_c limit of QCD has an exact contracted $SU(2N_f)_c$ symmetry when $N_c \rightarrow \infty$, N_f being the number of flavors. For ground state baryons the $SU(2N_f)$ symmetry is broken by corrections proportional to $1/N_c$ [5,6].

Analogous to s -wave baryons, consistency conditions which constrain the strong couplings of excited baryons to pions were derived in Ref. [7]. These consistency conditions predict the equality between pion couplings to excited states and pion couplings to s -wave baryons. These predictions are consistent with the nonrelativistic quark model.

A few years later, in the spirit of the Hartree approximation a procedure for constructing large N_c baryon wave functions with mixed symmetric spin-flavor parts has been proposed [8] and an operator analysis was performed for $\ell = 1$ baryons [9]. It was proven that, for such states, the $SU(2N_f)$ breaking occurs at

* Talk delivered by Fl. Stancu

order N_c^0 , instead of $1/N_c$, as it is the case for ground and also for symmetric excited states [56, ℓ^+] (for the latter see Refs. [10, 11]). This procedure has been extended to positive parity nonstrange baryons belonging to the $[70, \ell^+]$ multiplets with $\ell = 0$ and 2 [12]. In addition, in Ref. [12], the dependence of the contribution of the linear term in N_c , of the spin-orbit and of the spin-spin terms in the mass formula was presented as a function of the excitation energy or alternatively in terms of the band number N . Based on this analysis an impressive global compatibility between the $1/N_c$ expansion and the quark model results for $N = 0, 1, 2$ and 4 was found [13] (for a review see Ref. [14]). More recently the $[70, 1^-]$ multiplet was reanalyzed by using an exact wave function, instead of the Hartree-type wave function, which allowed to keep control of the Pauli principle at any stage of the calculations [21]. The novelty was that the isospin term, neglected previously [9] becomes as dominant in Δ resonances as the spin term in N^* resonances.

The purpose of this work is mainly to complete the analysis of the excited states by including the $N = 3$ band for which results were missing in the systematic analysis of Ref. [12]. An incentive for studying highly excited states with $\ell = 3$ has been given by a recent paper [15] where the compatibility between the two alternative pictures for baryon resonances namely the *quark-shell picture* and the *meson-nucleon scattering picture* defined in the framework of chiral soliton models [16, 17] has been proven explicitly. This work was an extension of the analysis made independently by Cohen and Lebed [18, 19] and Pirjol and Schat [20] for low excited states with $\ell = 1$.

As explained below, we shall analyze the resonances thought to belong to the $N = 3$ band by using the procedure we have proposed in Ref. [21] for the $N = 1$ band. Details can be found in Ref. [22].

2 Mixed symmetric baryon states

If an excited baryon belongs to a symmetric $SU(6)$ multiplet the N_c -quark system can be treated similarly to the ground state in the flavour-spin degrees of freedom, but one has to take into account the presence of an orbital excitation in the space part of the wave function [10, 11]. If the baryon state is described by a mixed symmetric representation of $SU(6)$, the $[70]$ at $N_c = 3$, the treatment becomes more complicated. In particular, the resonances up to about 2 GeV are thought to belong to $[70, 1^-]$, $[70, 0^+]$ or $[70, 2^+]$ multiplets and beyond to 2 GeV to $[70, 3^-]$, $[70, 5^-]$, etc.

There are two ways of studying mixed symmetric multiplets. The standard one is inspired by the Hartree approximation [8] where an excited baryon is described by a symmetric core plus an excited quark coupled to this core, see e.g. [9, 12, 23, 24]. The core is treated in a way similar to that of the ground state. In this method each $SU(2N_f) \times O(3)$ generator is separated into two parts

$$S^i = s^i + S_c^i; \quad T^a = t^a + T_c^a; \quad G^{ia} = g^{ia} + G_c^{ia}; \quad \ell^i = \ell_q^i + \ell_c^i, \quad (1)$$

where s^i , t^a , g^{ia} and ℓ_q^i are the excited quark operators and S_c^i , T_c^a , G_c^{ia} and ℓ_c^i the corresponding core operators.

As an alternative, we have proposed a method where all identical quarks are treated on the same footing and we have an exact wave function in the orbital-flavor-spin space. The procedure has been successfully applied to the $N = 1$ band [21, 25, 26]. In the following we shall adopt this procedure to analyze the $N = 3$ band.

3 The mass operator

When hyperons are included in the analysis, the $SU(3)$ symmetry must be broken and the mass operator takes the following general form [27]

$$M = \sum_i c_i O_i + \sum_i d_i B_i. \quad (2)$$

The formula contains two types of operators. The first type are the operators O_i , which are invariant under $SU(N_f)$ and are defined as

$$O_i = \frac{1}{N_c^{n-1}} O_\ell^{(k)} \cdot O_{SF}^{(k)}, \quad (3)$$

where $O_\ell^{(k)}$ is a k -rank tensor in $SO(3)$ and $O_{SF}^{(k)}$ a k -rank tensor in $SU(2)$ -spin. Thus O_i are rotational invariant. For the ground state one has $k = 0$. The excited states also require $k = 1$ and $k = 2$ terms. The rank $k = 2$ tensor operator of $SO(3)$ is

$$L^{(2)ij} = \frac{1}{2} \{L^i, L^j\} - \frac{1}{3} \delta_{i,-j} \mathbf{L} \cdot \mathbf{L}, \quad (4)$$

which we choose to act on the orbital wave function $|\ell m_\ell\rangle$ of the whole system of N_c quarks (see Ref. [12] for the normalization of $L^{(2)ij}$). The second type are the operators B_i which are $SU(3)$ breaking and are defined to have zero expectation values for non-strange baryons. Due to the scarcity of data in the $N = 3$ band hyperons, here we consider only one four-star hyperon $\Lambda(2100)7/2^-$ and accordingly include only one of these operators, namely $B_1 = -S$ where S is the strangeness.

The values of the coefficients c_i and d_i which encode the QCD dynamics are determined from numerical fits to data. Table 1 gives the list of O_i and B_i operators together with their coefficients, which we believe to be the most relevant for the present study. The choice is based on our previous experience with the $N = 1$ band [26]. In this table the first nontrivial operator is the spin-orbit operator O_2 . In the spirit of the Hartree picture [2] we identify the spin-orbit operator with the single-particle operator

$$\ell \cdot s = \sum_{i=1}^{N_c} \ell(i) \cdot s(i), \quad (5)$$

the matrix elements of which are of order N_c^0 . For simplicity we ignore the two-body part of the spin-orbit operator, denoted by $1/N_c (\ell \cdot S_c)$ in Ref. [9], as being of a lower order (we remind that the lower case operators $\ell(i)$ act on the excited quark and S_c is the core spin operator).

Table 1. Operators and their coefficients in the mass formula obtained from numerical fits. The values of c_i and d_i are indicated under the heading Fit n ($n = 1, 2, 3, 4$) from Ref. [22].

Operator	Fit 1 (MeV)	Fit 2 (MeV)	Fit 3 (MeV)	Fit 4 (MeV)
$O_1 = N_c \mathbf{1}$	$c_1 = 672 \pm 8$	$c_1 = 673 \pm 7$	$c_1 = 672 \pm 8$	$c_1 = 673 \pm 7$
$O_2 = \ell^i s^i$	$c_2 = 18 \pm 19$	$c_2 = 17 \pm 18$	$c_2 = 19 \pm 9$	$c_2 = 20 \pm 9$
$O_3 = \frac{1}{N_c} S^i S^i$	$c_3 = 121 \pm 59$	$c_3 = 115 \pm 46$	$c_3 = 120 \pm 58$	$c_3 = 112 \pm 42$
$O_4 = \frac{1}{N_c} [T^a T^a - \frac{1}{12} N_c (N_c + 6)]$	$c_4 = 202 \pm 41$	$c_4 = 200 \pm 40$	$c_4 = 205 \pm 27$	$c_4 = 205 \pm 27$
$O_5 = \frac{3}{N_c} L^i T^a G^{ia}$	$c_5 = 1 \pm 13$	$c_5 = 2 \pm 12$		
$O_6 = \frac{15}{N_c} L^{(2)ij} G^{ia} G^{ja}$	$c_6 = 1 \pm 6$		$c_6 = 1 \pm 5$	
$B_1 = -S$	$d_1 = 108 \pm 93$	$d_1 = 108 \pm 92$	$d_1 = 109 \pm 93$	$d_1 = 108 \pm 92$
χ_{dof}^2	1.23	0.93	0.93	0.75

The spin operator O_3 and the flavor operator O_4 are two-body and linearly independent. The expectation values of O_3 are simply equal to $\frac{1}{N_c} S(S+1)$ where S is the spin of the whole system. For nonstrange baryons the eigenvalue of O_4 is $\frac{1}{N_c} I(I+1)$ where I is the isospin. For the flavor singlet Λ the eigenvalue is $-(2N_c + 3)/4N_c$, favourably negative, as shown in Ref. [22].

Note that the definition of the operator O_4 , indicated in Table 1, is such as to recover the matrix elements of the usual $1/N_c (T^a T^a)$ in $SU(4)$, by subtracting $N_c(N_c + 6)/12$. This is understood by using Eq. (30) of Ref. [25] for the matrix elements of $1/N_c (T^a T^a)$ extended to $SU(6)$. Then, it turns out that the expectation values of O_4 are positive for octets and decuplets and of order N_c^{-1} , as in $SU(4)$, and negative and of order N_c^0 for flavor singlets.

The operators O_5 and O_6 are also two-body, which means that they carry a factor $1/N_c$ in the definition. However, as G^{ia} sums coherently, it introduces an extra factor N_c and makes all the matrix elements of O_6 of order N_c^0 [25]. These matrix elements are obtained from the formulas (B2) and (B4) of Ref. [26] where the multiplet $[70, 1^-]$ has been discussed. Interestingly, when $N_c = 3$, the contribution of O_5 cancels out for flavor singlets, like for $\ell = 1$ [26]. This property follows from the analytic form of the isoscalar factors given in Ref. [26].

We remind that the $SU(6)$ generators S^i , T^a and G^{ia} and the $O(3)$ generators L^i of Eq. (4) act on the total wave function of the N_c system of quarks as proposed in Refs. [21], [25] and [26]. The advantage of this procedure over the standard one, where the system is separated into a ground state core + an excited quark, is that the number of relevant operators needed in the fit is usually smaller than the number of data and it allows a better understanding of their role in the mass formula, in particular the role of the isospin operator O_4 which has always been omitted in the symmetric core + excited quark procedure. We should also mention that in our approach the permutation symmetry is exact [21].

Among the operators containing angular momentum components, besides the spin-orbit, we have included the operators O_5 and O_6 , to check whether or not they bring feeble contributions, as it was the case in the $N = 1$ band. From Table 1 one can see that their coefficients are indeed negligible either included together as in Fit 1 or separately as in Fit 2 and 3. Thus in the expansion series, besides O_1 , proportional to N_c , the most dominant operators are the pure spin O_3 and the pure isospin O_4 .

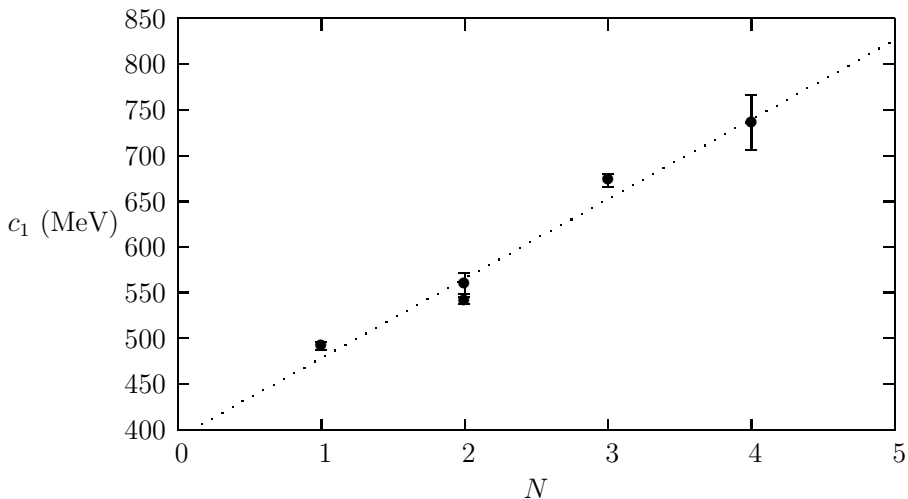


Fig. 1. The coefficient c_1 as a function of the band number N : $N = 1$ Ref. [26], $N = 2$ Ref. [10] for $[56, 2^+]$ and Ref. [12] for $[70, \ell^+]$, $N = 3$ Ref. [22], $N = 4$ Ref. [11]. The straight line is drawn to guide the eye.

4 Global results

The above analysis helps us to complete previous results for $N = 1, 2$ and 4 with the values of c_1 obtained for $N = 3$. Therefore we can draw now a complete picture of the dependence of the coefficients c_1 and c_2 on N in analogy to Ref. [12] where results for $N = 3$ were missing. The new pictures are shown in Figs. 1 and 2. One can see that the values of c_1 follow nearly a straight line which can give rise to a Regge trajectory. Remember that c_1 describes the bulk content of the baryon mass, $c_1 N_c$ being the most dominant mass term. In a quark model language it represents the kinetic plus the confinement energy. As discussed in Refs. [13, 14] the band number N also emerges from the spin independent part of a semi-relativistic quark model. If this part contributes to the total mass by a quantity denoted by M_0 , then one can make the identification

$$c_1^2 = M_0^2/9 \quad (6)$$

when $N_c = 3$. In this way one can compare the Regge trajectory obtainable from the above results with that of a standard constituent quark model. It turns out

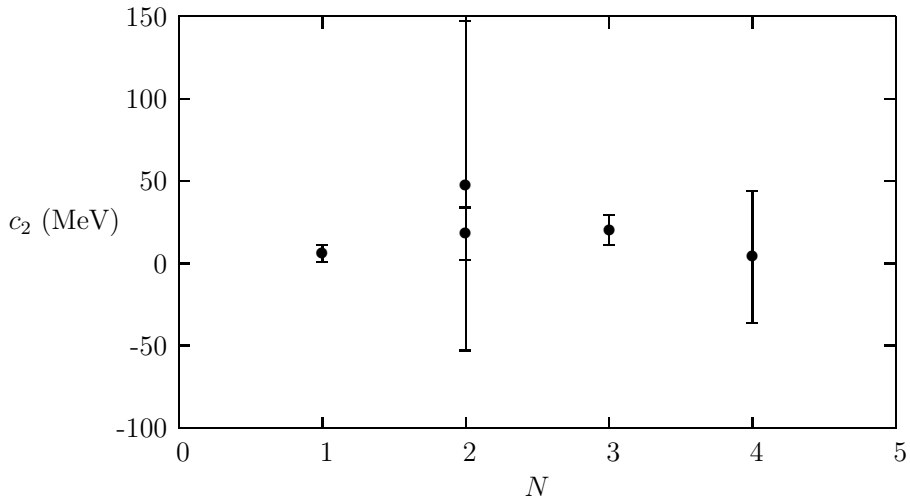


Fig. 2. Same as Figure 1 but for the coefficient c_2 .

that they are close to each other [13,14]. and the value obtained here for c_1 at $N = 3$, missing in the previous work, is entirely compatible with the previous picture.

The behaviour of c_2 shows that the spin-orbit operator contributes very little to the mass, at all energies, in agreement to quark models, where it is usually neglected. Note that the behaviour of c_2 in Fig. 2 is slightly different from that of [12], because we presently take the value of c_2 at $N = 1$ from Ref. [26] (Fit 3 giving the lowest χ^2_{dof}) for consistency with our treatment, instead of that of Ref. [9], based on the ground state core + excited quark, the only available at the time the paper [12] was published.

We refrain ourselves from presenting the global picture of c_3 , the spin term coefficient, because the results for positive parity mixed symmetric states are obtained on the one hand in the core + excited quark approach, where the isospin term is missing and on the other hand, for negative parity states where it is present, our approach is used. This term competes with the spin term. We plan to reanalyze the $[70, \ell^+]$ multiplets before drawing a complete picture of c_3 .

5 Conclusions

We have used a procedure which allows to write the mass formula by using a small number of linearly independent operators for spin-flavour mixed symmetric states of $SU(6)$. The numerical fits of the dynamical coefficients in the mass formula for $N = 3$ band resonances show that the pure spin and pure flavor terms are dominant in the $1/N_c$ expansion, like for $N = 1$ resonances. This proves that the isospin term cannot be neglected, as it was the case in the ground state + excited quark procedure. We have shown the dependence of the dynamical coefficients c_1 and c_2 as a function of the band number N or alternatively of the excitation energy for $N = 1, 2, 3$ and 4 bands.

References

1. G. 't Hooft, Nucl. Phys. **72** (1974) 461.
2. E. Witten, Nucl. Phys. **B160** (1979) 57.
3. J. L. Gervais and B. Sakita, Phys. Rev. Lett. **52** (1984) 87; Phys. Rev. **D30** (1984) 1795.
4. R. Dashen and A. V. Manohar, Phys. Lett. **B315** (1993) 425; *ibid* **B315** (1993) 438.
5. R. F. Dashen, E. Jenkins and A. V. Manohar, Phys. Rev. **D51** (1995) 3697.
6. E. Jenkins, Ann. Rev. Nucl. Part. Sci. **48** (1998) 81; AIP Conference Proceedings, Vol. 623 (2002) 36, arXiv:hep-ph/0111338; PoS E **FT09** (2009) 044 [arXiv:0905.1061 [hep-ph]].
7. D. Pirjol and T. M. Yan, Phys. Rev. D **57** (1998) 1449.
8. J. L. Goity, Phys. Lett. **B414** (1997) 140.
9. C. E. Carlson, C. D. Carone, J. L. Goity and R. F. Lebed, Phys. Rev. **D59** (1999) 114008.
10. J. L. Goity, C. Schat and N. N. Scoccola, Phys. Lett. **B564** (2003) 83.
11. N. Matagne and F. Stancu, Phys. Rev. **D71** (2005) 014010.
12. N. Matagne and F. Stancu, Phys. Lett. **B631** (2005) 7.
13. C. Semay, F. Buisseret, N. Matagne and F. Stancu, Phys. Rev. D **75** (2007) 096001.
14. F. Buisseret, C. Semay, F. Stancu and N. Matagne, Proceedings of the Mini-workshop Bled 2008, Few Quark States and the Continuum", Bled Workshops in Physics, vol. 9, no. 1, eds. B. Golli, M. Rosina and S. Sirca. arXiv:0810.2905 [hep-ph].
15. N. Matagne and F. Stancu, Phys. Rev. **D84** (2011) 056013.
16. A. Hayashi, G. Eckart, G. Holzwardt and H. Walliser, Phys. Lett. **147B** (1984) 5.
17. M. P. Mattis and M. E. Peskin, Phys. Rev. **D32** (1985) 58; M. P. Mattis, Phys. Rev. Lett. **56** (1986) 1103; Phys. Rev. **D39** (1989) 994; Phys. Rev. Lett. **63** (1989) 1455; M. P. Mattis and M. Mukerjee, Phys. Rev. Lett. **61** (1988) 1344.
18. T. D. Cohen and R. F. Lebed, Phys. Rev. Lett. **91**, 012001 (2003); Phys. Rev. **D67** (2003) 096008.
19. T. D. Cohen and R. F. Lebed, Phys. Rev. **D68** (2003) 056003.
20. D. Pirjol and C. Schat, Phys. Rev. **D67** (2003) 096009.
21. N. Matagne and F. Stancu, Nucl. Phys. A **811** (2008) 291.
22. N. Matagne and F. Stancu, Phys. Rev. D **85** (2012) 116003.
23. C. L. Schat, J. L. Goity and N. N. Scoccola, Phys. Rev. Lett. **88** (2002) 102002; J. L. Goity, C. L. Schat and N. N. Scoccola, Phys. Rev. **D66** (2002) 114014.
24. N. Matagne and F. Stancu, Phys. Rev. **D74** (2006) 034014; Nucl. Phys. Proc. Suppl. **174** (2007) 155.
25. N. Matagne and F. Stancu, Nucl. Phys. A **826** (2009) 161.
26. N. Matagne and F. Stancu, Phys. Rev. D **83** (2011) 056007.
27. E. Jenkins and R. F. Lebed, Phys. Rev. **D52** (1995) 282.



Poles as a link between QCD and scattering theory (old and contemporary knowledge)

A. Švarc

Rudjer Bošković Institute, Bijenička c. 54, 10 000 Zagreb, Croatia

An overview of existing knowledge about definition of a resonance, and quantification of resonance signals have been given. A special attention has paid to explaining why the definition of a resonance is in principle ill defined mathematical problem [1], and how it is overcome in physics reality [2]. A notion of scattering and resolvent resonances has been introduced, their interconnection and differences have been discussed, and reasons were presented why a pole as a resonance signal is the most acceptable solution [3]. The importance of multi-channel analysis has been demonstrated for pole extraction giving the example of $N(1710) P_{11}$ resonance where single channel πN elastic data are insufficient to establish its existence. Only inclusion of inelastic channels (η production and/or $K\Lambda$ channels) is needed [4]. The dangers when using Breit-Wigner parameters for quantifying resonance properties have been discussed, and use of phase-shift as a link between QCD and scattering theory has been mentioned by using Lüscher's theorem [5]. The present state of the art of baryon spectroscopy has been presented by showing the highlights from the Camogli Workshop [6].

References

1. B. Simon, International Journal of Quantum Chemistry, **vol. XIV**, 529 (1978.)
2. P. Exner and J. Lipovský, in "Adventures in Mathematical Physics" (Proceedings, Cergy-Pontoise 2006), AMS "Contemporary Mathematics" Series, **vol. 447**, Providence, R.I., 2007; pp. 73-81.
3. R. H. Dalitz and R. G. Moorhouse, Proc. R. Soc. Lond. **A 318**, 279 (1970).
4. S. Ceci, A. Švarc, and B. Zauner, Phys. Rev. Lett. **97**, 062002 (2006).
5. M. Lüscher, Commun. Math. Phys. **105**, 153 (1986); M. Lüscher, Nucl. Phys. **B 354**, 531 (1991).
6. International Workshop on NEW PARTIAL WAVE ANALYSIS TOOLS FOR NEXT GENERATION HADRON SPECTROSCOPY EXPERIMENTS, ATHOS 2012, June 20-22, 2012, Camogli, Italy. [<http://www.ge.infn.it/athos12/ATHOS/Welcome.html>]



Complete Experiments for Pion Photoproduction

L. Tiator

Institut für Kernphysik, Johannes Gutenberg-Universität, D-55099 Mainz, Germany

Abstract. The possibilities of a model-independent partial wave analysis for pion, eta or kaon photoproduction are discussed in the context of ‘complete experiments’. It is shown that the helicity amplitudes obtained from at least 8 polarization observables including beam, target and recoil polarization can not be used to analyze nucleon resonances. However, a truncated partial wave analysis, which requires only 5 observables will be possible with minimal model assumptions.

1 Introduction

Around the year 1970 people started to think about how to determine the four complex helicity amplitudes for pseudoscalar meson photoproduction from a complete set of experiments. In 1975 Barker, Donnachie and Storrow [1] published their classical paper on ‘Complete Experiments’. After reconsiderations and careful studies of discrete ambiguities [2–4], in the 90s it became clear that such a model-independent amplitude analysis would require at least 8 polarization observables which have to be carefully chosen. There are plenty of possible combinations, but all of them would require a polarized beam and target and in addition also recoil polarization measurements. Technically this was not possible until very recently, when transverse polarized targets came into operation at Mainz, Bonn and JLab and furthermore recoil polarization measurements by nucleon rescattering has been shown to be doable. This was the start of new efforts in different groups in order to achieve the complete experimental information and a model-independent partial wave analysis [5–8].

2 Complete experiments

A complete experiment is a set of measurements which is sufficient to predict all other possible experiments, provided that the measurements are free of uncertainties. Therefore it is first of all an academic problem, which can be solved by mathematical algorithms. In practise, however, it will not work in the same way and either a very high statistical precision would be required, which is very unlikely, or further measurements of other polarization observables are necessary. Both problems, first the mathematical problem but also the problem for a physical experiment can be studied with the help of state-of-the-art models like MAID or partial wave analyses (PWA) like SAID. With high precision calculations the complete sets of observables can be checked and with pseudo-data, generated from models and PWA, real experiments can be simulated under realistic conditions.

2.1 Coordinate Frames

Experiments with three types of polarization can be performed in meson photo-production: photon beam polarization, polarization of the target nucleon and polarization of the recoil nucleon. Target polarization will be described in the frame $\{x, y, z\}$, see Fig. 1, with the z -axis pointing into the direction of the photon momentum $\hat{\mathbf{k}}$, the y -axis perpendicular to the reaction plane, $\hat{\mathbf{y}} = \hat{\mathbf{k}} \times \hat{\mathbf{q}} / \sin \theta$, and the x -axis is given by $\hat{\mathbf{x}} = \hat{\mathbf{y}} \times \hat{\mathbf{z}}$. For recoil polarization, traditionally the frame $\{x', y', z'\}$ is used, with the z' -axis defined by the momentum vector of the outgoing meson $\hat{\mathbf{q}}$, the y' -axis is the same as for target polarization and the x' -axis given by $\hat{\mathbf{x}}' = \hat{\mathbf{y}}' \times \hat{\mathbf{z}}'$.

The photon polarization can be linear or circular. For a linear photon polarization ($P_T = 1$) in the reaction plane ($\hat{\mathbf{x}}, \hat{\mathbf{z}}$), $\varphi = 0$. Perpendicular, in direction $\hat{\mathbf{y}}$, the polarization angle is $\varphi = \pi/2$. Finally, for right-handed circular polarization, $P_\odot = +1$.

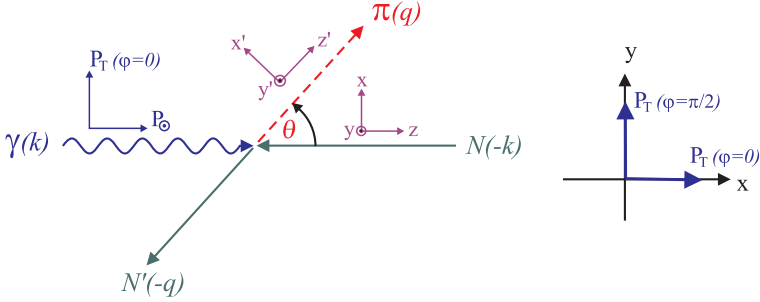


Fig. 1. Frames for polarization vectors in the CM.

The polarized differential cross section can be classified into three classes of double polarization experiments:

polarized photons and polarized target (types (S, BT))

$$\frac{d\sigma}{d\Omega} = \sigma_0 \{ 1 - P_T \Sigma \cos 2\varphi + P_x (-P_T H \sin 2\varphi + P_\odot F) + P_y (T - P_T P \cos 2\varphi) + P_z (P_T G \sin 2\varphi - P_\odot E) \}, \quad (1)$$

polarized photons and recoil polarization (types (S, BR))

$$\frac{d\sigma}{d\Omega} = \sigma_0 \{ 1 - P_T \Sigma \cos 2\varphi + P_{x'} (-P_T O_{x'} \sin 2\varphi - P_\odot C_{x'}) + P_{y'} (P - P_T T \cos 2\varphi) + P_{z'} (-P_T O_{z'} \sin 2\varphi - P_\odot C_{z'}) \}, \quad (2)$$

polarized target and recoil polarization (types (S, TR))

$$\frac{d\sigma}{d\Omega} = \sigma_0 \{ 1 + P_y T + P_{y'} P + P_{x'} (P_x T_{x'} - P_z L_{x'}) + P_{y'} P_y \Sigma + P_{z'} (P_x T_{z'} + P_z L_{z'}) \}. \quad (3)$$

In these equations σ_0 denotes the unpolarized differential cross section, Σ, T, P are single-spin asymmetries (S), E, F, G, H the beam-target asymmetries (BT),

$O_{x'}$, $O_{z'}$, $C_{x'}$, $C_{z'}$ the beam-recoil asymmetries (\mathcal{BR}) and $T_{x'}$, $T_{z'}$, $L_{x'}$, $L_{z'}$ the target-recoil asymmetries (\mathcal{TR}). The polarization quantities are described in Fig. 1. The signs of the 16 polarization observables of Eq. (1,2,3) are in principle arbitrary, except for the cross section σ_0 , which is naturally positive. For the 15 asymmetries we use the sign convention of Barker et al. [1], which is also used by the MAID and SAID partial wave analysis groups. For other sign conventions, see Ref. [9].

2.2 Amplitude analysis

Pseudoscalar meson photoproduction has 8 spin degrees of freedom, and due to parity conservation it can be described by 4 complex amplitudes of 2 kinematical variables. Possible sets of amplitudes are: Invariant amplitudes A_i , CGLN amplitudes F_i , helicity amplitudes H_i or transversity amplitudes b_i . All of them are linearly related to each other and further combinations are possible. Most often in the literature the helicity basis was chosen and the 16 possible polarization observables can be expressed in bilinear products

$$O_i(W, \theta) = \frac{q}{k} \sum_{k, \ell=1}^4 \alpha_{k, \ell} H_k(W, \theta) H_\ell^*(W, \theta), \quad (4)$$

where O_1 is the unpolarized differential cross section σ_0 and all other observables are products of asymmetries with σ_0 , for details see Table 1.

From a complete set of 8 measurements $\{O_i(W, \theta)\}$ one can determine the moduli of the 4 amplitudes and 3 relative phases. But there is always an unknown overall phase, e.g. $\phi_1(W, \theta)$, which can not be determined by additional measurements. This is, however, not a principal problem as with the principally undetermined phase of a quantum mechanical wave function. Already in 1963 Goldberger et al. [10] discussed a method using the idea of a Hanbury-Brown and Twiss experiment, and very recently in 2012, Ivanov [11] discussed another method using vortex beams to measure the phase of a scattering amplitude. Both methods, however, are highly impractical for a meson photoproduction experiment.

Therefore, the complete information is contained in a set of 4 reduced amplitudes,

$$\tilde{H}_i(W, \theta) = H_i(W, \theta) e^{-i \phi_1(W, \theta)} \quad (5)$$

of which \tilde{H}_1 is a real function, the others are complex, resulting in a total of 7 real values for any given W and θ .

Figure 2 shows two of such amplitude analyses with a complete set of 8 observables and an overcomplete set of 10 observables. The data used for this analysis has been generated as pseudo-data from Monte-Carlo events according to the Maid2007 solution, see Sect. 3. The figure shows the real parts of two out of four reduced helicity amplitudes, $\text{Re}\tilde{H}_1$ and $\text{Re}\tilde{H}_4$. While the solution with the complete set of 8 observables results in a rather bad description of the true amplitudes, the solution of the overcomplete set gives a satisfactory result.

Table 1. Spin observables for pseudoscalar meson photoproduction involving beam, target and recoil polarization in 4 groups, \mathcal{S} , \mathcal{BT} , \mathcal{BR} , \mathcal{TR} . A phase space factor q/k has been omitted in all expressions and the asymmetries are given by $\Lambda = \hat{\Lambda}/\sigma_0$. In column 2 the observables are expressed in terms of the Walker helicity amplitudes [12] and in column 3 in $\sin \theta$ and $x = \cos \theta$ with the leading terms for an S, P wave truncation.

Spin Obs	Helicity Representation	Partial Wave Expansion
σ_0	$\frac{1}{2}(H_1 ^2 + H_2 ^2 + H_3 ^2 + H_4 ^2)$	$A_0^\sigma + A_1^\sigma x + A_2^\sigma x^2 + \dots$
$\hat{\Sigma}$	$\text{Re}(H_1 H_4^* - H_2 H_3^*)$	$\sin^2 \theta (A_0^\Sigma + \dots)$
\hat{T}	$\text{Im}(H_1 H_2^* + H_3 H_4^*)$	$\sin \theta (A_0^T + A_1^T x + \dots)$
\hat{P}	$-\text{Im}(H_1 H_3^* + H_2 H_4^*)$	$\sin \theta (A_0^P + A_1^P x + \dots)$
\hat{G}	$-\text{Im}(H_1 H_4^* + H_2 H_3^*)$	$\sin^2 \theta (A_0^G + \dots)$
\hat{H}	$-\text{Im}(H_1 H_3^* - H_2 H_4^*)$	$\sin \theta (A_0^H + A_1^H x + \dots)$
\hat{E}	$\frac{1}{2}(- H_1 ^2 + H_2 ^2 - H_3 ^2 + H_4 ^2)$	$A_0^E + A_1^E x + A_2^E x^2 + \dots$
\hat{F}	$\text{Re}(H_1 H_2^* + H_3 H_4^*)$	$\sin \theta (A_0^F + A_1^F x + \dots)$
$\hat{O}_{x'}$	$-\text{Im}(H_1 H_2^* - H_3 H_4^*)$	$\sin \theta (A_0^{O_{x'}} + A_1^{O_{x'}} x + A_2^{O_{x'}} x^2 + \dots)$
$\hat{O}_{z'}$	$\text{Im}(H_1 H_4^* - H_2 H_3^*)$	$\sin^2 \theta (A_0^{O_{z'}} + A_1^{O_{z'}} x + \dots)$
$\hat{C}_{x'}$	$-\text{Re}(H_1 H_3^* + H_2 H_4^*)$	$\sin \theta (A_0^{C_{x'}} + A_1^{C_{x'}} x + A_2^{C_{x'}} x^2 + \dots)$
$\hat{C}_{z'}$	$\frac{1}{2}(- H_1 ^2 - H_2 ^2 + H_3 ^2 + H_4 ^2)$	$A_0^{C_{z'}} + A_1^{C_{z'}} x + A_2^{C_{z'}} x^2 + A_3^{C_{z'}} x^3 + \dots$
$\hat{T}_{x'}$	$\text{Re}(H_1 H_4^* + H_2 H_3^*)$	$\sin^2 \theta (A_0^{T_{x'}} + A_1^{T_{x'}} x + \dots)$
$\hat{T}_{z'}$	$\text{Re}(H_1 H_2^* - H_3 H_4^*)$	$\sin \theta (A_0^{T_{z'}} + A_1^{T_{z'}} x + A_2^{T_{z'}} x^2 + \dots)$
$\hat{L}_{x'}$	$-\text{Re}(H_1 H_3^* - H_2 H_4^*)$	$\sin \theta (A_0^{L_{x'}} + A_1^{L_{x'}} x + A_2^{L_{x'}} x^2 + \dots)$
$\hat{L}_{z'}$	$\frac{1}{2}(H_1 ^2 - H_2 ^2 - H_3 ^2 + H_4 ^2)$	$A_0^{L_{z'}} + A_1^{L_{z'}} x + A_2^{L_{z'}} x^2 + A_3^{L_{z'}} x^3 + \dots$

2.3 Truncated partial wave analysis

Even with the help of unitarity in form of Watson's theorem, the angle-dependent phase $\phi_1(W, \theta)$ cannot be provided. This has very strong consequences, namely a partial wave decomposition would lead to wrong partial waves, which would be useless for nucleon resonance analysis. It becomes obvious in the following schematic formula

$$f_\ell(W) = \frac{2}{2\ell + 1} \int \tilde{H}(W, \theta) e^{i\phi(W, \theta)} P_\ell(\cos \theta) d \cos \theta, \quad (6)$$

where the desired partial wave $f_\ell(W)$ cannot be obtained from the reduced helicity amplitudes $\tilde{H}(W, \theta)$ alone, as long as the angle dependent phase $\phi(W, \theta)$ is unknown.

Our main goal in the data analysis of photoproduction is the search for nucleon resonances and their properties. To better reach this goal, one can directly perform a partial wave analysis from the observables without going through the underlying helicity amplitudes. Such an analysis would be a truncated partial wave analysis (TPWA) with a minimal model dependence (i) from the truncation of the series at a maximal angular momentum ℓ_{\max} and (ii) from an overall unknown phase as in the case of the amplitude analysis in the previous paragraph. However, in the TPWA the overall phase would be only a function of energy and with additional theoretical help it can be constrained without strong model as-

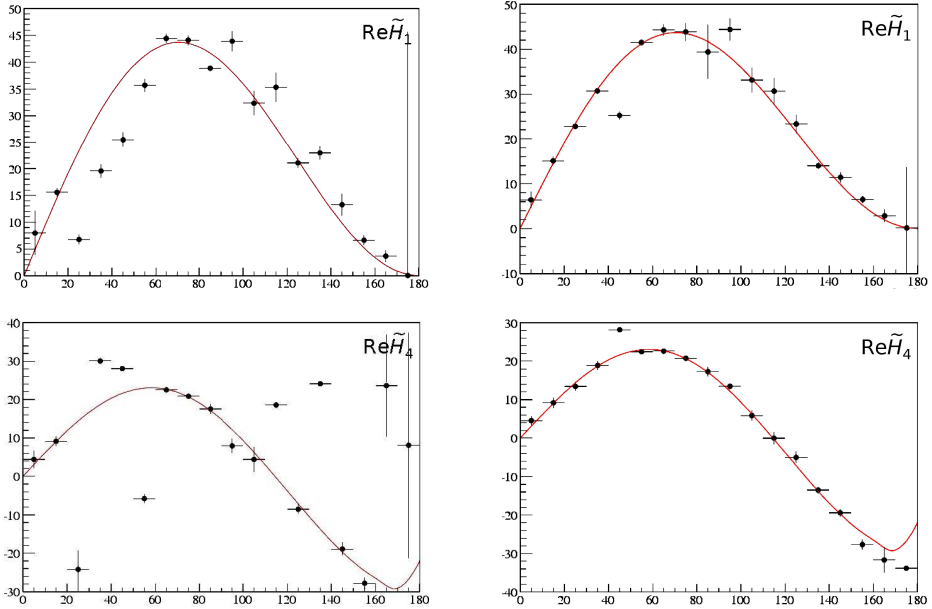


Fig. 2. Comparison of the reduced helicity amplitudes $\text{Re}\tilde{H}_1$ and $\text{Re}\tilde{H}_4$ between a pseudo-data analysis with a complete dataset of 8 observables: $\sigma_0, \Sigma, T, P, E, G, O_{x'}, C_{x'}$ (left 2 panels) and with an overcomplete dataset of 10 observables with additional F, H (right 2 panels) for $\gamma p \rightarrow \pi^0 p$ at $E = 320$ MeV as a function of the c.m. angle θ . The solid red curves show the MAID2007 solutions. Amplitudes are in units of $10^{-3}/m_{\pi^+}$.

sumptions. Such a concept was already discussed and applied for γ, π in the 80s by Grushin [13] for a PWA in the region of the $\Delta(1232)$ resonance.

Formally, the truncated partial wave analysis can be performed in the following way. All observables can be expanded either in a Legendre series or in a $\cos \theta$ series

$$O_i(W, \theta) = \frac{q}{k} \sin^{\alpha_i} \theta \sum_{k=0}^{2\ell_{\max} + \beta_i} A_k^i(W) \cos^k \theta, \quad (7)$$

$$A_k^i(W) = \sum_{\ell, \ell'=0}^{\ell_{\max}} \sum_{k, k'=1}^4 \alpha_{\ell, \ell'}^{k, k'} \mathcal{M}_{\ell, k}(W) \mathcal{M}_{\ell', k'}^*(W), \quad (8)$$

where k, k' denote the 4 possible electric and magnetic multipoles for each πN angular momentum $\ell \geq 2$, namely $\mathcal{M}_{\ell, k} = \{E_{\ell+}, E_{\ell-}, M_{\ell+}, M_{\ell-}\}$. For an S, P truncation ($\ell_{\max} = 1$) there are 4 complex multipoles $E_{0+}, E_{1+}, M_{1+}, M_{1-}$ leading to 7 free real parameters and an arbitrary phase, which can be put to zero for the beginning. In Table 1 we list the expansion coefficients for all observables that appear in an S, P wave expansion. Already from the 8 observables of the first two groups (S, BT) one can measure a set of 16 coefficients, from which we only need 8 well selected ones for a unique mathematical solution. This can be achieved by a measurement of the angular distributions of only 5 observables, e.g. $\sigma_0, \Sigma, T, P, F$ or $\sigma_0, \Sigma, T, F, G$. In the first example one gets even 10 coefficients, from which e.g.

A_1^P and A_0^F can be omitted. In the second case, there are 9 coefficients, of which A_0^F can be omitted. In practise one can select those coefficients, which have the smallest statistical errors, and therefore, the biggest impact for the analysis by keeping in mind that all discrete ambiguities are resolved.

As has been shown by Omelaenko [14] the same is true for any PWA with truncation at ℓ_{\max} . For the determination of the $8\ell_{\max} - 1$ free parameters one has the possibility to measure $(8\ell_{\max}, 8\ell_{\max}, 8\ell_{\max} + 4, 8\ell_{\max} + 4)$ coefficients for types (S, BT, BR, TR), respectively.

3 Partial wave analysis with pseudo-data

In a first numerical attempt towards a model-independent partial wave analysis, a procedure similar to the second method, the TPWA, described above, has been applied [6], and pseudo-data, generated for γ, π^0 and γ, π^+ have been analyzed.

Events were generated over an energy range from $E_{\text{lab}} = 200 - 1200$ MeV and a full angular range of $\theta = 0 - 180^\circ$ for beam energy bins of $\Delta E_\gamma = 10$ MeV and angular bins of $\Delta\theta = 10^\circ$, based on the MAID2007 model predictions [15]. For each observable, typically $5 \cdot 10^6$ events have been generated over the full energy range. For each energy bin a single-energy (SE) analysis has been performed using the SAID PWA tools [16].

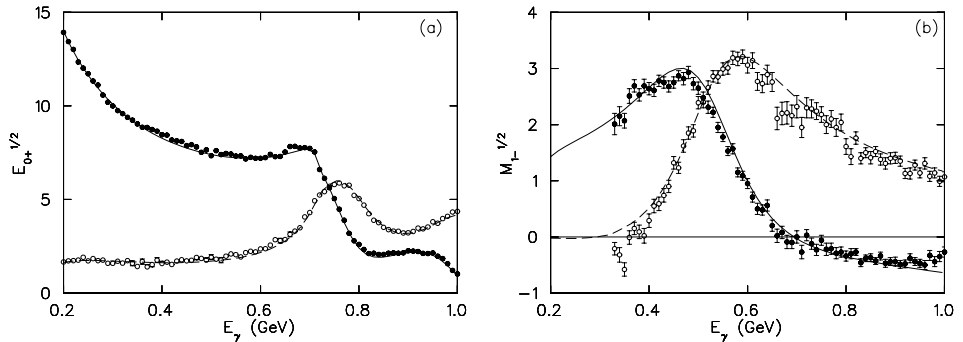


Fig. 3. Real and imaginary parts of (a) the S_{11} partial wave amplitude $E_{0+}^{1/2}$ and (b) the P_{11} partial wave amplitude $M_{1-}^{1/2}$. The solid (dashed) line shows the real (imaginary) part of the MAID2007 solution, used for the pseudo-data generation. Solid (open) circles display real (imaginary) single-energy fits (SE6p) to the following 6 observables without any recoil polarization measurement: $d\sigma/d\Omega$, two single-spin observables Σ, T and three beam-target double polarization observables E, F, G . Multipoles are in millifermi units.

A series of fits, SE4p, SE6p and SE8p have been performed [6] using 4, 6 and 8 observables, respectively. Here the example using 6 observables ($\sigma_0, \Sigma, T, E, F, G$) is demonstrated, where no recoil polarization has been used. As explained before, such an experiment would be incomplete in the sense of an ‘amplitude analysis’, but complete for a truncated partial wave analysis. In Fig. 3 two multipoles $E_{0+}^{1/2}$ and $M_{1-}^{1/2}$ for the S_{11} and P_{11} channels are shown and the SE6p fits are compared to the MAID2007 solution. The fitted SE solutions are very close to the MAID

solution with very small uncertainties for the S_{11} partial wave. For the P_{11} partial wave we obtain a larger statistical spread of the SE solutions. This is typical for the $M_{1-}^{1/2}$ multipole, which is generally much more difficult to obtain with good accuracy [15], because of the weaker sensitivity of the observables to this magnetic multipole. But also this multipole can be considerably improved in an analysis with 8 observables [6].

4 Summary and conclusions

It is shown that for an analysis of N^* resonances, the amplitude analysis of a complete experiment is not very useful, because of an unknown energy and angle dependent phase that can not be determined by experiment and can not be provided by theory without a strong model dependence. However, the same measurements or even less will be very useful for a truncated partial wave analysis with minimal model dependence due to truncations and extrapolations of Watson's theorem in the inelastic energy region. A further big advantage of such a PWA is a different counting of the necessary polarization observables, resulting in very different sets of observables. While it is certainly helpful to have polarization observables from 3 or 4 different types, for a mathematical solution of the bilinear equations one can find minimal sets of only 5 observables from only 2 types, where either a polarized target or recoil polarization measurements can be completely avoided.

I would like to thank R. Workman, M. Ostrick and S. Schumann for their contributions to this ongoing work. I want to thank the Deutsche Forschungsgemeinschaft for the support by the Collaborative Research Center 1044.

References

1. I. S. Barker, A. Donnachie, J. K. Storrow, Nucl. Phys. B **95**, 347 (1975).
2. C. G. Fasano, F. Tabakin, B. Saghai, Phys. Rev. C **46**, 2430 (1992).
3. G. Keaton and R. Workman, Phys. Rev. C **54**, 1437 (1996).
4. W.-T. Chiang and F. Tabakin, Phys. Rev. C **55**, 2054 (1997).
5. R. L. Workman, Phys. Rev. C **83**, 035201 (2011).
6. R. L. Workman, M. W. Paris, W. J. Briscoe, L. Tiator, S. Schumann, M. Ostrick and S. S. Kamalov, Eur. Phys. J. A **47**, 143 (2011).
7. B. Dey, M. E. McCracken, D. G. Ireland, C. A. Meyer, Phys. Rev. C **83**, 055208 (2011).
8. A. M. Sandorfi, S. Hoblit, H. Kamano, T. -S. H. Lee, J. Phys. G **38**, 053001 (2011).
9. A. M. Sandorfi, B. Dey, A. Sarantsev, L. Tiator and R. Workman, AIP Conf. Proc. **1432**, 219 (2012).
10. M. L. Goldberger, H. W. Lewis and K. M. Watson, Phys. Rev. **132**, 2764 (1963).
11. I. P. Ivanov, Phys. Rev. D **85**, 076001 (2012).
12. R. L. Walker, Phys. Rev. **182**, 1729 (1969).
13. V. F. Grushin, in *Photoproduction of Pions on Nucleons and Nuclei*, edited by A. A. Komar, (Nova Science, New York, 1989), p. 1ff.
14. A. S. Omelaenko, Sov. J. Nucl. Phys. **34**, 406 (1981).
15. D. Drechsel, S. S. Kamalov, L. Tiator, Eur. Phys. J. A **34**, 69 (2007).
16. R. A. Arndt, R. L. Workman, Z. Li *et al.*, Phys. Rev. C **42**, 1853 (1990).



News from Belle: Recent Spectroscopy Results

M. Bračko*

University of Maribor, Smetanova ulica 17, SI-2000 Maribor, Slovenia and
Jožef Stefan Institute, Jamova cesta 39, SI-1000 Ljubljana, Slovenia

Abstract. This paper reports on some of the latest spectroscopic measurements performed with the experimental data collected by the Belle spectrometer, which has been operating at the KEKB asymmetric-energy e^+e^- collider in the KEK laboratory in Tsukuba, Japan.

1 Introduction

The Belle detector [1] at the asymmetric-energy e^+e^- collider KEKB [2] has accumulated about 1 ab^{-1} of data by the end of its operation in June 2010. The KEKB collider, called a *B-factory*, most of the time operated near the $\Upsilon(4S)$ resonance, but it has accumulated substantial data samples also at other Υ resonances, like $\Upsilon(1S)$, $\Upsilon(2S)$ and $\Upsilon(5S)$, as well as in the nearby continuum. In particular, the data samples at the $\Upsilon(4S)$ and $\Upsilon(5S)$ resonances are by far the largest available in the world, corresponding to integrated luminosities of 798 fb^{-1} and 123 fb^{-1} , respectively. Large amount of collected experimental data and excellent detector performance enabled many interesting spectroscopic results, including discoveries of new hadronic states and studies of their properties. This report covers most recent and interesting spectroscopic measurements—performed with either charmonium(-like) and bottomonium(-like) states.

2 Bottomonium and Bottomonium-like States

The Belle collaboration used a data sample at the CM energy around the $\Upsilon(5S)$ mass 10.89 GeV , and found large signals for decays into $\pi^+\pi^-\Upsilon(1S)$, $\pi^+\pi^-\Upsilon(2S)$ and $\pi^+\pi^-\Upsilon(3S)$ final states [3]. If these transitions are only from the $\Upsilon(5S)$ resonance, then the corresponding partial widths are more than two orders of magnitude larger than the corresponding partial widths for $\Upsilon(4S)$, $\Upsilon(3S)$ and $\Upsilon(2S)$ decays to $\pi^+\pi^-\Upsilon(1S)$. These results motivate a search for the $h_b(mP)$ resonances in the $\Upsilon(5S)$ data. $h_b(1P)$ and $h_b(2P)$ states are observed in the missing mass spectrum of $\pi^+\pi^-$ pairs for the $\Upsilon(5S)$ decays, with significances of 5.5σ and 11.2σ , respectively [4]. This is the first observation of the $h_b(1P)$ and $h_b(2P)$ spin-singlet bottomonium states in the reaction $e^+e^- \rightarrow h_b(mP)\pi^+\pi^-$ at the $\Upsilon(5S)$ energy. Later $h_b(1P)$ and $h_b(2P)$ were studied in the $\Upsilon(5S) \rightarrow h_b\pi^+\pi^- \rightarrow \gamma\eta_b(1S)\pi^+\pi^-$

* Representing the Belle Collaboration.

Decay mode	Branching fraction in %
$h_b(1P) \rightarrow \gamma\eta_b(1S)$	$49.2 \pm 5.7^{+5.6}_{-3.3}$
$h_b(2P) \rightarrow \gamma\eta_b(1S)$	$22.3 \pm 3.8^{+3.1}_{-3.3}$
$h_b(2P) \rightarrow \gamma\eta_b(2S)$	$47.5 \pm 10.5^{+6.8}_{-7.7}$

Table 1. The branching fractions for $h_b \rightarrow \gamma\eta_b$ decays, as measured by Belle.

decay [5]. In the same final state, Belle observes [5] also the first evidence for a $\eta_b(2S)$ in $\Upsilon(5S) \rightarrow h_b(2P)\pi^+\pi^- \rightarrow \gamma\eta_b(2S)\pi^+\pi^-$ decay. The width of $\eta_b(2S)$ is small, with $\Gamma = (4 \pm 8)$ MeV. Branching fractions for observed radiative h_b decays are summarized in Table 1.

Comparable rates of $h_b(1P)$ and $h_b(2P)$ production indicate a possible exotic process that violates heavy quark spin-flip and this motivates a further study of the resonant structure in $\Upsilon(5S) \rightarrow h_b(mP)\pi^+\pi^-$ and $\Upsilon(5S) \rightarrow \Upsilon(nS)\pi^+\pi^-$ decays [6]. Due to the limited statistics, only the study of $M(h_b(mP)\pi)$ distribution is possible for $h_b(mP)\pi^+\pi^-$, while in the case of $\Upsilon(nS)\pi^+\pi^-$ decay modes the Dalitz plot analysis can be performed. As a result, two charged bottomonium-like resonances, $Z_b(10610)$ and $Z_b(10650)$, are observed with signals in five different decay channels, $\Upsilon(nS)\pi^\pm$ ($n = 1, 2, 3$) and $h_b(mP)\pi^\pm$ ($m = 1, 2$). The averaged values for the mass and widths of the two states are calculated to be: $M(Z_b(10610)) = (10607.2 \pm 2.0)$ MeV, $\Gamma(Z_b(10610)) = (18.4 \pm 2.4)$ MeV and $M(Z_b(10650)) = (10652.2 \pm 1.5)$ MeV, $\Gamma(Z_b(10650)) = (11.5 \pm 2.2)$ MeV. The measured masses are only a few MeV above the thresholds for the open beauty channels $B^*\bar{B}$ (10604.6 MeV) and $B^*\bar{B}^*$ (10650.2 MeV) [9], which could indicate a molecular nature of the two observed states. Angular analysis of charged pion distributions favours the $J^P = 1^+$ spin-parity assignment for both $Z_b(10610)$ and $Z_b(10650)$.

3 Charmonium and Charmonium-like States

There has been a renewed interest in charmonium spectroscopy since 2002. The attention to this field was drawn by the discovery of the two missing $c\bar{c}$ states below the open-charm threshold, $\eta_c(2S)$ and $h_c(1P)$ [7,8] with $J^{PC}=0^{-+}$ and 1^{+-} , respectively, but even with the discoveries of new new charmonium-like states (so called “XYZ” states).

3.1 The X(3872) news

The story about the so called “XYZ” states began in 2003, when Belle reported on $B^+ \rightarrow K^+J/\psi\pi^+\pi^-$ analysis, where a new state decaying to $J/\psi\pi^+\pi^-$ was discovered [10]. The new state, called X(3872), was soon confirmed and also intensively studied by the CDF, DØ and BABAR collaborations [11–19]. So far it has been established that this narrow state ($\Gamma = (3.0^{+1.9}_{-1.4} \pm 0.9)$ MeV) has a mass of

(3872.2 ± 0.8) MeV, which is very close to the $D^0\bar{D}^{*0}$ threshold [9]. The intensive studies of several $X(3872)$ production and decay modes suggest two possible J^{PC} assignments, 1^{++} and 2^{-+} , and establish the $X(3872)$ as a candidate for a loosely bound $D^0\bar{D}^{*0}$ molecular state. However, results provided substantial evidence that the $X(3872)$ state must contain a significant $c\bar{c}$ component as well.

Recently, Belle performed a study of $B \rightarrow (c\bar{c}\gamma)K$ using the final data sample with 772 million of $B\bar{B}$ pairs collected at the $\Upsilon(4S)$ resonance [20]. Pure $D^0\bar{D}^{*0}$ molecular model [21] predicts $\mathcal{B}(X(3872) \rightarrow \psi'\gamma)$ to be less than $\mathcal{B}(X(3872) \rightarrow J/\psi\gamma)$. Results by the *BABAR* collaboration [19] show that $\mathcal{B}(X(3872) \rightarrow \psi'\gamma)$ is almost three times that of $\mathcal{B}(X(3872) \rightarrow J/\psi\gamma)$, which is inconsistent with the pure molecular model, and can be interpreted as a large $c\bar{c} - D^0\bar{D}^{*0}$ admixture. We observe $X(3872) \rightarrow J/\psi\gamma$ together with an evidence for $\chi_{c2} \rightarrow J/\psi\gamma$ in $B^\pm \rightarrow J/\psi\gamma K^\pm$ decays, while in our search for $X(3872) \rightarrow \psi'\gamma$ no significant signal is found. We also observe $B \rightarrow \chi_{c1}K$ decays in both, charged as well as neutral B decays. The obtained results suggest that the $c\bar{c}$ - $D^0\bar{D}^{*0}$ admixture in $X(3872)$ may not be as large as discussed above.

New results for the $X(3872) \rightarrow J/\psi\pi^+\pi^-$ decay modes in $B^+ \rightarrow K^+X(3872)$ and $B^0 \rightarrow K^0 (\rightarrow \pi^+\pi^-)X(3872)$ decays are obtained with the complete Belle data set of 772 million $B\bar{B}$ pairs collected at the $\Upsilon(4S)$ resonance [22]. The results for the $X(3872)$ mass and width are obtained by a 3-dimensional fit to distributions of the three variables: beam-constrained-mass $M_{bc} = \sqrt{(E_{beam}^{cms})^2 - (p_B^{cms})^2}$ (with the beam energy E_{beam}^{cms} and the B-meson momentum p_B^{cms} both measured in the centre-of-mass system), the invariant mass $M_{inv}(J/\psi\pi^+\pi^-)$ and the energy difference $\Delta E = E_B^{cms} - E_{beam}^{cms}$ (where E_B^{cms} is the B-meson energy in the centre-of-mass system). As a first step, the fit is performed for the reference channel $\psi' \rightarrow J/\psi\pi^+\pi^-$, and the resolution parameters are then fixed for the fit of the $X(3872)$. The mass, determined by the fit, is $(3871.84 \pm 0.27 \pm 0.19)$ MeV. Including the new Belle result, the updated world-average mass of the $X(3872)$ is $m_X = (3871.67 \pm 0.17)$ MeV. If the $X(3872)$ is an S-wave $D^{*0}\bar{D}^0$ molecular state, the binding energy E_b would be given by the mass difference $m(X) - m(D^{*0}) - m(D^0)$. With the current value of $m(D^0) + m(D^{*0}) = (3871.79 \pm 0.30)$ MeV [9], a binding energy of $E_b = (-0.12 \pm 0.35)$ MeV can be calculated, which is surprisingly small and would indicate a very large radius of the molecular state.

The best upper limit for the $X(3872)$ width was 2.3 MeV (with 90% C.L.), obtained by previous Belle measurement [10]. The 3-dimensional fits are more sensitive to the natural width, which is smaller than the detector resolution ($\sigma \sim 4$ MeV). Due to the fit sensitivity and the calibration performed on the reference channel $\psi' \rightarrow J/\psi\pi^+\pi^-$, the updated upper limit for the $X(3872)$ width is about 1/2 of the previous value: $\Gamma(X(3872)) < 1.2$ MeV at 90% C.L.

Previous studies performed by several experiments suggested two possible J^{PC} assignments for the $X(3872)$, 1^{++} and 2^{-+} . In the recent Belle analysis [20], the $X(3872)$ quantum numbers were also studied with the full available data sample collected at the $\Upsilon(4S)$ resonance. At the current level of statistical sensitivity it is not possible to distinguish completely between the two possible quantum number assignments, so both hypotheses are still allowed. Possible C-odd neu-

tral partners of $X(3872)$ are also searched, but no signal is found for this type of states.

4 Summary and Conclusions

Many new particles have already been discovered during the operation of the Belle experiment at the KEKB collider, and some of them are mentioned in this report. Some recent Belle results also indicate that analogs to exotic charmonium-like states can be found in $b\bar{b}$ systems. Although the operation of the experiment has finished, data analyses are still ongoing and therefore more interesting results on charmonium(-like) and bottomonium(-like) spectroscopy can still be expected from Belle in the near future.

References

1. Belle Collaboration, *Nucl. Instrum. Methods A* **479**, 117 (2002).
2. S. Kurokawa and E. Kikutani, *Nucl. Instrum. Methods A* **499**, 1 (2003), and other papers included in this Volume.
3. Belle Collaboration, *Phys. Rev. Lett.* **100**, 112001 (2008); *Phys. Rev. D* **82**, 091106 (2010).
4. Belle Collab., *Phys. Rev. Lett.* **108**, 032001 (2012).
5. Belle Collab., arXiv:1205.6351 [hep-ex], to appear in *Phys. Rev. Lett.* .
6. Belle Collaboration, *Phys. Rev. Lett.* **108**, 122001 (2012).
7. Belle Collaboration, *Phys. Rev. Lett.* **89**, 102001 (2002).
8. Cleo Collaboration, *Phys. Rev. Lett.* **95**, 102003 (2005).
9. K. Nakamura *et al.* (Particle Data Group), *J. Phys. G* **37**, 075021 (2010).
10. Belle Collaboration, *Phys. Rev. Lett.* **91**, 262001 (2003).
11. CDF Collaboration, *Phys. Rev. Lett.* **93**, 072001 (2004); DØ Collaboration, *Phys. Rev. Lett.* **93**, 162002 (2004); BABAR Collaboration, *Phys. Rev. D* **71**, 071103 (2005).
12. Belle Collaboration, arXiv:hep-ex/0505037, arXiv:hep-ex/0505038; submitted to the Lepton-Photon 2005 Conference.
13. Belle Collaboration, *Phys. Rev. Lett.* **97**, 162002 (2006).
14. BABAR Collaboration, *Phys. Rev. D* **74**, 071101 (2006).
15. Belle Collaboration, arXiv:0809.1224v1 [hep-ex]; contributed to the ICHEP 2008 Conference.
16. Belle Collaboration, arXiv:0810.0358v2 [hep-ex]; contributed to the ICHEP 2008 Conference.
17. CDF Collaboration, *Phys. Rev. Lett.* **98**, 132002 (2007).
18. BABAR Collaboration, *Phys. Rev. D* **77**, 011102 (2008).
19. BABAR Collaboration, *Phys. Rev. Lett.* **102**, 132001 (2009).
20. Belle Collaboration, *Phys. Rev. Lett.* **107**, 091803 (2011).
21. E. S. Swanson, *Phys. Rep.* **429**, 243 (2006).
22. Belle Collaboration, *Phys. Rev. D* **84**, 052004(R) (2011).
23. CDF Collaboration, *Phys. Rev. Lett.* **103**, 152001 (2009).
24. BABAR Collaboration, *Phys. Rev. D* **77**, 111101(R) (2008).
25. LHCb Collab., Proc. XIX International Workshop on Deep-Inelastic Scattering and Related Subjects (DIS2011), LHCb-CONF-2011-021.



Meson electro-production in the region of the Delta(1700) D33 resonance

B. Golli

Faculty of Education, University of Ljubljana, 1000 Ljubljana, Slovenia and Jožef Stefan Institute, 1000 Ljubljana, Slovenia

Abstract. We apply a coupled channel formalism incorporating quasi-bound quark-model states to calculate the D13, D33 and D15 scattering and electro-production amplitudes. The meson-baryon vertices for πN , $\pi\Delta$ (s- and d-waves), ρN , $\pi N(1440)$, $\pi N(1535)$, $\pi\Delta(1600)$ and $\sigma\Delta(1600)$ channels are determined in the Cloudy Bag Model. We use the same values for the model parameters as in the case of the P11, P33 and S11 partial waves except for the strength of the coupling of the d-wave mesons to quarks which has to be increased in order to reproduce the width of the observed D-wave resonances. The electro-production amplitudes exhibit a consistent behavior in all channels but are too weak in the resonance region.

1 Introduction

This work is a continuation of a joint project on the description of baryon resonances performed by the Coimbra group (Manuel Fiolhais and Pedro Alberto) and the Ljubljana group (Simon Širca and B. G.) [1–9]. In our previous works [5–7] we have successfully applied our method which incorporates excited baryons represented as quasi-bound quark-model states into a coupled channel formalism using the K-matrix approach [5] to calculate the scattering and the electro-production amplitudes in the P11, P33 and S11 partial waves. In the present work we extend of the approach to low lying negative parity D-wave resonances.

In the next section we give a short review of the method and in the following sections we discuss in more detail scattering and electro-production in the D13 and D33 and D15 partial waves.

2 The method

We limit ourselves to a class of chiral quark models in which mesons couple linearly to the quark core. In such cases the elements of the K matrix in the basis with good total angular momentum J and isospin T can be cast in the form [5]:

$$K_{M'B'MB}^{JT} = -\pi \mathcal{N}_{M'B'} \langle \Psi_{JT}^{MB} \| V_{M'}(\mathbf{k}) \| \tilde{\Psi}_{B'} \rangle, \quad \mathcal{N}_{MB} = \sqrt{\frac{\omega_M \bar{E}_B}{k_M W}}. \quad (1)$$

Here ω_M and k_M are the energy and momentum of the incoming (outgoing) meson, $|\tilde{\Psi}_B\rangle$ is properly normalized baryon state and E_B is its energy, W is the invariant energy of the meson-baryon system, and $|\Psi^{MB}\rangle$ is the principal value state

$$|\Psi_{JT}^{MB}\rangle = \mathcal{N}_{MB} \left\{ [a^\dagger(k_M)|\tilde{\Psi}_B\rangle]^{JT} + \sum_{\mathcal{R}} c_{\mathcal{R}}^{MB} |\Phi_{\mathcal{R}}\rangle + \sum_{M'B'} \int \frac{dk \chi^{M'B'MB}(k, k_M)}{\omega_k + E_{B'}(k) - W} [a^\dagger(k)|\tilde{\Psi}_{B'}\rangle]^{JT} \right\}. \quad (2)$$

The first term represents the free meson ($\pi, \eta, \rho, K, \dots$) and the baryon ($N, \Delta, \Lambda, \dots$) and defines the channel, the next term is the sum over *bare* tree-quark states $\Phi_{\mathcal{R}}$ involving different excitation of the quark core, the third term introduces meson clouds around different isobars, $E(k)$ is the energy of the recoiled baryon. We assume that the two pion decay proceeds either through an unstable meson (ρ -meson, σ -meson, ...) or through a baryon resonance ($\Delta(1232), N^*(1440) \dots$). The meson amplitudes $\chi^{M'B'MB}(k, k_M)$ are proportional to the (half) off-shell matrix elements of the K-matrix and are determine by solving a Lippmann-Schwinger type of equation. The resulting matrix elements of the K-matrix take the form

$$K_{M'B'MB}(k, k_M) = - \sum_{\mathcal{R}} \frac{\mathcal{V}_{B\mathcal{R}}^M(k_M) \mathcal{V}_{B'\mathcal{R}}^{M'}(k)}{Z_{\mathcal{R}}(W)(W - W_{\mathcal{R}})} + K_{M'B'MB}^{\text{bkg}}(k, k_M), \quad (3)$$

where the first term represents the contribution of various resonances while $K_{M'B'MB}^{\text{bkg}}(k, k_M)$ originates in the non-resonant background processes. Here $\mathcal{V}_{B\mathcal{R}}^M$ is the dressed matrix element of the quark-meson interaction between the resonant state and the baryon state in the channel MB, and $Z_{\mathcal{R}}$ is the wave-function normalization. The physical resonant state \mathcal{R} is a superposition of the dressed states built around the bare 3-quark states $\Phi_{\mathcal{R}'}$. The T matrix is finally obtained by solving the Heitler's equation

$$T_{MBM'B'} = K_{MBM'B'} + i \sum_{M''B''} T_{MBM''B''} K_{M''B''M'B'}. \quad (4)$$

Considering meson electro-production, the T matrix for $\gamma N \rightarrow MB$ satisfies

$$T_{MB\gamma N} = K_{MB\gamma N} + i \sum_{M'B'} T_{MBM'B'} K_{M'B'\gamma N}. \quad (5)$$

In the vicinity of a chosen resonance (\mathcal{R}) we write (see (3)):

$$K_{MB\gamma N} = - \frac{\mathcal{V}_{B\mathcal{R}}^M \mathcal{V}_{N\mathcal{R}}^\gamma}{Z_{\mathcal{R}}(W)(W - W_{\mathcal{R}})} - \sum_{\mathcal{R}' \neq \mathcal{R}} \frac{\mathcal{V}_{B\mathcal{R}'}^M \mathcal{V}_{N\mathcal{R}'}^\gamma}{Z_{\mathcal{R}'}(W)(W - W_{\mathcal{R}'})} + B_{MB\gamma N}^{\text{bkg}}. \quad (6)$$

We manipulate the first term:

$$\frac{\mathcal{V}_{B\mathcal{R}}^M \mathcal{V}_{N\mathcal{R}}^\gamma}{Z_{\mathcal{R}}(W)(W - W_{\mathcal{R}})} = \frac{\mathcal{V}_{B\mathcal{R}}^M{}^2}{Z_{\mathcal{R}}(W)(W - W_{\mathcal{R}})} \frac{\mathcal{V}_{N\mathcal{R}}^\gamma}{\mathcal{V}_{B\mathcal{R}}^M} = \left(K_{MBMB} - K_{MBMB}^{\text{bkg}} \right) \frac{\mathcal{V}_{N\mathcal{R}}^\gamma}{\mathcal{V}_{B\mathcal{R}}^M}$$

so that (5) takes the form

$$\begin{aligned}
T_{MB\gamma N} &= \left(K_{MB\ MB} + i \sum_{M'B'} T_{MB\ M'B'} K_{M'B'\ MB} \right) \frac{\mathcal{V}_{NR}^\gamma}{\mathcal{V}_{BR}^M} \\
&\quad + K_{MB\ \gamma N}^{\text{bkg}} + i \sum_{M'B'} T_{MB\ M'B'} K_{M'B'\ \gamma N}^{\text{bkg}} \\
&= \frac{\mathcal{V}_{NR}^\gamma}{\mathcal{V}_{BR}^M} T_{MB\ MB} + T_{MB\ MB}^{\text{bkg}} \equiv T_{MB\ \gamma N}^{\text{res}} + T_{MB\ \gamma N}^{\text{bkg}}, \quad (7)
\end{aligned}$$

which means that the T matrix for elektro-production can be split into the resonant part and the background part; the latter is the solution of the Heitler equation with the "background" K-matrix defined as

$$K_{MB\ \gamma N}^{\text{bkg}} = -K_{MB\ MB}^{\text{bkg}} \frac{\mathcal{V}_{NR}^\gamma}{\mathcal{V}_{BR}^M} - \sum_{R' \neq R} \frac{\mathcal{V}_{BR}^M \mathcal{V}_{NR'}^\gamma}{Z_{R'}(W)(W - W_{R'})} + B_{MB\ \gamma N}^{\text{bkg}}.$$

Note that $\mathcal{V}_{NR}^\gamma(k_\gamma)$ is proportional to the helicity amplitudes while the strong amplitude $\mathcal{V}_{BR}^M(k_M)$ to $\sqrt{\Gamma_{MB}}$ and to ζ , the sign of the phase of the meson decay.

3 The D-wave resonances in the Cloudy Bag Model

In the quark model, the negative parity D-wave resonances are described by a single quark $l = 1$ orbital excitation. The two D13 (flavor octet, $J = \frac{3}{2}$) resonances are the superposition of the $S = \frac{1}{2}$ and $S = \frac{3}{2}$ configurations, the D33 resonance (flavour decouplet) has $S = \frac{1}{2}$, while the D15 resonance (octet, $J = \frac{5}{2}$) has $S = \frac{3}{2}$. We use the j-j coupling scheme in which the resonances take the following forms:

$$\begin{aligned}
N(1520)D13 &= -\sin \vartheta_d |^4 \mathbf{8}_{3/2} \rangle + \cos \vartheta_d |^2 \mathbf{8}_{3/2} \rangle \\
&= c_S^1 |(1s)^2 1p_{3/2} \rangle_{MS} + c_A^1 |(1s)^2 1p_{3/2} \rangle_{MA} + c_P^1 |(1s)^2 1p_{1/2} \rangle, \quad (8)
\end{aligned}$$

$$\begin{aligned}
N(1700)D13 &= \cos \vartheta_d |^4 \mathbf{8}_{3/2} \rangle + \sin \vartheta_d |^2 \mathbf{8}_{3/2} \rangle \\
&= c_S^2 |(1s)^2 1p_{3/2} \rangle_{MS} + c_A^2 |(1s)^2 1p_{3/2} \rangle_{MA} + c_P^2 |(1s)^2 1p_{1/2} \rangle, \quad (9)
\end{aligned}$$

$$\Delta(1700)D33 = |^2 \mathbf{10}_{3/2} \rangle = \frac{\sqrt{5}}{3} |(1s)^2 1p_{3/2} \rangle - \frac{2}{3} |(1s)^2 1p_{1/2} \rangle, \quad (10)$$

$$N(1675)D15 = |^4 \mathbf{8}_{5/2} \rangle = |(1s)^2 1p_{3/2} \rangle. \quad (11)$$

Here MS and MA denote the mixed symmetric and the mixed antisymmetric representation, and

$$c_S^1 = \frac{2}{3} \sin \vartheta_d + \sqrt{\frac{5}{18}} \cos \vartheta_d, \quad c_A^1 = -\frac{\sqrt{2}}{2} \cos \vartheta_d, \quad c_P^1 = -\frac{\sqrt{5}}{3} \sin \vartheta_d + \frac{\sqrt{2}}{3} \cos \vartheta_d. \quad (12)$$

The $l = 2$ pions couple only to $j = 3/2$ quarks; the corresponding interaction in the Cloudy Bag Model takes the form

$$V_{2\pi t}^\pi(k) = \frac{1}{2f_\pi} \sqrt{\frac{\omega_{p_{3/2}} \omega_s}{(\omega_{p_{3/2}} - 2)(\omega_s - 1)}} \frac{\sqrt{2}}{2\pi} \frac{k^2}{\sqrt{\omega_k}} \frac{j_2(kR)}{kR} \sum_{i=1}^3 \tau_t(i) \Sigma_{2m}^{[\frac{1}{2} \frac{3}{2}]}(i), \quad (13)$$

where

$$\Sigma_{1m}^{[\frac{1}{2}\frac{3}{2}]} = \sum_{m_s m_j} C_{\frac{1}{2}m_j 1m}^{\frac{1}{2}m_s} |sm_s\rangle \langle p_{3/2} m_j|, \quad \omega_s = 2.043, \quad \omega_{p_{3/2}} = 3.204.$$

In the case of P11, P33 and S11 waves we have used the bag radius $R = 0.83$ fm which determines the range of quark-pion interaction corresponding to the cut-off $\Lambda \sim 550$ MeV/c, and the value for $f_\pi = 76$ MeV which reproduces the experimental value of the πNN coupling constant. For the d-wave pions it turns out that the range predicted by (13) is too large while the resulting coupling strength is too weak. We have therefore modified the interaction in such a way as to correspond to $\Lambda \sim 550$ MeV/c, while the coupling strength has been increased by a factor 1.7 – 2.75 (depending on the considered resonance).

4 Scattering amplitudes

The effect of the form factor and the strength of quark-meson coupling discussed in the previous section is most clearly seen in the case of the D15 where the background effects as well as the influence of other resonances are almost negligible. Using our standard value for the cut-off parameter we have to increase the quark model coupling constant by a factor of 2.75 in order to obtain an almost perfect fit to the data in the region of the resonance.

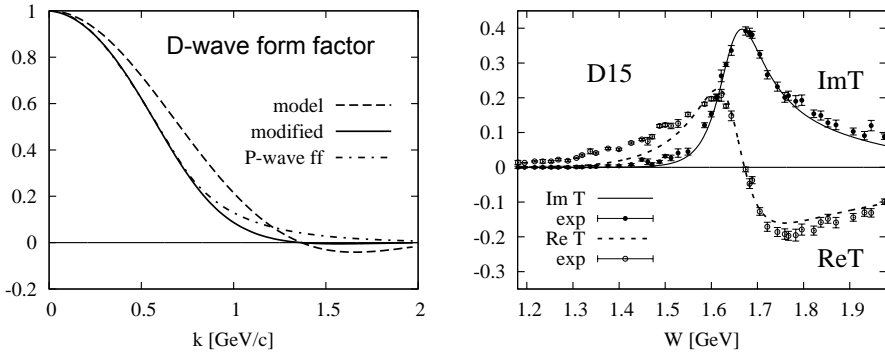


Fig. 1. The form factor for the D-wave pions (left panel), and the real and the imaginary part of the D15 scattering amplitude (right). The data points are from [10].

The data for elastic scattering in the D13 partial wave show almost no sign of the second resonance N(1700). Since the $l = 2$ pions most strongly couple to the $|(1s)^2 1p_{3/2}\rangle_{MA}$ configuration, the absence of the second resonance can be most easily explained by the vanishing of the c_Λ^2 coefficient in (9), $c_\Lambda^2 = -\sin\theta_d/\sqrt{2}$. This suggests $\theta_d = 0$. In our model the resonances are mixed through the pion interaction which changes slightly the above conclusion leading to the choice $\theta_d \approx 10^\circ$ for the optimal mixing. At this energy range the effect of the cut-off is less pronounced; the quark-model prediction for the πNR coupling constant has to be increased by a factor of 1.7, while that to the Δ decreased by a factor of one half.

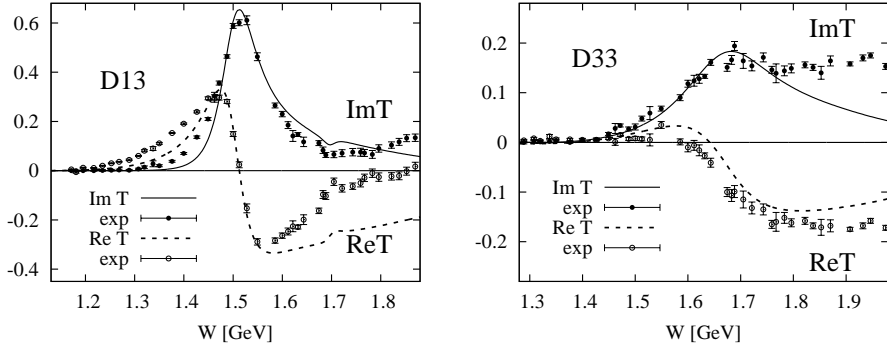


Fig. 2. The real and the imaginary part of the D13 wave scattering amplitude (left), and for the D33 wave (right). The data points are from [10].

In the vicinity of the D33 resonance the elastic amplitude is dominated by the coupling of the elastic channel to the $\pi\Delta(1232)$ channel. The d-wave pion coupling to the nucleon is increased by a factor of 2.5 with respect to the quark model value, while the model value for s-wave coupling to the $\Delta(1232)$ is not modified. Increasing the latter coupling brings the real part of the amplitude closer to the data, however the behavior of the photo-production amplitudes, presented in the next section, is deteriorated.

5 Electro-production

The electro-production amplitudes are obtained by evaluating the EM current consisting of the quark and the pion part between the nucleon ground state and the resonant state. The corresponding helicity amplitude $\mathcal{V}_{N\mathcal{R}}^\gamma$ in (7) reads

$$\mathcal{V}_{N\mathcal{R}}^\gamma(k_\gamma) = \frac{e}{\sqrt{2\omega_\gamma}} \langle \mathcal{R} | j_{EM}(k_\gamma) | N \rangle,$$

where the resonant state stemming from the second and the third term in (2) consists of the bare-quark part and the meson cloud

$$|\mathcal{R}\rangle = \frac{1}{\sqrt{Z_{\mathcal{R}}}} \left\{ |\Phi_{\mathcal{R}}\rangle - \sum_{MB} \int \frac{dk}{\omega_k + E_B - W} \mathcal{V}_{B\mathcal{R}}^M(k) [a^\dagger(k) |\tilde{\Psi}_B\rangle]^{JT} \right\}. \quad (14)$$

The background term entering (7) is dominated by the pion-pole term and the u-channel process which originate from the first term in (2).

In Figs. 3 – 6 the transverse photo-production amplitudes for the partial D13, D33 and D15 partial waves calculated in our model are compared to the data as well as to the analysis of the MAID group [11]. While our calculation correctly reproduce the behavior of the amplitudes at the energies close to the threshold where they are dominated by the pion-pole term, their strength in the resonance region is typically a factor 0.5 to 0.7 weaker compared to the value of the electric transverse amplitude as deduced from the experiment, and even weaker in the case of the magnetic amplitude. The pertinent multipoles are sensitive to the

nucleon's periphery which is apparently not adequately reproduced in the bag model, as we have already noticed when analyzing the coupling of the resonance to the d-wave pions. Here the pion cloud effect are relatively weak as a consequence of cancellations of different terms, and contribute at the level of 10 % to 20 % to the amplitudes.

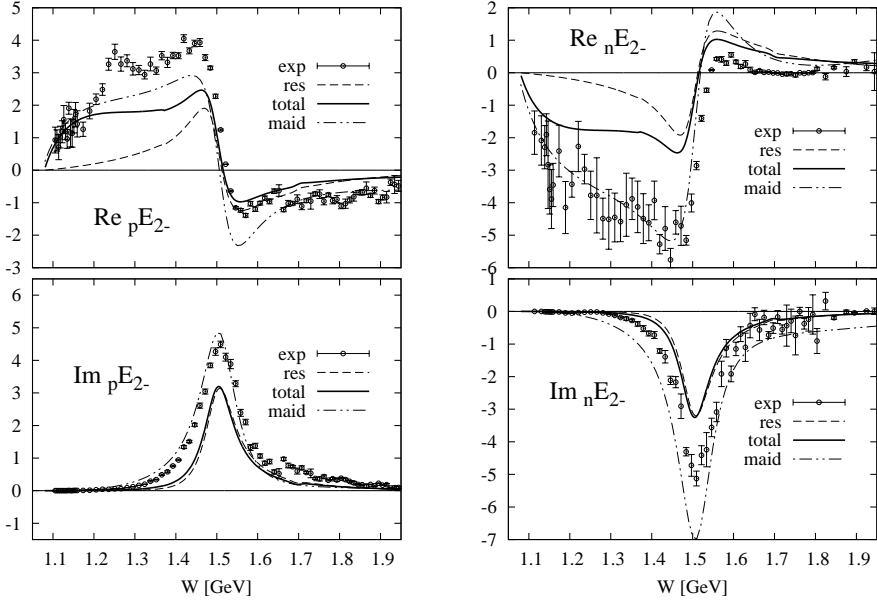


Fig. 3. The real and the imaginary part of the proton and neutron multipoles E_{2-} for the D13 wave in units $10^{-3}/m_\pi$ (preliminary). The data points are from [10], "maid" corresponds to the partial wave analysis from [11].

Nonetheless, we should stress that the amplitudes exhibit a consistent behavior in all considered partial waves. In particular, our model correctly predicts that in the D13 partial wave the ${}_n E_{2-}^{1/2}$ multipole amplitude is weaker than the corresponding ${}_n E_{2-}^{1/2}$ amplitude, and that the ${}_n M_{2-}^{1/2}$ amplitude almost vanishes. Similarly, for the D15 partial wave the quark model predicts that the quark contribution to the ${}_p M_{2-}^{1/2}$ multipole vanishes and only the pion cloud contributes to the resonant part of the amplitude. The non-zero quark contribution in the case of the neutron multipole is however too weak to reproduce the data.

6 Discussion

Comparing the present results with the results for other partial waves obtained in chiral quark models we notice a general trend that the quark core alone does not provide sufficient strength to reproduce the observed resonance excitation amplitudes. The best known example is the P33 partial wave in which case the quark contribution to the electric dipole excitation of the $\Delta(1232)$ is estimated

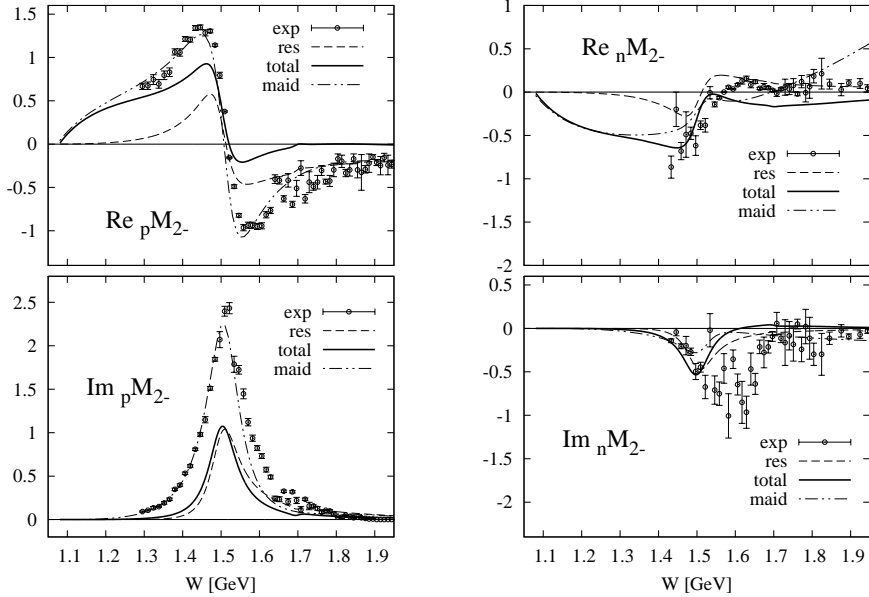


Fig. 4. The M_{2-} multipole, notation as in Fig. 3.

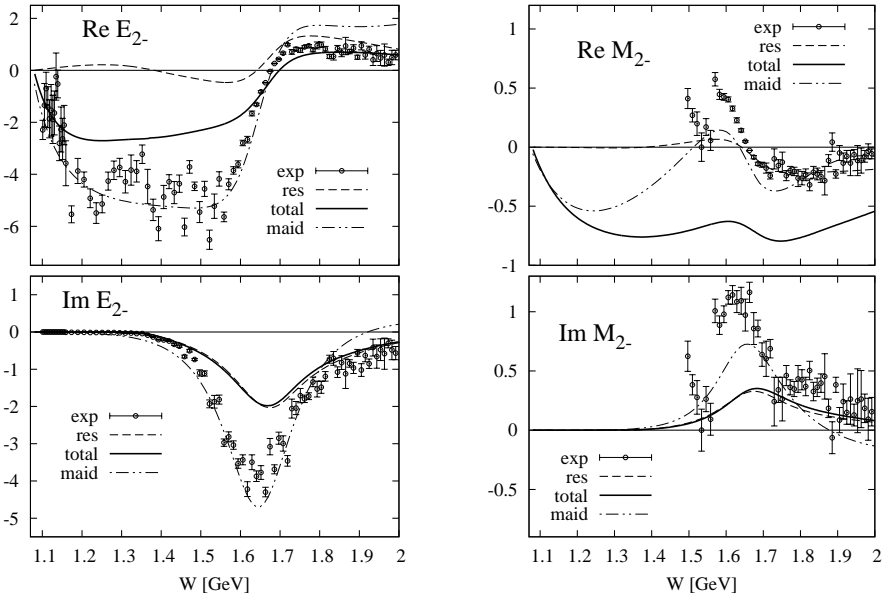


Fig. 5. E_{2-} and M_{2-} amplitudes for the D33 wave, notation as in Fig. 3.

by only 60 % while the rest is attributed to the pion cloud [1]. In the present calculation the pion cloud effects turn out not to be that important. In fact, we have noticed a considerable cancellation of different contributions of the meson cloud, e.g. the vertex correction due to pion loops and the genuine contribution

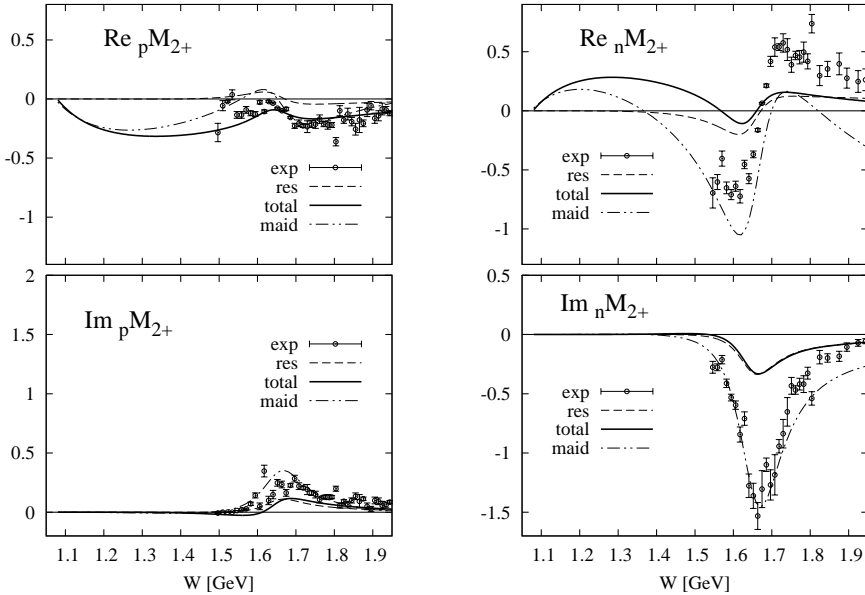


Fig. 6. The M_{2+} amplitudes for the D15 wave, notation as in Fig. 3.

of the pion cloud to the EM current. It is therefore possible that a calculation in a more elaborate chiral quark model could provide a better agreement with the data. To conclude, the overall qualitative agreement with the multipole analysis in the D13, D33 and D15 partial waves prove that the quark-model explanation of the D-wave resonance as the p-wave excitation of the quark core supplemented by the meson cloud is sensible and that no further degrees of freedom are needed.

References

1. M. Fiolhais, B. Golli, S. Širca, Phys. Lett. B **373**, 229 (1996)
2. P. Alberto, M. Fiolhais, B. Golli, and J. Marques, Phys. Lett. B **523**, 273 (2001).
3. B. Golli, S. Širca, L. Amoreira, M. Fiolhais Phys.Lett. B **553** (2003) 51-60
4. P. Alberto, L. Amoreira, M. Fiolhais, B. Golli, and S. Širca, Eur. Phys. J. A **26**, 99 (2005).
5. B. Golli and S. Širca, Eur. Phys. J. A **38**, (2008) 271.
6. B. Golli, S. Širca, and M. Fiolhais, Eur. Phys. J. A **42**, 185 (2009)
7. B. Golli, S. Širca, Eur. Phys. J. A **47** (2011) 61.
8. B. Golli, talk given at the Sixth International Workshop on Pion-Nucleon Partial-Wave Analysis and the Interpretation of Baryon Resonances, 23–27 May, 2011, Washington, DC, U.S.A., http://gwddac.phys.gwu.edu/pwa2011/Thursday/b_golli.pdf
9. Simon Širca, Bojan Golli, Manuel Fiolhais and Pedro Alberto, in Proceedings of the XIV International Conference on Hadron Spectroscopy (hadron2011), Munich, 2011, edited by B. Grube, S. Paul, and N. Brambilla, eConf C110613 (2011) [<http://arxiv.org/abs/1109.0163>].
10. R. A. Arndt, W. J. Briscoe, I. I. Strakovsky, R. L. Workman, Phys. Rev. C **74** (2006) 045205.
11. D. Drechsel, S.S. Kamalov, L. Tiator, Eur. Phys. J. A **34**, 69 (2007).



Scattering phase shifts and resonances from lattice QCD

S. Prelovšek^{a,b}

^a Jožef Stefan Institute, Jamova 39, 1000 Ljubljana, Slovenia

^b Faculty of Mathematics and Physics, University of Ljubljana, Jadranska 19, 1000 Ljubljana, Slovenia

Most of hadrons are hadronic resonances - they decay quickly via the strong interactions. Among all the resonances, only the ρ meson has been properly simulated as a resonance within lattice QCD up to know. This involved the simulation of the $\pi\pi$ scattering in p-wave, extraction of the scattering phase shift and determination of m_R and Γ via the Breit-Wigner like fit of the phase shift.

In the past year, we performed first exploratory simulations of $D\pi$, $D^*\pi$ and $K\pi$ scattering in the resonant scattering channels [1,2]. Our simulations are done in lattice QCD with two-dynamical light quarks at a mass corresponding to $m_\pi \approx 266$ MeV and the lattice spacing $a = 0.124$ fm.

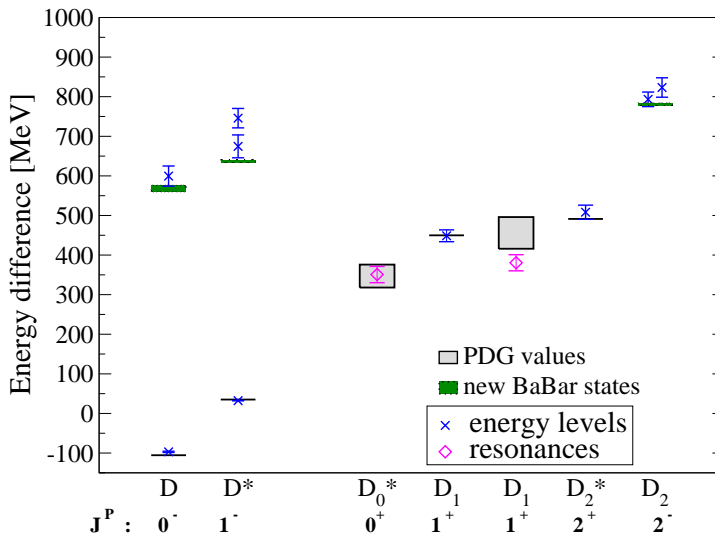


Fig. 1. Energy differences $\Delta E = E - \frac{1}{4}(M_D + 3M_{D^*})$ for D meson states in our simulation [1] and in experiment; the reference spin-averaged mass is $\frac{1}{4}(M_D + 3M_{D^*}) \approx 1971$ MeV in experiment. Magenta diamonds give resonance masses for states treated properly as resonances, while those extracted naively assuming $m_n = E_n$ are displayed as blue crosses [1].

The masses and widths of the broad scalar $D_0^*(2400)$ and the axial $D_1(2430)$ charmed-light resonances are extracted by simulating the corresponding $D\pi$ and $D^*\pi$ scattering on the lattice [1]. The resonance parameters are obtained using a Breit-Wigner fit of the elastic phase shifts. The resulting $D_0^*(2400)$ mass is 351 ± 21 MeV above the spin-average $\frac{1}{4}(m_D + 3m_{D^*})$, in agreement with the experimental value of 347 ± 29 MeV above. The resulting $D_0^* \rightarrow D\pi$ coupling $g^{\text{lat}} = 2.55 \pm 0.21$ GeV is close to the experimental value $g^{\text{exp}} = 1.92 \pm 0.14$ GeV, where g parametrizes the width $\Gamma \equiv g^2 p^*/s$. The resonance parameters for the broad $D_1(2430)$ are also found close to the experimental values; these are obtained by appealing to the heavy quark limit, where the neighboring resonance $D_1(2420)$ is narrow. The simulation of the scattering in these channels incorporates quark-antiquark as well as $D^{(*)}\pi$ interpolators, and we use distillation method for contractions. The resulting D-meson spectrum is compared to the experimental one in Fig. 1.

In addition, the ground and several excited charm-light and charmonium states with various J^P are calculated using standard quark-antiquark interpolators. The lattice results for the charmonium are compared to the experimental levels in Fig. 2.

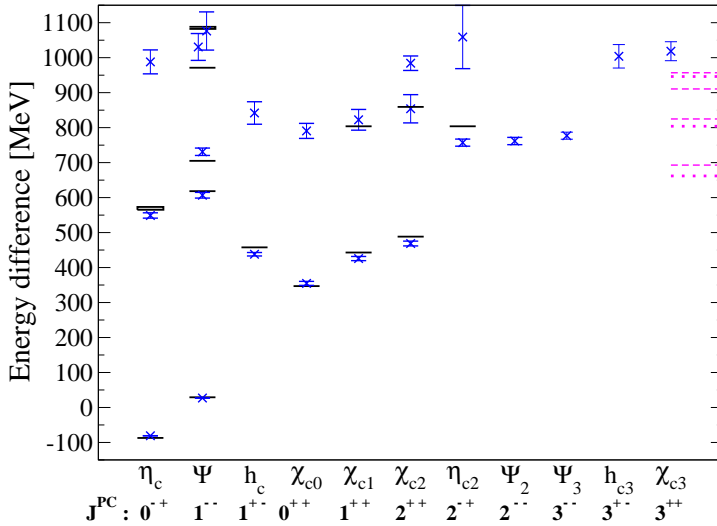


Fig. 2. Energy differences $\Delta E = E - \frac{1}{4}(M_{\eta_c} + 3M_{J_\Psi})$ for charmonium states in our simulation [1] and in experiment; reference spin-averaged mass is $\frac{1}{4}(M_{\eta_c} + 3M_{J_\Psi}) \approx 3068$ MeV in experiment. The magenta lines on the right denote relevant lattice and continuum $\bar{D}^{(*)}D^{(*)}$ thresholds.

We also simulated $K\pi$ scattering in s-wave and p-wave for both isospins $I = 1/2, 3/2$ using quark-antiquark and meson-meson interpolating fields [2]. Fig. 3 shows the resulting energy levels of $K\pi$ in a box. In all four channels we observe the expected $K(\eta)\pi(-\eta)$ scattering states, which are shifted due to the interaction. In both attractive $I = 1/2$ channels we observe additional states that are related

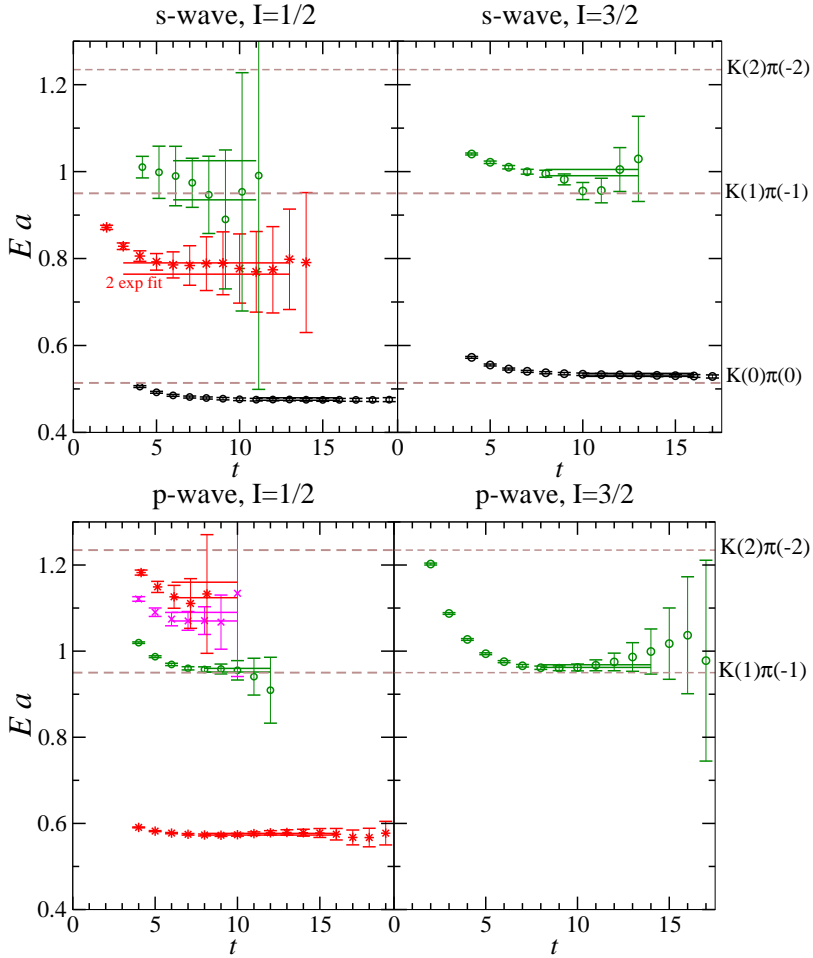


Fig. 3. The energy levels $E(t)a$ of the $K\pi$ in the box for all four channels (multiply by $a^{-1} = 1.59$ GeV to get the result in GeV). The horizontal broken lines show the energies $E = E_K + E_\pi$ of the non-interacting scattering states $K(n)\pi(-n)$ as measured on our lattice; $K(n)\pi(-n)$ corresponds to the scattering state with $p^* = \sqrt{n} \frac{2\pi}{L}$. Note that there is no $K(0)\pi(0)$ scattering state for p-wave. Black and green circles correspond to the shifted scattering states, while the red stars and pink crosses correspond to additional states related with resonances.

to resonances; we attribute them to $K_0^*(1430)$ in s-wave and $K^*(892)$, $K^*(1410)$ and $K^*(1680)$ in p-wave. We extract the elastic phase shifts δ at several values of the $K\pi$ relative momenta. The resulting phases exhibit qualitative agreement with the experimental phases in all four channels, as shown in Fig. 4. In addition to the values of the phase shifts shown in Fig. 4, we also extract the values of the phase shift close to the threshold, which are expressed in terms of the scattering lengths in [2].

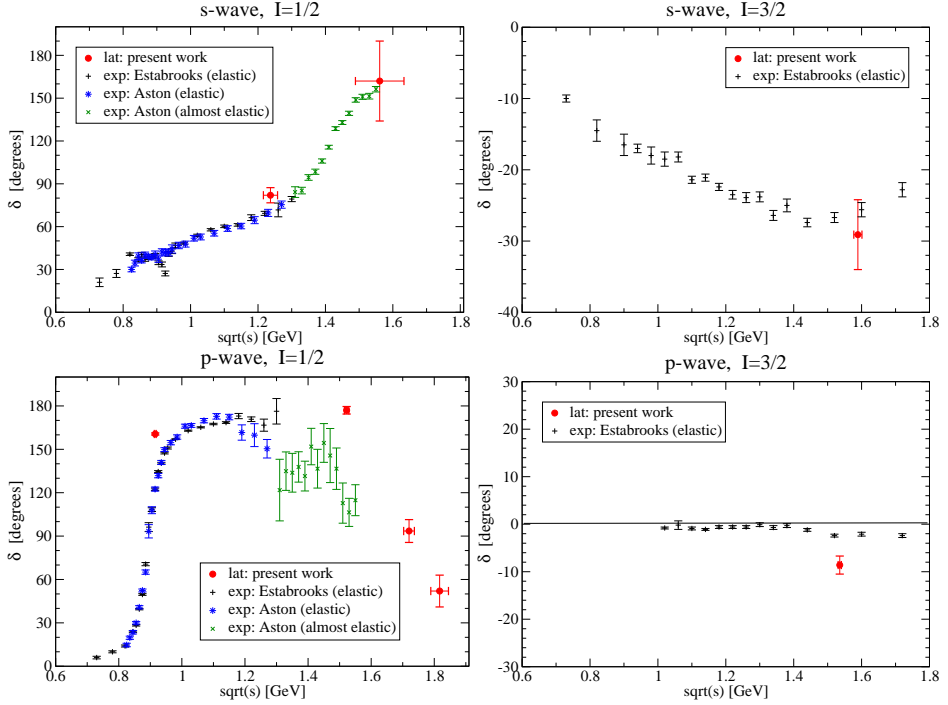


Fig. 4. The extracted $K\pi$ scattering phase shifts δ_l^I in all four channels $l = 0, 1$ and $I = 1/2, 3/2$. The phase shifts are shown as a function of the $K\pi$ invariant mass $\sqrt{s} = M_{K\pi} = \sqrt{(p_\pi + p_K)^2}$. Our results (red circles) apply for $m_\pi \simeq 266$ MeV and $m_K \simeq 552$ MeV in our lattice simulation. In addition to the phases provided in four plots, we also extract the values of $\delta_0^{1/2, 3/2}$ near threshold $\sqrt{s} = m_\pi + m_K$, but these are provided in the form of the scattering length in the main text (as they are particularly sensitive to $m_{\pi,K}$). Our lattice results are compared to the experimental elastic phase shifts (both are determined up to multiples of 180 degrees).

We believe that these simulations of the $D\pi$, $D^*\pi$ and $K\pi$ scattering in the resonant channels represent encouraging step to simulate resonances properly from first principle QCD. There are many other exciting resonances waiting to be simulated along the similar lines.

References

1. D. Mohler, S. Prelovsek and R. Woloshyn, *D π scattering and D meson resonances from lattice QCD*, arXiv:1208.4059.
2. C. B. Lang, Luka Leskovec, Daniel Mohler, Sasa Prelovsek, *K π scattering for isospin 1/2 and 3/2 in lattice QCD*, Phys. Rev. D.86. (2012) 054508, arXiv:1207.3204.



Scattering of nucleon on a superheavy neutron ^{*}

Norma Mankoč Borštnik^a and Mitja Rosina^{a,b}

^aFaculty of Mathematics and Physics, University of Ljubljana, Jadranska 19, P.O. Box 2964, 1001 Ljubljana, Slovenia

^bJ. Stefan Institute, 1000 Ljubljana, Slovenia

Abstract. The scattering cross section of a superheavy baryon on a nucleon is estimated. The possibility that such a superheavy baryon (from a higher quark family) might be a viable candidate for the dark matter, is discussed.

1 Introduction

The purpose of this talk is twofold.

(i) Scattering of a light cluster on a superheavy cluster is a challenging few-body problem. The energy scales and consequently the sizes of both clusters differ by 5-6 orders of magnitude. Due to colour neutrality of unperturbed clusters, the strong interaction acts only at a very short distance via the virtual colour-octet colour-octet Van der Waals excitation. The novel feature is the van der Waals interaction at contact separation. Moreover, due to the small size of the superheavy cluster the effective quark-quark interaction is expected to be coulomb-like and this feature might be tested even in bottomium collisions.

(ii) We want to show that clusters of strongly interacting particles are viable candidates for dark matter provided their masses are large enough. Then both the number density of dark matter particles is small and their cross section is small due to their small size.

We require that the number of collisions of dark matter particles against the detector is either consistent with the DAMA experiment [1] (if confirmed) or lower (if DAMA is not confirmed). It turns out that superheavy quarks must have a mass of about 100 TeV or more in order to have a low enough collision rate by weak interaction. Surprisingly, at this mass the strong cross section is much smaller than the weak cross section and can be neglected.

As an example we take the superheavy quarks from the unified *Spin-Charge-Family* theory [2–6] which has been developed by one of the authors (SNMB) in the recent two decades. For a short review, we invite the reader to read the Bled 2010 Proceedings [7]. In this theory eight families of quarks and leptons are predicted, with the fifth family decoupled from the lower ones and therefore rather stable. The most promising candidates for dark matter are the superheavy neutrons (the $n_5 = u_5 d_5 d_5$ clusters) of the fifth family.

* Talk delivered by M. Rosina

There is a danger in this proposal. Either the charged baryon $u_5u_5u_5$ or the charged baryon $d_5d_5d_5$ could be the lightest, depending on whether u_5 or d_5 is lighter. Charged clusters cannot, of course, constitute dark matter. Forming the atoms with the first family electrons they would have far too large scattering amplitude to be consistent with the properties of dark matter. However, if one takes into account also the electro-weak interaction between quarks, then the neutral baryon $n_5 = u_5d_5d_5$ can be the lightest, provided the u-d mass difference is not too large. We have put limits on the u-d quark mass differences in ref. [7] and we briefly repeat the result (choosing $\alpha_{EM} = 1/128$, $\alpha_W = 1/32$, $\alpha_Z = 1/24$).

For superheavy quarks, the colour interaction is assumed to be coulombic and we solve the Hamiltonian for the three-quark system

$$H = 3m_5 + \sum_i \frac{\mathbf{p}_i^2}{2m_5} - \frac{(\sum_i \mathbf{p}_i)^2}{6m_5} - \sum_{i<j} \frac{2}{3} \frac{\alpha_s}{r_{ij}}.$$

For the choice of the average quark mass $m_5 = 100$ TeV and $\alpha_s = 1/13$ the binding energy is $E_0 = -\eta\alpha_s^2 m_5 = -0.39$ TeV and the average quark momentum $p = \sqrt{2m_5 E_{kin}/3} = 5.1$ TeV. (The coefficient η has been obtained variationally).

The electroweak interaction prefers the neutral $u_5d_5d_5$ and it cannot decay into $d_5d_5d_5$ or $u_5u_5d_5$ provided

$$-0.026 \text{ TeV} < m_{u_5} - m_{d_5} < 0.39 \text{ TeV}.$$

This limits are not very narrow, but they are narrow compared to the mass scale of $m_5 = 100$ TeV.

2 The weak ($u_5d_5d_5$) – ($u_1d_1d_1$) cross section

It is easy to calculate the scattering amplitude since the superheavy neutron is a point particle compared to the range of the weak interaction and its quark structure is not important. Only Z-exchange matters since there is not enough energy to excite $u_5d_5d_5$ into $d_5d_5d_5$ or $u_5u_5d_5$ via W-exchange. We consider only the scattering on neutron (the ‘‘charge’’ of proton almost happens to cancel!). Also, we consider only the Fermi (vector) matrix element, since it adds coherently in heavy nuclei, while the Gamov-Teller (axial) has many cancellations in spin coupling.

$$\begin{aligned} \mathcal{M} &= \left[\frac{1}{2} t_0(1) - \sin^2 \vartheta_W e(1) \right] \frac{g_Z^2}{m_Z^2} \left[\frac{1}{2} t_0(5) - \sin^2 \vartheta_W e(5) \right] = \frac{G_F}{2\sqrt{2}} \\ \sigma_n &= 2\pi |\mathcal{M}|^2 \frac{4\pi p_1^2}{(2\pi)^3 v^2} = \frac{m_{n1}^2}{\pi} |\mathcal{M}|^2 = \frac{G_F^2 m_{n1}^2}{8\pi} = 1.9 \times 10^{-13} \text{ fm}^2. \end{aligned}$$

We should note that the cross section does not depend on the mass m_{n5} provided it is much larger than m_{n1} of the first family. For a heavy target

$$\sigma_A = \sigma_n (A - Z)^2 A^2$$

The rate at a detector of $^{23}_{11}\text{Na}$ $^{127}_{53}\text{I}$ per kilogram of detector is

$$R_{1\text{kg}} = \sigma_A N_A \frac{\rho_{n5} \times v}{m_{n5}}$$

$$R_{1\text{kg}} = \sigma_n [(A_{Na} - Z_{Na})^2 A_{Na}^2 + (A_I - Z_I)^2 A_I^2] \frac{N_{\text{avogadro}}}{A_{Na} + A_I} \frac{\rho_{n5} \times v}{m_{n5}} = 1.3/\text{day}$$

We used the data $\rho_{n5} = 0.3 \text{ GeV cm}^{-3}$, $m_{n5} = 300 \text{ TeV}$, $v = 230 \text{ km/s}$.

This can be compared to the rate claimed by the DAMA collaboration:

$$\Delta R_{1\text{kg}}(\text{DAMA}) = 0.02/\text{day}, \quad R_{1\text{kg}}(\text{DAMA}) \sim (0.1 \leftrightarrow 1)/\text{day}.$$

This comparison was used to decide about the choice of m_5 in our example. If DAMA results are not confirmed, m_5 should be even larger.

3 The strong MESON – meson cross section

This Section is a **lesson** for a future realistic calculation of the $(u_5 d_5 d_5) - (u_1 d_1 d_1)$ scattering. We want to show that for superheavy quarks the strong cross section is much smaller than the weak cross section and can be neglected. For this purpose we need only an estimate and not a detailed calculation. Meson-meson scattering offers a good estimate since the baryon in a quark-diquark approximation resembles a meson. However, this lesson is very relevant for botonium scattering and for future heavy baryons in the 10-100 GeV region.

Here we present the trial functions of the light and heavy meson, together with relevant quantities such as the chromomagnetic dipole moment D of the heavy meson sitting in the dipole field G of the light meson. Note that m and M are quark masses and $\alpha = \frac{4}{3}\alpha_s$.

$$\begin{aligned} \mathbf{r} &= \mathbf{r}_q - \mathbf{r}_{\bar{q}}, & b &= 1/(\frac{1}{2}m)\alpha & \mathbf{R} &= \mathbf{R}_Q - \mathbf{R}_{\bar{Q}}, & B &= 1/(\frac{1}{2}M)\alpha \ll b \\ \psi_0 &= (2/\sqrt{4\pi b^3}) \exp(-r/b) & \Psi_0 &= (2/\sqrt{4\pi B^3}) \exp(-R/B) \\ \psi_z &= \frac{2^{-3/2}}{\sqrt{4\pi f^3}} (r/f) \cos \vartheta \exp(-r/f) & \Psi_z &= \frac{2^{-3/2}}{\sqrt{4\pi B^3}} (R/B) \cos \Theta \exp(-R/B) \\ \epsilon_0 &= -(1/2)(\frac{1}{2}m)\alpha^2 & E_0 &= -(1/2)(\frac{1}{2}M)\alpha^2 \\ \epsilon_{z,\text{kin}} &= +(1/8)(\frac{1}{2}m)\alpha^2 (b/f)^2 & E_z &= -(1/8)(\frac{1}{2}M)\alpha^2 \\ G_z &= \langle \psi_z | z / (r/2)^3 | \psi_0 \rangle = \gamma / \sqrt{fb^3} & D &= \langle \Psi_z | Z | \Psi_0 \rangle = \beta B \\ \gamma &= 16\sqrt{2}/3 = 7.542 & \beta &= 2^{15/2}/3^5 = 0.745 \end{aligned}$$

The meson wavefunctions get "decorated" with colour factors

$$\phi_0 = \psi_0 \frac{(r[\text{gb}] + g[\text{br}] + b[\text{rg}])}{\sqrt{3}}, \quad \phi_{z3} = \psi_z \frac{(r[\text{gb}] - g[\text{br}])}{\sqrt{2}}$$

$$\Phi_0 = \Psi_0 \frac{(r[gb] + g[br] + b[rg])}{\sqrt{3}}, \quad \Phi_{z3} = \Psi_z \frac{(r[gb] - g[br])}{\sqrt{2}}$$

We write explicitly only the spatial excitation in the z -direction and colour excitation in the "third colour" $\omega = 3$. Others behave similarly.

We shall need the colour matrix element

$$\left\langle \frac{r[gb] - g[br]}{\sqrt{2}} \left| \frac{\lambda_q^3}{2} - \frac{\lambda_{\bar{q}}^3}{2} \right| \frac{r[gb] + g[br] + b[rg]}{\sqrt{3}} \right\rangle = \sqrt{\frac{2}{3}}$$

For color neutral hadrons, the dominant term in the expansion yields the effective dipole-dipole, colour-octet – colour-octet potential

$$\hat{V}_{\text{dipole}} = \alpha_s \left(\mathbf{R}_Q \frac{\vec{\lambda}_Q}{2} + \mathbf{R}_{\bar{Q}} \frac{\vec{\lambda}_{\bar{Q}}}{2} \right) \left(\frac{\mathbf{r}_q}{r_q^3} \frac{\vec{\lambda}_q}{2} + \frac{\mathbf{r}_{\bar{q}}}{r_{\bar{q}}^3} \frac{\vec{\lambda}_{\bar{q}}}{2} \right),$$

The perturbation term between the unperturbed ground state and the virtual excitation is then

$$V'_{z,3} = \alpha_s \langle \Psi_z \Psi_z | \left\{ \frac{Z}{2} \right\} \sqrt{\frac{2}{3}} \left\{ \frac{z/2}{(r/2)^3} \right\} \sqrt{\frac{2}{3}} | \Psi_0 \Psi_0 \rangle = \frac{\alpha_s D_z G_z}{6}$$

$$V'_{x,\omega} = V'_{y,\omega} = V'_{z,\omega} \equiv V' \quad \text{equal for all } \omega.$$

The second order perturbation theory then gives the effective potential between the two clusters

$$V_{\text{eff}} = -24 \frac{V'^2}{(E_z - E_0) + \epsilon_{z,\text{kin}}}$$

We have neglected $\epsilon_{z,\text{pot}}$ and ϵ_0 . The factor 24 comes from 3 spacial and 8 colour degrees of freedom.

$$V_{\text{eff}} = -\frac{2}{3} \frac{(\alpha_s D_z G_z)^2}{(3/8)(\frac{1}{2}M)(4\alpha_s/3)^2 + (1/8)(\frac{1}{2}m)(4\alpha_s/3)^2 (b/f)^2}$$

$$V_{\text{eff}} = -\frac{2(\beta\gamma B)^2}{fb^3(M + (1/3)m(b/f)^2)}$$

Note that α_s has canceled. Minimization with respect to f gives $f/b = \sqrt{m/3M} \ll 1$. Finally, we get

$$V_{\text{eff}} = -\frac{\sqrt{3}\beta^2\gamma^2}{b^3} \left(\frac{m}{M}\right)^{3/2} \frac{B}{m}$$

Here we took the distance between the two clusters $U = 0$. We assume

$$V_{\text{eff}}(U) = V_{\text{eff}}(U = 0) \exp(-2U/b).$$

In Born approximation (with the mass of the lighter cluster $m_q + m_{\bar{q}} = 2m$) we get

$$\alpha = \frac{(2m)}{2\pi} \int V_{\text{eff}}(U) d^3U = \sqrt{3}\beta^2\gamma^2 \left(\frac{m}{M}\right)^{3/2} B.$$

Let us give a numerical example with the choice

$$m = 300 \text{ MeV}, \quad M = \frac{1}{2}m_Q = 100 \text{ TeV}, \quad m/M = 3 \cdot 10^{-6}, \quad \alpha_s = 1/13$$

$$\alpha = \sqrt{3}\beta^2\gamma^2 \left(\frac{m}{M}\right)^{3/2} B = 1.1 \cdot 10^{-11} \text{ fm}$$

$$\sigma = 4\pi\alpha^2 = 1.5 \cdot 10^{-21} \text{ fm}^2$$

4 Conclusion

Regarding the weak interaction, the scattering rate of superheavy clusters is inversely proportional to their mass because (i) their weak cross section is independent of the heavy mass if it is large enough and (ii) because their number density is inversely proportional to their mass for the known dark matter density. This argument requires the superheavy quark mass to be about 100 TeV (if DAMA experiment is confirmed) or more.

For such a heavy mass, **the strong cross section is MUCH SMALLER than the weak cross section**. The reason is (i) the small size of the heavy hadron, $B = 3.8 \cdot 10^{-5} \text{ fm}$ and moreover, (ii) the suppression factor $(m/M)^3$ which is a consequence of colour neutrality of both clusters so that they interact only by induced color dipoles (“van der Waals interaction”).

The lesson from the heavy hadron – light hadron scattering will be useful also for not-so-exotic processes such as bottomium and bbb scattering.

References

1. R. Bernabei et al., Int. J. Mod. Phys. D **13** (2004) 2127-2160; Eur. Phys. J. C **56** (2008) 333-355.
2. N. S. Mankoč Borštnik, Phys. Lett. B **292** (1992) 25; J. Math. Phys. **34** (1993) 3731; Int. J. Theor. Phys. **40** (2001) 315; Modern Phys. Lett. **A 10** (1995) 587.

3. A. Borštnik, N. S. Mankoč Borštnik, in *Proceedings to the Euroconference on Symmetries Beyond the Standard Model*, Portorož, July 12-17, 2003, hep-ph/0401043, hep-ph/0401055, hep-ph/0301029; Phys. Rev. D **74** (2006) 073013, hep-ph/0512062.
4. G. Bregar and N. S. Mankoč Borštnik, Phys. Rev. D **80** (2009) 083534.
5. G. Bregar, M. Breskvar, D. Lukman, N.S. Mankoč Borštnik, New J. of Phys. **10** (2008) 093002.
6. N. S. Mankoč Borštnik, in "What comes beyond the standard models", Bled Workshops in Physics **11** (2010) No.2
7. N. S. Mankoč Borštnik and M. Rosina, *Bled Workshops in Physics* **11** (2010) No. 1, 64; also <http://www-f1.ijs.si/BledPub/>.
8. Z. Ahmed et al., Phys. Rev. Lett. **102** (2009) 011301.
9. K. Nakamura et al. (Particle Data Group), J. Phys. G **37** (2010) 075021.



Approaching the spin structure of ^3He by polarization observables

S. Širca^{a,b}

^a Faculty of Mathematics and Physics, University of Ljubljana, Jadranska 19, 1000 Ljubljana, Slovenia

^b Jožef Stefan Institute, Jamova 39, 1000 Ljubljana, Slovenia

Abstract. The E05-102 experiment at Jefferson Laboratory (TJNAF) was devised to study the double-polarization asymmetries in electron-induced deuteron, proton, and neutron knockout from polarized ^3He at low momentum transfers, in a wide range of missing momenta. With this advanced experimental technique, we strive to obtain a much clearer insight into the ground-state structure of ^3He , the cornerstone nucleus widely used as the effective neutron target. An order of magnitude improvement in the statistical uncertainties with respect to existing measurements is anticipated. We report on the status of the ongoing data analysis.

1 Physics motivation

The primary motivation to study electron-induced processes involving the ^3He nucleus (see [1] and references therein) is to understand the ground-state structure of this nucleus. This structure is not only interesting by itself; it is also important to study it in order to be able to interpret all data “on the neutron” for which ^3He acts as an effective target to a very good approximation. Contrary to common belief, there is no widely adopted consensus about the exact level at which this approximation can be treated as “good” or “good enough”.

A precise understanding of the transition between the experimental data acquired on ^3He targets and the observables corresponding to the neutron has become a burning issue since the statistical precision of recently performed (or future) experiments is so large that the systematical uncertainties of this computational transition procedure have become comparable to it. Some of the most interesting observables fall into this category, like e.g. the neutron elastic form-factors

$$G_E^n, \quad G_M^n,$$

and the polarized quark structure functions corresponding to the neutron,

$$G_E^n, \quad G_M^n, \quad A_1^n, \quad g_1^n, \quad g_2^n,$$

as well as the studies of the GDH sum rule.

One of the main complications, of course, is that the protons in ${}^3\text{He}$ partly polarized due to the presence of S' - and D-state components of the ground-state wave-function. (The ground-state configuration of ${}^3\text{He}$ is intimately connected to another open question of differences in RMS-radii, $\langle r^2 \rangle^{1/2}$, of ${}^3\text{H}$ as opposed to ${}^3\text{He}$, a matter largely unresolved due to an almost complete lack of measurements on tritium.) The manifestations of the distribution of spin, orbital angular momentum and isospin within ${}^3\text{He}$ appear to be most prominent and unambiguous in double-polarization asymmetries for electron-induced deuteron, proton, and neutron knockout from polarized ${}^3\text{He}$. Numerous discrepancies among the state-of-the-art theories persist for these observables.

In short, understanding the role of D and S' states as the two most relevant sub-leading components of the ${}^3\text{He}$ wave-function, and of the spin- and isospin-dependence of reaction mechanisms on ${}^3\text{He}$ is one of the key issues in the "Standard Model" of few-body theory.

2 The measurements

The exclusive cross-section for electron-induced deuteron knockout (with both the beam and the target polarized) has the form

$$\frac{d\sigma(\mathbf{h}, \mathbf{S})}{d\Omega_e dE_e d\Omega_d dp_d} = \frac{d\sigma_0}{d\Omega_e dE_e d\Omega_d dp_d} [1 + \mathbf{S} \cdot \mathbf{A}^0 + h(\mathbf{A}_e + \mathbf{S} \cdot \mathbf{A})] .$$

In the experiment described in this contribution, we measured two components of \mathbf{A} (or linear combinations thereof), which correspond to the transverse and longitudinal double-polarization asymmetries

$$A_{x,z} = \frac{[d\sigma_{++} + d\sigma_{--}] - [d\sigma_{+-} + d\sigma_{-+}]}{[d\sigma_{++} + d\sigma_{--}] + [d\sigma_{+-} + d\sigma_{-+}]},$$

where the subscript signs denote the helicities of the electron beam and the orientation of the target spin. The target was polarized along the beam-line and perpendicular to it (in both sideways directions). Similarly, the asymmetries for exclusive processes in which the proton and the neutron were knocked out (with obvious modifications to the above formulas) have been measured.

Since the transverse and longitudinal asymmetries in each channel have very distinct sensitivities to the dominant S and the sub-dominant D and S' component of the ${}^3\text{He}$ as functions of missing momentum, our experiment carries an immense resolving power for testing theories mentioned below. The fact that several exclusive channels were measured at the same time at approximately the same four-momentum transfer of about 0.2 to 0.3 $(\text{GeV}/c)^2$, in a large range of missing momenta, and with excellent statistical and systematical uncertainties, is another landmark feature of this experiment.

The resulting asymmetries will be compared to state-of-the-art theories of the ${}^3\text{He}$ nucleus. We exploit the calculations of the Bochum/Krakow group [4] that

apply a full Faddeev approach with the AV18 NN-potential and the Urbana IX three-nucleon force, together with a complete treatment of final-state interactions (FSI) and meson-exchange currents (MEC).

Also available to use are the calculations of the Hannover/Lisbon group [5] that are also full Faddeev, but with a coupled-channel extension and refit of the CD-Bonn NN-potential. They also incorporate FSI and MEC, while the effective three-nucleon force and two-body currents are provided by inclusion of the Δ as an active degree-of-freedom. Coulomb interaction for outgoing charged baryons is also included.

The group from Pisa has also provided us with their calculations based on the AV18 potential and the Urbana IX force in which the FSI are included by means of the variational pair-hyperspherical harmonics expansion, and MEC are also accounted for. This is not a Faddeev-type calculation, but its accuracy is assumed to be completely equivalent to it [6]. All three predictions (full calculations only) are presented in comparison to the anticipated experimental uncertainties in Fig. 1.

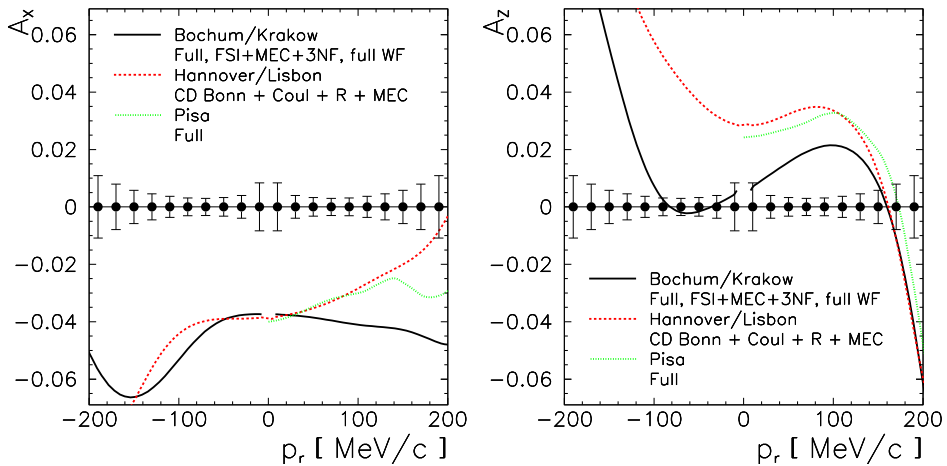


Fig. 1. The predictions for the asymmetries A_x and A_y in the quasi-elastic ${}^3\text{He}(e, e'd)$ process. The anticipated experimental uncertainties and three calculations by the Bochum/Krakow, Hannover/Lisbon and Pisa groups are shown.

3 Status of data analysis

The polarizations of the electron beam and the target have been established, and the beam and target monitoring apparatus have been calibrated. The magneto-optical properties of the BigBite spectrometer that was used to detect the charged hadrons have been determined [3], and the tracking and PID detectors have been calibrated, along with the neutron detector and the spectrometer used to detect the electrons. Presently the analysis work is focused on the correct averaging of

the theoretical asymmetries over the relatively large experimental acceptance. To this purpose, we have obtained the calculations of the asymmetries on a rather dense grid of points in the (E_e, θ_e) plane that covers the majority of our acceptance, as shown in Fig. 2. The additional dimension in which averaging is performed is the deuteron (or proton) emission angle with respect to the virtual photon.

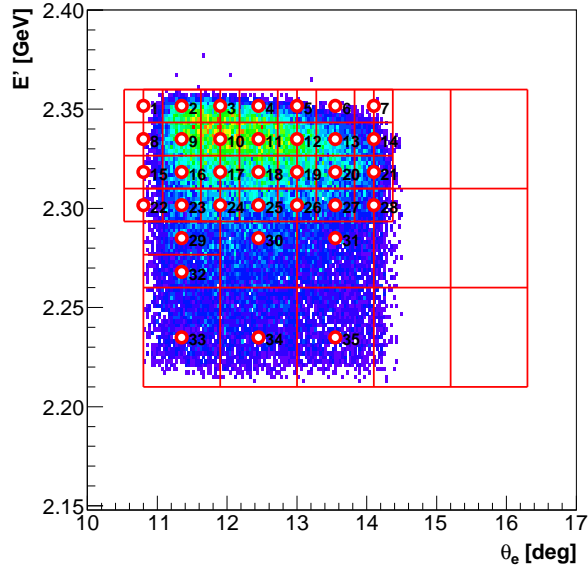


Fig. 2. The grid in (E_e, θ_e) plane on which the theoretical calculations will be performed, thus covering the most relevant parts of the experimental acceptance in the ${}^3\text{He}(e, e'd)$ channel. The high density of points is needed for reliable acceptance averaging because the asymmetries have a strong dependence on the energy transfer $E_e - E'_e$ (vertical axis).

The statistics of the data is sufficient to achieve a precision better than 2% on the asymmetries in each 20 MeV/c bin in missing momentum, ranging to about 200 MeV/c in the deuteron channel and about 300 MeV/c in the proton channels. Similar accuracy will be achieved in the neutron channel, and an even better one in the inclusive channels, which are a “bonus” of our experiment.

References

1. S. Širca, *Few-Body Systems* **47** (2010) 39.
2. S. Širca, S. Gilad, D. W. Higinbotham, W. Korsch, B. E. Norum (spokespersons), *Measurement of A_x and A_z asymmetries in the quasi-elastic ${}^3\text{He}(e, e'd)$* , JLab Experiment E05-102, June 2005.
3. M. Mihovilović et al. (Hall A Collaboration), *Nucl. Instr. Meth. A* **686** (2012) 20.
4. J. Golak, R. Skibiński, H. Witała, W. Glöckle, A. Nogga, H. Kamada, *Phys. Reports* **415** (2005) 89.
5. A. Deltuva et al., *Phys. Rev. C* **70** (2004) 034004.
6. L. E. Marcucci, M. Viviani, R. Schiavilla, A. Kievsky, S. Rosati, *Phys. Rev. C* **72** (2005) 014001.

BLEJSKE DELAVNICE IZ FIZIKE, LETNIK 13, ŠT. 1, ISSN 1580-4992

BLED WORKSHOPS IN PHYSICS, VOL. 13, NO. 1

Zbornik delavnice 'Hadronske resonance',
Bled, 1. – 8. julij 2012

Proceedings of the Mini-Workshop 'Hadronic Resonances',
Bled, July 1 – 8, 2012

Uredili in oblikovali Bojan Golli, Mitja Rosina, Simon Širca

Publikacijo sofinancira Javna agencija za knjigo Republike Slovenije

Tehnični urednik Matjaž Zaveršnik

Založilo: DMFA – založništvo, Jadranska 19, 1000 Ljubljana, Slovenija

Natisnila tiskarna Birografika Bori v nakladi 100 izvodov

Publikacija DMFA številka 1882

Brezplačni izvod za udeležence delavnice
